UNIVERSITY OF SIENA

DEPARTMENT OF BIOTECHNOLOGY, CHEMISTRY AND PHARMACY

DOCTORAL THESIS IN BIOCHEMISTRY AND MOLECULAR BIOLOGY
Cycle XXXVI

Coordinator: Prof. Lorenza Trabalzini

THE ANTIMICROBIAL PEPTIDE SET-M33: *IN VIVO* EFFICACY AND TOXICITY IN DIFFERENT ANIMAL SPECIES AND ENCAPSULATION IN INHALABLE POLYMERIC NANOPARTICLES FOR PULMONARY DELIVERY

SCIENTIFIC-DISCIPLINARY SECTOR: BIO/10

TUTOR: **Prof. Alessandro Pini**

PhD STUDENT: **Laura Cresti**

Firmato digitalmente da Laura Cresti
Data: 12.04.2024 12:20:44 CEST

Academic year: 2022/2023

ABSTRACT

SET-M33 is a synthetic peptide that is being developed as a new antibiotic against major Gram-negative bacteria. In this Ph.D. thesis the results about *in vivo* efficacy and toxicity in different animal species are reported, concluding the preclinical development of the peptide. Furthermore, the construction of a biocompatible nanosystem where the antimicrobial peptide SET-M33 is encapsulated into polymeric nanoparticles (NPs) of poly(lactide-co-glycolide) (PLGA) conjugated with polyethylene glycol (PEG) is also described.

In the first study SET-M33 was administered to CD-1 mice by snout inhalation exposure for 1 h/day for 7 days at doses of 5 and 20 mg/kg/day. The results showed adverse clinical signs and effects on body weight at the higher dose, as well as some treatment-related histopathology findings (lungs and bronchi, nose/turbinates, larynx and tracheal bifurcation). On this basis, the no observable adverse effect level (NOAEL) was considered to be 5 mg/kg/day. In the same study, an efficacy evaluation of the peptide in an endotoxin (LPS)-induced pulmonary inflammation model. Intratracheal administration of SET-M33 at 0.5, 2 and 5 mg/kg significantly inhibited BAL neutrophil cell counts after an LPS challenge was presented. A significant reduction in pro-inflammatory cytokines, KC, MIP-1α, IP-10, MCP-1 and TNF-α was also recorded after SET-M33 administration.

In the second study, dose range finding experiments determined the doses to use in toxicokinetic evaluation, clinical biochemistry analysis, necroscopy and in neurological and respiratory measurements. Clinical laboratory investigations in dogs and rats showed a dose-related increase in creatinine and urea levels, indicating that the kidneys are the target organ. This was also confirmed by necroscopy studies of animal tissues, where signs of degeneration and regeneration were found in the kidney when SET-M33 was administered at the highest doses in the two animal species. Neurological toxicity measurements by the Irwin method and respiratory function evaluation in rats did not reveal any toxic effect even at the highest dose. Finally, repeated administration of SET-M33 by short infusion in dogs revealed a NOAEL of 0.5 mg/kg/day.

In the third study, the system peptide-NPs was conceived for the better delivery of the peptide to the lungs by aerosol. The encapsulated peptide showed prolonged antibacterial activity, due to its controlled release, and much lower toxicity than the free molecule. The peptide-based nanosystem killed *Pseudomonas aeruginosa* in planktonic and sessile forms in a dose-dependent manner, remaining active up to 72 hours after application. The encapsulated peptide showed no detectable cytotoxicity when incubated with human bronchial epithelial cells from healthy individuals and from cystic fibrosis patients, unlike the free peptide which showed an EC_{50} of about 22 μM. *In vivo* acute toxicity studies in experimental animals showed that the peptide nanosystem did not cause any appreciable side effects, and confirmed its ability to mitigate the toxic and lethal effects of free SET-M33.

TABLE OF CONTENTS

INTRODUCTION

ANTIBIOTICS AND RESISTANCE

Fleming's discovery of penicillin in 1928 marked the beginning of a new era in medicine, leading to the development of various classes of antibiotics. Antibiotics have revolutionized medicine by significantly reducing the mortality rates associated with bacterial infections [1]. They are a milestone of modern healthcare, used to treat various bacterial illnesses, from minor infections to life-threatening diseases [2]. However, the overuse and misuse of antibiotics have led to the emergence of antibiotic resistance, one of the most pressing global health threats we face today [3].

Antimicrobial resistance (AMR) occurs when bacteria adapt and evolve, becoming resistant to the effects of antibiotics. Bacteria can develop resistance through genetic mutations, horizontal gene transfer, and the selection of resistant strains through excessive antibiotic exposure [4]. The ability of bacteria to adapt and survive against these drugs poses a serious threat to global health. The misuse of antibiotics, such as not completing prescribed courses, using them when they're not necessary (for viral infections like the common cold or flu), and their widespread use in agriculture and livestock, are some of the primary contributors to the development of resistance [5].

In February 2017, to focus and guide research and development related to new antibiotics, the World Health Organization (WHO) published its list of pathogens for which new antimicrobial development is urgently needed [6]. Within this broad list, ESKAPE (*Enterococcus faecium*, *Staphylococcus aureus*, *Klebsiella pneumoniae*, *Acinetobacter baumannii*, *Pseudomonas aeruginosa* and *Enterobacter* species) pathogens were designated “priority status” [7].

The implications of AMR are profound. It reduces the effectiveness of antibiotics, leading to prolonged illnesses, increased mortality, and higher healthcare costs. Common infections that were once easily treatable can become untreatable, posing a significant risk, especially to vulnerable populations, such as the elderly, young children, and those with weakened immune systems [8]. In addition, the economic cost of the resistance to antibiotics is enormous. Antibiotic resistance is single-handedly killing more people than cancer and road traffic accidents combined deaths, killing 700,000 people every year, and another 10 million are anticipated to die from it by the year 2050, with a cost for the global economy of US$100 trillion (Figure 1) [9-10].

Since the turn of the 1990s, the development and commercialization of novel antibiotics have slowed. In recent years 11 new antimicrobial therapies were approved by the U.S. Food and Drug Administration (U.S. FDA) [11-12]. Of these 11 antimicrobials, 4 were approved by the European Union European Medicines Agency (E.U. EMA): the meropenem-vaborbactam combination (Vaborem) [13], eravacycline (Xerava) [14], delafloxacin (Baxdela/Quofenix) [15], and the imipenem-cilastatin-relebactam combination (Recarbrio; a positive opinion toward the granting of marketing authorization was recommended in December 2019, and approval was provided in February 2020) [16]. Global initiatives to deliver new antibacterial therapies or complementing alternative therapies are urgently needed.

Research and innovation play a vital role in the fight against antibiotic resistance. Scientists are exploring alternative therapies, such as phage therapy, which uses viruses to target and destroy bacteria [17], the discovery of new types of molecules that could have an antimicrobial activity and the development of new vaccines against superbugs [18]. Additionally, there's a growing emphasis on developing rapid diagnostic tools to enable healthcare providers to prescribe the most effective antibiotics promptly, reducing unnecessary or ineffective treatments [19].

A globally integrated strategy that includes different approaches (antibiotics, vaccines, diagnostics, antibodies, and new tools targeting the host, the microbiome, or delivered by phages) seems to be required to fight AMR effectively [20].

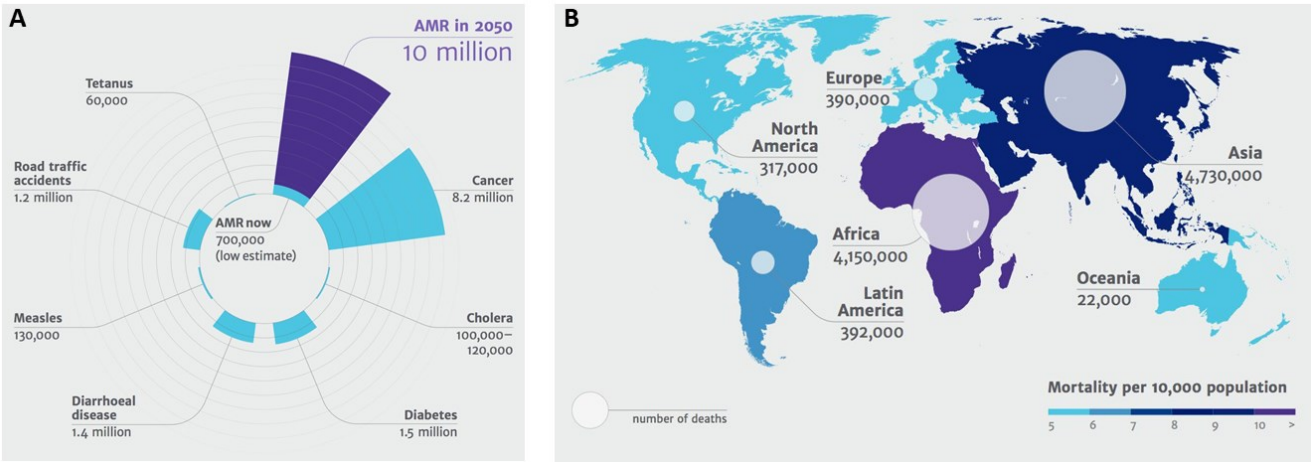

Figure 1. *(A) Deaths attributable to AMR every year compared to other major causes of death. (B) Deaths attributable to AMR every year by 2050 [10].*

ANTIMICROBIAL PEPTIDES (AMPs): AN OVERVIEW

The widespread growth of resistance to traditional antibiotics worldwide has prompted a significant surge in research efforts directed towards introducing new and unconventional anti-infective medications to the market. Antimicrobial peptides (AMPs) have captured the attention of the scientific community, as demonstrated by the rapid increased number of articles published (Figure 2) [21].

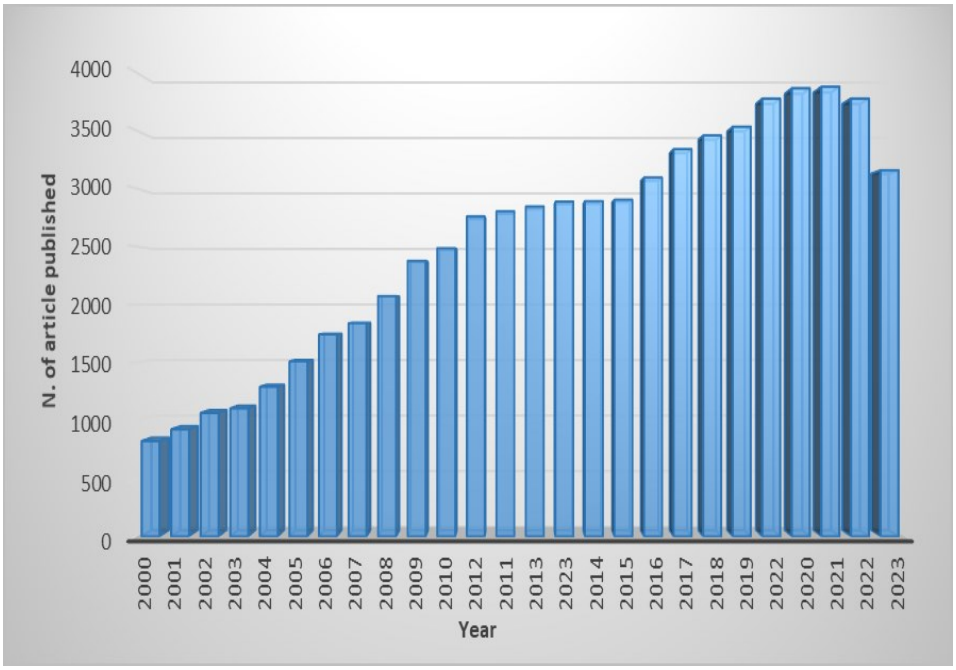

Figure 2. *Number of scientific articles published in academic journals since 2000. The keywords used for the resource in PubMed database were "antimicrobial peptides" OR "AMPs" OR "host defence peptides" OR "HDPs". The research of data was performed on January 2024.*

AMPs are bioactive small proteins generally composed of 10–50 amino acids, with a molecular weight of less than 10 KDa. Most AMPs are positively charged (2–13 net positive charges) that are derived primarily from lysine and arginine (a few may be histidine) in the sequence, forming a specific cationic domain [22-23]. Only a few AMPs are negatively charged, such as cattle chromatin, with 12 net negative charges, or daptomycin [24].

To emphasize the multifaceted nature of these molecules, the term "Host Defense Peptide" (HDP) [25-26] is now more commonly used to encompass the breadth of biological processes that are influenced by these versatile biomolecules, although the terms AMP are still accurate when considering only activities against bacteria [27].

Gramicidin, the first AMP, was discovered in 1939 from the soil bacterium *Brevibacillus* and showed *in vitro* and *in vivo* antibacterial activity against various Gram-positive bacteria [28]. Subsequently, AMPs were gradually isolated from bacteria, fungi and animals. In microorganisms, they are produced to kill other bacteria that compete for the same ecological niche. Instead, in plants and insects that do not have an immune system, they represent the primary defence against pathogens. Finally, in superior organisms like mammals, AMPs constitute roles as effectors in the innate immunity, primarily responsible for direct inhibition of pathogens as well as modulating innate and adaptive immune responses [29-31].

Natural AMPs can be classified based on their origin in bacteriophage/viral AMPs, bacterial AMPs, fungal AMPs, plant-derived AMPs and animal-derived AMPs [32].

Among them, insect-derived antimicrobial peptides are widely studied. Some examples of insect AMPs are defensins, cecropins, proline-rich peptides and attacins and have been identified in several insect orders, such as Diptera, Hymenoptera, Hemiptera, Coleoptera and Lepidoptera [33].

Focusing on the mammalian-derived AMPs, the two major families are human cathelicidins and defensins, mainly produced by epithelial cells and neutrophils [34-35].

The Antimicrobial Peptide Database (APD3; available at https://aps.unmc.edu/) is one of the largest databases [36]. It contains 3940 peptides, including 3146 natural antimicrobial peptides (AMPs) from the six life kingdoms (383 bacteriocins/peptide antibiotics from bacteria, 5 from archaea, 8 from protists, 29 from fungi, 250 from plants, and 2463 from animals), 190 predicted and 314 synthetic AMPs (Last updated: Jan 2024 | Copyright 2003-2023 Dept of Pathology & Microbiology, UNMC) (Figure 3).

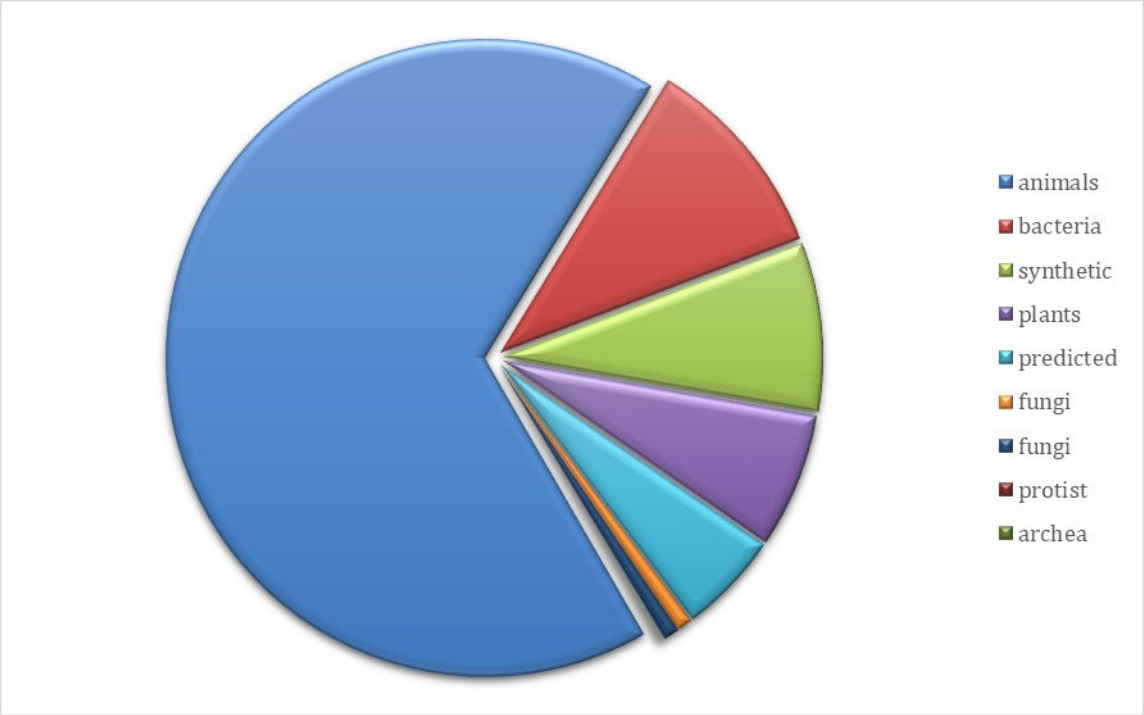

Figure 3. *Sources of antimicrobial peptides (total 3940) as of January 2024 from the APD3 Antimicrobial Peptide Database*

AMPs have a variety of biological activities such as antibacterial, antiviral, anticancer, immune regulation, prevention and/or eradication of biofilm, wound healing, antioxidant and many others [37].

AMPs can have different mechanisms of action (MoA). Most AMPs exert a direct antibacterial activity by destroying the membrane integrity of the bacteria, while some others are able to cross the microbial membrane to reach intracellular targets. The direct bactericidal mechanism of AMPs is performed through interacting with negatively charged membranes, resulting in increased membrane permeability, cell membrane lysis, or release of intracellular contents, which ultimately leads to cell death. There are four main models, widely described in the literature, of membrane-pore formation: barrel-stave model, toroidal-pore model, carpet model and aggregate model [38]. After AMPs penetrate into the phospholipid membrane, their hydrophobic regions combine with the internal hydrophobic regions of the phospholipid bilayer, while their hydrophilic regions are exposed to the outside. Another bactericidal mechanism is that AMPs penetrate into the cytoplasm and have different effects, such as inhibiting DNA, RNA and protein synthesis, inhibiting protein folding, inhibiting enzyme activity and cell wall synthesis, or promoting the release of enzymes to destroy cell structures [39-40]. Another type of AMPs classification is based on

the secondary structure: alpha-helical structure [41], beta-sheet structure [42], extended structure and loop structure [43]. Alpha-helical cathelicidian and beta-sheet defensin structures are common in humans. The typical representative of the extended structure is indolicidin, which contains abundant tryptophan and glycine. The loop structure of AMPs of bactenecin contains an intramolecular covalent disulfide bond on its C-end, which results in a loop. In addition, there are a large number of AMPs, such as human lactoferricin, whose structure is a mixture of the common structures mentioned above [44-45].

In addition to the large number of natural AMPs just described, synthetic AMPs can be obtained using other methods. One strategy to develop novel synthetic AMPs is *de novo* design of new sequences thanks to the assistance of specific softwares [46]. The rational or computational design of new peptides is an approach known and used for several years, but the Artificial Intelligence and Machine Learning applications (AI/ML) are fundamentally revolutionizing the drug development process, and therefore also the research in the field of peptides [47-48]. Several AI tools and platforms can be involved in different stages of this process. Keep in mind that the *de novo* design of antimicrobial peptides is a complex task, and a multidisciplinary approach involving expertise in biology, chemistry, and bioinformatics is essential for success [49].

A completely different strategy to identify new sequences could be Phage Display technique. Phage display is a highly effective and robust technology used to identify ligands of biological targets, first reported by Smith in 1985 [50]. Phage display is a selection technique in which a library of peptide or protein variants is expressed on the outside of a phage virion (i.e. M13 phage), while the genetic material encoding each variant resides on the inside. This creates a physical linkage between each variant protein sequence and the DNA encoding it, which allows rapid partitioning based on binding affinity to a given target molecule (antibodies, enzymes, cell-surface receptors, etc.) by an *in vitro* selection process called panning. Rapidly, panning is carried out by incubating a library of phage-displayed peptides with the target, washing away the unbound phage, and eluting the specifically bound phage. The eluted phages are then amplified and taken through additional binding/amplification cycles to enrich the pool in favour of binding sequences. After 3–4 rounds, individual clones are characterized by DNA sequencing and binding assays. This technique allowed the discovery of several new peptide candidates [51].

Extracting and purifying natural antimicrobial peptides (AMPs) from animals and plants poses challenges. Recently, the application of genetic engineering technology for the

recombinant expression of AMPs has emerged as a significant development in their commercial production. Commonly, AMPs are expressed using either prokaryotic or eukaryotic systems. Prokaryotic expression offers advantages such as short expression periods, high quantity, and low cost, but challenges may arise during purification due to a lack of post-translational modification. On the other hand, eukaryotic expression is advantageous for its non-toxicity to host cells and simplified purification through extracellular expression. However, the drawbacks include a higher expression cost and longer expression periods [52].

E. coli expression is a widely used prokaryotic expression system in the field of genetic engineering to industrialize antimicrobial peptide production [53]. Yeast expression system could be used as well, with *Saccharomyces cerevisiae* and *Pichia pastoris* that are commonly used [54]. Both expression systems show negative and positive aspects at the same time, regarding expression efficiency, timing of procedures, expression cost and effects of non biological activity. In recent years, researchers have utilized transgenic technology to introduce antimicrobial peptide (AMP) genes into plants like corn and soybean [55]. Plants, as advanced eukaryotes, offer a suitable environment for expressing AMPs. However, only a few studies have focused on extracting AMPs from plants used as expression hosts, so the development of a fully functional expression system for producing AMPs in plants requires further investigation [56].

Another method for obtaining AMPs is the chemical synthesis in the laboratory using an automatic synthesizer. The chemical synthesis of peptides is well-developed, particularly solid-phase peptide synthesis (SPPS) technology described by Merrifield in 1963 [57]. The SPPS technology has undergone significant enhancements, playing a pivotal role in contemporary peptide production. This approach is based on coupling and deprotection of amino acid in a single reactor, leading to the development of automated peptide synthesizers. In comparison to recombinant technology, SPPS yields crude peptides that are more homogeneous, avoiding additional biological compounds. Furthermore, impurities in the final SPPS product are easily identifiable, primarily originating from incomplete or side reactions during the synthesis process, simplifying subsequent purification efforts [58]. Following the synthesis, techniques like mass spectrometry, nuclear magnetic resonance (NMR), and high-performance liquid chromatography (HPLC) assess the purity of the peptide.

PROCESS OF AMP-BASED DRUG DISCOVERY

Drug development is a complex, expensive and long lasting process that begins with the design, synthesis, and optimization of a therapeutic compound [59].

First, during an initial phase of development the antimicrobial compound is identified with different techniques and origins (as previously reported), i.e. of natural or synthetic origin. An important phase of the development is the establishment and the scale-up of the manufacturing process. In preclinical phase, several *in vitro* tests are performed to study different aspects of the molecule, including physiochemical properties, potency/cellular activity (e.g. based on minimum inhibitory concentration and minimum bactericidal concentration), mechanism of action, efficacy and toxicity (especially in human cell lines), mechanism of resistance, genotoxicity and interaction. An identified molecule can undergo an optimization process aimed at improving some aspects, such as affinity for the target, efficacy or toxicity. Then, an *in vivo* model in different animal species must be set up in order to evaluate the safety and efficacy of potential drug candidates. This is accomplished using relevant animal models and validated procedures. The ultimate goal is to translate the animal model responses into an understanding of the risk for human subjects. To this end, the toxicologist must be aware of the international guidelines for safety evaluation in humans. The typical toxicology profile consists of safety pharmacology, genetic toxicology, acute and subchronic toxicology, chronic toxicology, absorption, distribution, metabolism, and excretion (ADME) studies, reproductive and developmental toxicology, and an evaluation of carcinogenic potential [60-61].

In clinical phase I, tolerability and potential dosing is assessed in a small number of healthy volunteers. In clinical phase II, a study with a small group of volunteer patients who have the disease is conducted to prove the positive impact on the disease. In clinical phase III, the medicine is tested in large, randomized, placebo-controlled trials with larger numbers of patient volunteers to confirm the efficacy and safety profile by generating statistically significant data. The clinical trials from all phases deliver the data required to prepare submissions for regulatory approval to agencies around the world. Teams of various disciplines (e.g. scientists, physicians, pharmacologists) need to work together until a new biopharmaceutical is finally developed and approved by the regulatory agencies (e.g. EMA, European Medicines Agency; FDA, U.S. Food and Drug Administration) to be delivered to the patients [62-63].

Timings are dependent on a number of factors and can vary greatly. A minimum to maximum range for complete development (discovery to market) is 8–18 years (average 13–14 years). The cost per molecule/candidate (in million euros, m€) does not include extended costs for attrition (failed programmes) and lost opportunities associated with increased cycle time until reaching the next development phase; such extensions can increase the required budget for the early stages up to 50–100 m€ [64] (Figure 4).

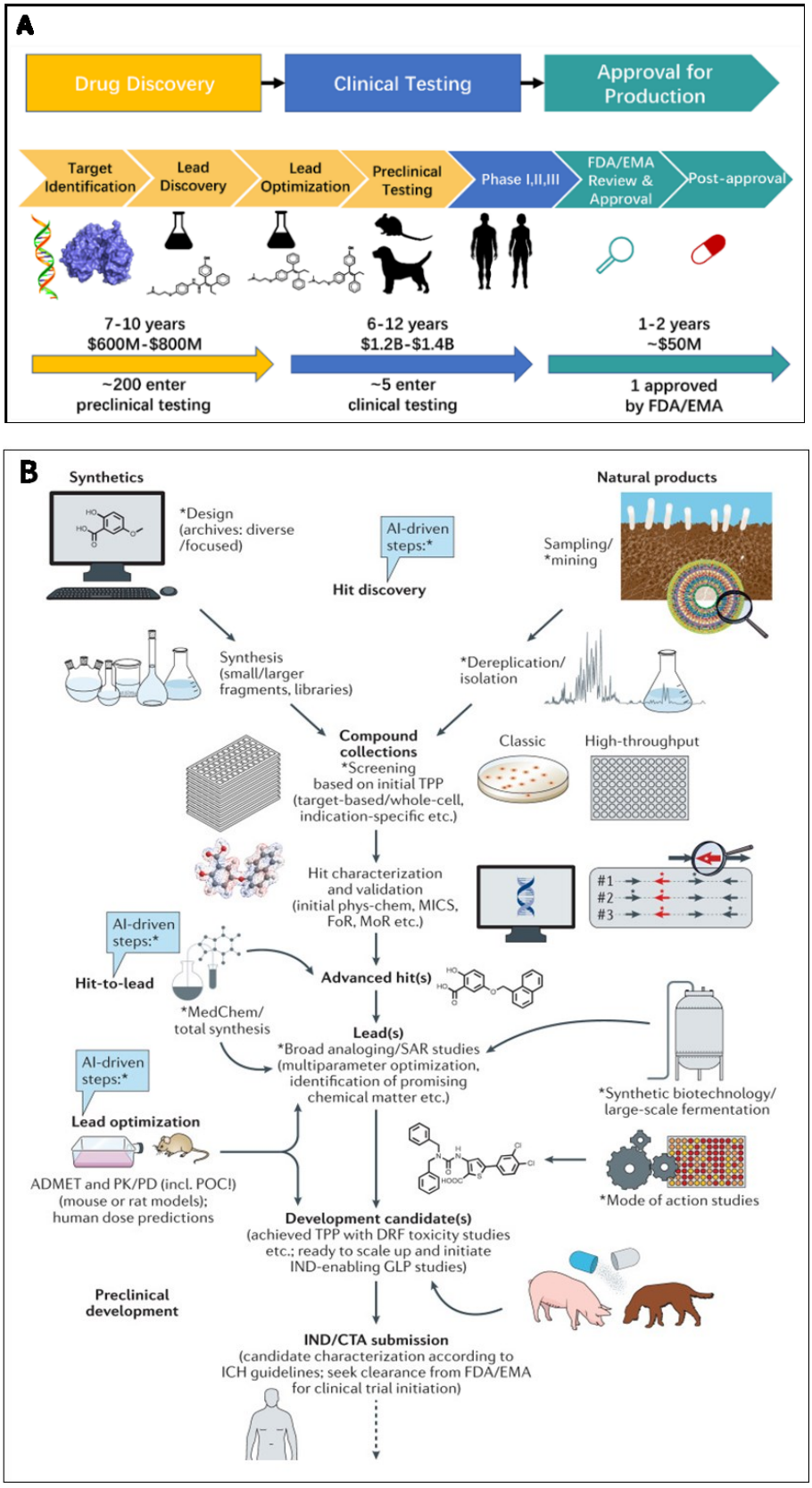

Figure 4. *(A) General scheme of the pipeline of antimicrobial drug development. (B) Summary of major steps and processes in antibacterial drug discovery and development.*

PEPTIDES IN PHARMACEUTICAL INDUSTRY

Peptide drugs account about 5-6% of the global pharmaceutical market, with an impressive global sales reported in the recently updated "*Global Peptide Therapeutics Market (by Type, Synthesis Technology, Manufacturing Type, Application & Region): Insights & Forecast with Potential Impact of COVID-19 (2022-2026)*" (https://www.researchandmarkets.com/). The global peptide therapeutics market is expected to record a value of US $44.43 billion in 2026, progressing at a compound annual growth rate (CAGR) of 6.95%, over the period 2022-2026 (Figure 5A). To further confirm these data, the "*Peptide Therapeutics Market By Application, By Route of administration, By Distribution Channel: Global Opportunity Analysis and Industry Forecast, 2021-2031*" (https://www.researchandmarkets.com/) reported that the peptide therapeutics market is estimated to reach US $64.3 billion by 2031, growing at a CAGR of 6.8% from 2022 to 2031 (Figure 5B). The fastest growing regional market is North America due to increasing research and development activities for the development of innovative peptide therapeutics and improvements in healthcare infrastructure coupled with growing prescription of peptide therapeutics on account of high presence of a large number of patients with chronic diseases such as diabetes and cancer. The global peptide therapeutics market is led by international companies, including Takeda Pharmaceutical, Pzifer, Merk & Co., Eli Lilly and Company, Sanofi S.A., AstraZeneca plc, GlaxoSmithKline (GSK). Over the years the demand for peptide therapeutics has increased significantly, leading to more than 100 peptide-based drug approval (Figure 5C). They have different therapeutic indications such as oncology, anti-inflammatory, autoimmune, metabolic and antimicrobial as well (Figure 5D). The latter could represent promising new antibiotics or a valid support to the traditional antibiotic therapy [65-67].

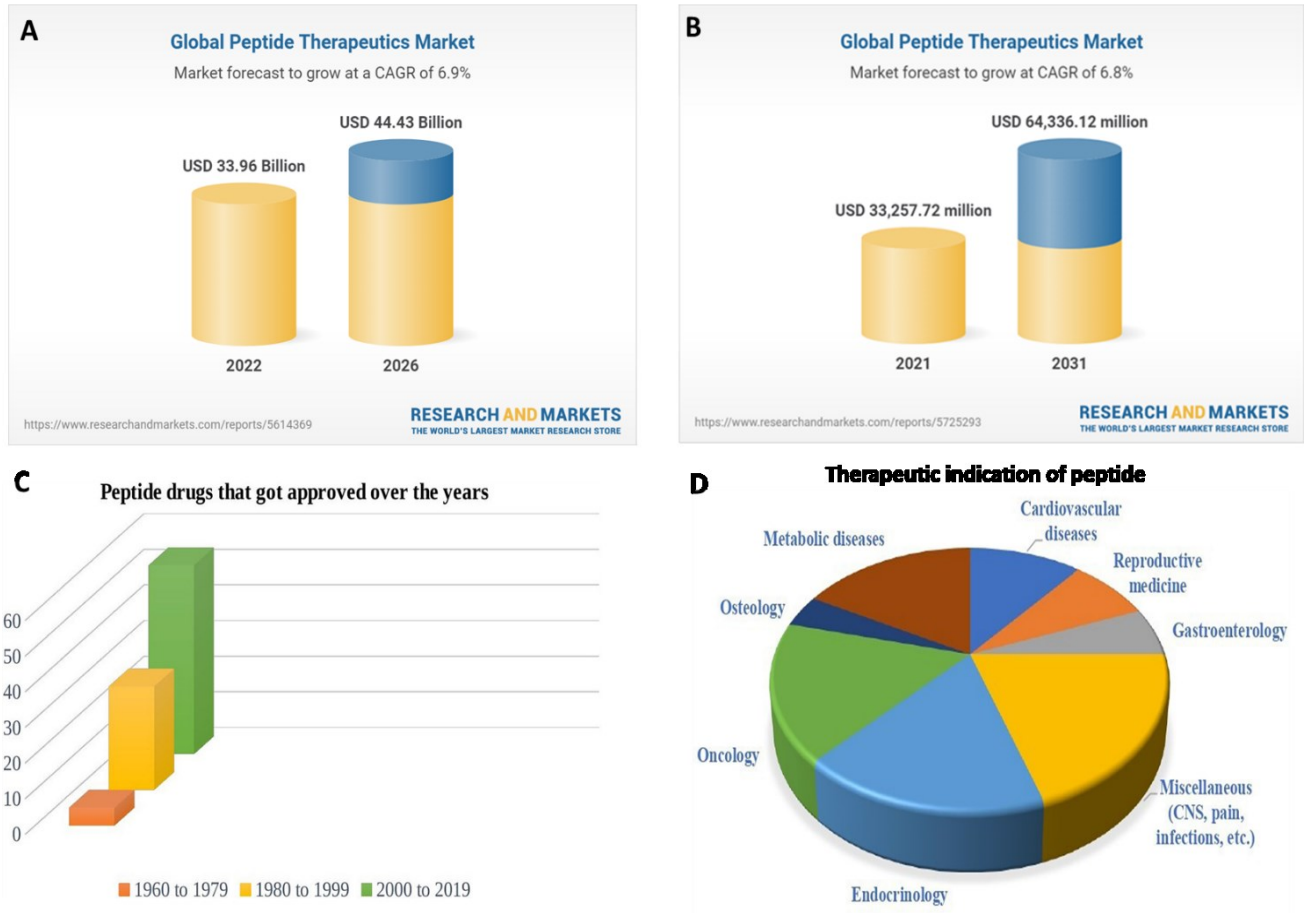

Figure 5. *(A) Global Peptide Therapeutics Market, 2022-2026. (B) Global Peptide Therapeutics Market, 2021-2031. (C) Peptide drugs that have gained approval over the years [67] (D) Indications for which peptide drugs are most commonly used [67]*

APPROVED THERAPEUTIC AMPs IN MARKET

Bacitracin is a group of cyclic polypeptides produced by organisms of the licheniformis group of *Bacillus subtilis*. It has antimicrobial activity against many Gram-positive bacteria, including staphylococci, streptococci and clostridia, and was approved by FDA in 1948 [68]. It is applied topically to treat local infections, mainly infections of the skin, ear and eye.

Colistin (**Polymyxin E**) and **Polymyxin B** (**PMB**) belong to the Polymyxin class and they are lipopeptide antibiotics with activity against many Gram-negative bacteria. The polymyxins were approved for clinical use in the late 1950s but fell out of favour during the mid-1970s owing to concerns over their potential to cause nephrotoxicity and neurotoxicity [69]. Over time they have undergone many modifications, with new approvals from the FDA (i.e. colistimethate sodium, a form of colistin, was approved in 1999), not least the interest

in the conjugation of this class of molecules with already known antibiotics (i.e. the clinical trial for the combination of colistin and rifampicin administered i.v. [70])

Daptomycin is a lipopeptide isolated in the 1980s with impressive activity against Gram-positive, but not Gram-negative, bacteria [71]. It received approval from the US FDA in 2003 and it is currently widely used for *Staphylococcus* spp. and *Enterococcus* spp. infections [72].

Vancomycin is a tryciclic glycopeptide with an antibacterial effect against Gram-positive bacteria, includind methicillin-resistant strain of *S. aureus*, by inhibiting the synthesis of the peptidoglycan layer of the bacterial cell wall. It was first approved for use in the United States in 1958 and it continues to be widely used, particularly with the recent rise in incidence of serious MRSA infections [73].

Dalbavancin, Oritavancin and Telavancin are small lipoglycopeptide derived from vancomycin. They are more potent and bactericidal than their prototype, and they are effective against vancomycin-resistant bacteria. They inhibit bacterial cell wall formation, and telavancin and oritavancin also disrupt bacterial cell membranes and affect membrane permeability. They were approved by the FDA between 2009 and 2014 [74].

Teicoplanin is a glycopeptide produced by *Actinoplanes teichomiceticus* that is effective against Gram-positive bacteria resistant to β-lactam antibiotics. It has been used clinically for the treatment of methicillin-resistant *Staphylococcus aureus* (MRSA) infections. Teicoplanin is currently not approved by the FDA for use in the USA but is widely used in Europe, Asia and South America. Some recent studies documented its activity against SARS-CoV2, reporting that teicoplanin could become a drug of choice in the treatment of COVID-19 patients. Teicoplanin stops the replication of the virus and at the same time avoids the development of Gram-positive bacterial co-infections [75].

Gramicidin, derived from the soil bacteria *Bacillus brevis*, is active against most of the Gram-positive and few Gram-negative bacteria and fungi. It is often formulated with other active ingredients in topical creams, lotions and powders, topical and ophthalmic ointments and ophthalmic and otic solutions. Gramicidin is unsuitable for systemic use due to its toxicity [76].

AMPs IN CLINICAL DEVELOPMENT

As for many other classes of drugs, the number of AMPs entering in clinical trials is significantly lower than the total number of compounds initially identified, and the percentage of those receiving marketing approval is even lower. The image with which the drug discovery process is classically represented is a funnel, which gives a good idea of the number of molecules which decreases as the phases progress. So, many AMPs result under clinical trials for the prevention and the treatment of many infections.

The landscape of drug development is dynamic, and the status of specific compounds is constantly evolving. For the latest information on AMPs in clinical phases, including their current development status, it is recommended to check the updated clinical trial databases. However, the information about some peptides could not be obtained because the licences were transferred to other companies or the preclinical or clinical trials were discontinued for unknown reasons.

Just a short description of some AMPs currently in clinical trials is presented below.

hLF1-11 is a short synthetic peptide derived from the N-terminal region of human lactoferrin, an antimicrobial protein found in human milk and other bodily fluids. Interestingly, hLF1-11 shows poor antimicrobial activity under physiological conditions *in vitro*, but *in vivo* activity against bacteria (both gram positive and negative) and fungi is highly effective, including infections caused by methicillin-resistant *S. aureus* (MRSA), *K. pneumoniae*, and *Listeria monocytogenes*. hLF1-11 also exhibits an immunomodulatory mechanism, such as stimulation of monocyte differentiation and release of pro-inflammatory cytokines [77]

EA-230 is a newly developed synthetic linear tetrapeptide derived from human chorionic gonadotropin. EA-230 exerted immunomodulatory and renoprotective effects in preclinical models [78] and its safety and efficacy was demonstrated in phase I and II clinical trials [79].

The specifically targeted antimicrobial peptide (STAMP) **C16G2** was developed to target the cariogenic oral pathogen *Streptococcus ssp* mutants [80]. *Streptococcus ssp* mutants are believed to be a critical factor in the cause of dental caries or tooth decay. C16G2 is being developed for the prevention of dental caries in adults, adolescents and pediatrics. C3 Jian, Inc., a biotechnology company focused on reengineering the human microbiome to deliver novel health-care products, started the Phase II clinical study, that is a randomised, double-blind, safety and microbiology study in healthy adult subjects, with a preliminary data announced in 2015 [81].

NP213 (Novexatin®) is a novel antifungal peptide specifically designed for the topical treatment of onychomycosis. NP213 was designed using host defense peptides (HDP), essential components of the innate immune response to infection, as a template. NP213 was efficacious in two phase IIa human trials, confirming it as a promising peptide-based candidate for the topical treatment fungal infection of the skin [82].

Dusquetide (SGX942) is a first-in-class Innate Defense Regulator (IDR) that modulates the innate immune response to both PAMPs and DAMPs by binding to p62, a key adaptor protein that functions downstream to the key sensing receptors (e.g., toll-like receptors [TLRs], etc.) that trigger innate immune activation. There are no other candidates that target the p62 protein [83]. A phase III clinical trial sponsored by Soligenix Inc. for the treatment of the oral mucositis, a side effect of treatment of squamous cell carcinoma of the oral cavity, is ongoing [84].

Omiganan (CLS001) is an AMP that is analogous to indolicidin, a bovine member of the cathelicidin family. It showed antibacterial and antifungal activity throughout a range of preclinical and clinical studies, with a favourable safety profile. Although the phase IIIb trial for catheter-associated urinary tract infection caused by *S. aureus* failed [85], the phase III trial for the treatment of topical skin antisepsis and rosacea [86], as well as the phase II trial for vulvar intraepithelial neoplasia, acne, and atopic dermatitis are still ongoing [87].

Ramoplanin (NTI-851), sponsored by Nanotherapeutics, is a peptide produced by *Actinoplanes* spp. That exhibits bactericidal activity by blocking the cell wall peptidoglycan synthesis of gram-positive bacteria. It results in phase III clinical trials for the oral treatment of vancomycin-resistant enterococcus (VRE) infection and it is also in phase II clinical trials for the treatment of *C. difficile* [88].

CHALLENGE AND STRATEGY TOWARD CLINICAL APPLICATION OF AMPs

The progress of developing AMPs for clinical applications is confronted by numerous challenges, including elevated costs associated with both development and production, concerns related to reduced efficacy in clinically significant settings, and the unexpected emergence of bacterial resistance. Furthermore, AMPs are mainly active on membranes but

they are not completely selective to microbial cells and may be toxic for eukaryotic cells as well. Several AMPs cause haemolytic and/or cytotoxic effects at antimicrobial concentrations, limiting their wider utilization [89]. Another drawback for the clinical development of AMPs is the lower antimicrobial activity in clinically relevant environments [90]. AMPs may lose their bactericidal activity under physiological salt conditions due to loss of electrostatic interactions between AMPs and cell membranes. In the presence of serum, AMPs may bind to proteins such as albumin [91]. Additionally, AMPs can be susceptible to proteolytic degradation [92]. With the aim of overcoming some of these limitations, several strategies have been implemented to improve the performance of AMPs, in order to make them suitable for clinical use.

RESISTANCES TO AMPs

Different from traditional antibiotics, which perform a function by breaking the cell envelope, or interrupting DNA replication or protein synthesis process [93], some AMPs have been shown to possess multiple modes of action with non-specific targets and are less liable to develop resistance [94]. Meanwhile, some organisms can produce several different AMPs, which would also reduce the chance of resistance development [95]. For these and other reasons it was believed for a long time, and erroneously, that resistance to AMPs was very difficult to occur and that it therefore was not a big concern [96]. However, as several recent studies have shown, resistance to AMPs not only could be an intrinsic mechanism, but can also could be acquired or evolve at high rates (at least *in vitro*), generating mutants with, sometimes high, levels of resistance [97].

Intrinsic resistance to AMPs can be a passive or inducible mechanism. Passive AMP resistance occurs in some bacterial species including *Proteus*, *Morganella*, *Providencia*, *Serratia* and *Burkholderia* as a result of an inherently more positively charged lipid A that reduces AMP interaction. The induction of AMP-resistance in other bacteria is tightly regulated in response to environmental conditions and serves as a mechanism for bacterial survival in various natural environments in which they would experience the threat of AMPs [98]. Some of the mechanisms involved in the AMPs resistance [99-100], including proteolytic degradation, prevention of AMPs from targeting bacterial membrane by bacterial secreted proteins or outer membrane vesicles (OMVs) or capsule, activation of bacterial

efflux pump and decreased net anionic charge in cell envelope, are schematically represented in Figure 6 [101].

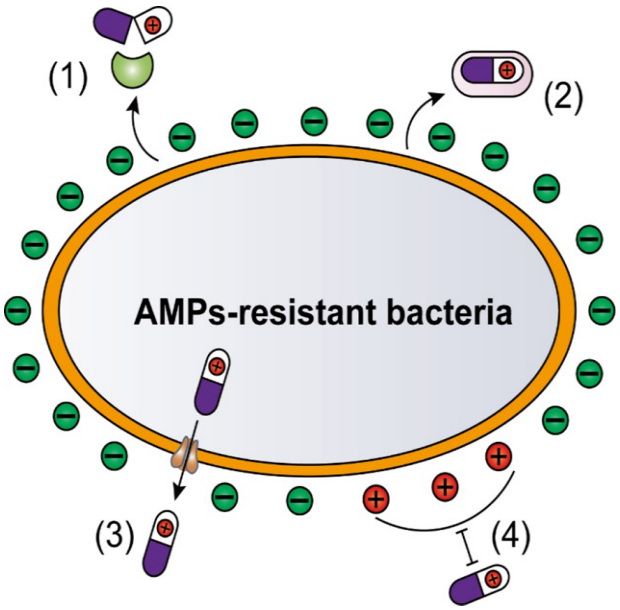

Figure 6. *Bacteria have evolved multiple strategies to antagonize the activity of AMPs, including the production of microbial proteases to hydrolyze AMPs (1), generation of specific proteins such as Staphylococcus aureus staphylokinase or outer membrane vesicles (OMVs) or capsule to prevent AMPs from targeting bacterial membrane (2), activation of efflux pump (3) and reduction of the net anionic charge of the bacterial cell envelope, thereby suppressing its affinity with AMPs (4) [101].*

As regards the acquired resistance, Liu *et al.* reported a case of resistance to AMPs due to a horizontal gene transfer in *E. coli* [102]. A plasmid containing the *mcr-1* gene was shown to mediate colistin resistance by encoding a phosphoethanolamine transferase that modifies lipid A reducing its negative charge. The reduced affinity between colistin and LPS anchored to the bacterial outer membrane decreases the colistin efficacy in the clinic practice [103]. The *mcr-1*-containing-plasmid was initially isolated in Chinese livestock animals, and since its initial characterization the *mcr-1* gene has been identified retroactively in 3 of 1267 human faecal microbiome samples taken from China prior to 2011 indicating animal to human gene transfer [104].

Hence, while most AMPs generally show a reduced likelihood of developing drug resistance in comparison to traditional antibiotics based on current understanding, it's important to stay vigilant against the potential development of resistance to AMPs within clinical and environmental settings.

CHEMICAL MODIFICATIONS

According to the relationship between structure and activity, the order, the position and the configuration of the amino acids play an important role in the biological activity of the peptide. Several chemical modifications are possible in order to improve some properties (i.e. antibacterial activity, permeability), to make AMPs more stable and, therefore, more suitable for an *in vivo* use. Some of the possible modifications are reported below.

PEGylation

The term PEGylation describes the modification of biological molecules by covalent conjugation with polyethylene glycol (PEG), a non-toxic, non-immunogenic polymer, and is used as a strategy to overcome some disadvantages associated with the molecule of interest [105]. The advantage of PEG residues is a very good solubility in both aqueous and organic environments, great flexibility, high hydration that increases its hydrodynamic volume, and a range of molecular weight species with low polydispersity. All of these properties are acquired by compounds to which PEG is covalently bound. Proteins conjugated with PEG exhibit increased solubility, become resistant to antibodies, proteolytic enzymes and cells, and, because of their increased size, are ultra-filtered by the kidneys more slowly [106]. So the PEGylation of AMPs enhance their overall pharmacodynamic properties. Starting from the introduction of the first PEGylated protein, Adagen®, in 1990, the increasing number of pegylated products on the market is increasing [107].

Lipidation

Another strategy to enhance the antimicrobial potency of AMPs without modifying to their properties is lipidation, that is the attachment of a portion of a fatty acid to N-terminal residues or lysine side chains. The incorporation of lipid tails of different lengths enhances the hydrophobicity of AMPs and confers better membrane interaction, better permeability, and protection against enzymatic proteolysis [108]. It is likely that the improved potency is correlated to the length of the acyl chain, which also influences their specificity and enhances the interactions between the bacterial cell membrane and the fatty acid conjugated on the peptide [109]. However, as acyl chains grow in length, there is an increased tendency for self-assembly in an aqueous solution, which determines a loss of peptide interaction with bacterial membranes. In addition, the length of the conjugated fatty acids may increase hydrophobicity, enhancing the selectivity toward mammalian cells with consequent toxicity. Thus, although the increase in the hydrophobicity of peptides can improve antimicrobial

activity, it is crucial to preserve the right hydrophilicity/hydrophobicity balance to avoid an increase in toxicity. Clearly, a well-chosen chain length is key to determining the balance between improved antibacterial properties and selectivity [110-111].

D amino acids

Natural AMPs are composed of L amino acids. Replacing L amino acids with their D stereoisomers results in peptides that are not recognized by naturally occurring proteases or immune system receptors, due to their spatial configuration, and this is one of the strategies used for overcoming the problem of biostability *in vivo* [112]. The natural amino acids in AMPs are easily recognized by the host proteolytic enzyme, resulting in peptide proteolysis. Introducing D amino acids at the site of the proteolytic cleavage will interfere with this recognition, thus avoiding peptide degradation [113]. Considering the resistance of degradation by proteases, the D amino acids substitution strategy is also employed to enhance the stability of the peptide. Furthermore, the isomerization of AMPs' amino acids broadens the antimicrobial spectrum to Gram-positive bacteria. The SET-M33 antimicrobial peptide was shown to be very active against Gram-negative bacteria. The isomeric version synthetized with D amino acids showed 4 to 16-fold higher activity against Gram-positive pathogens, including *S. aureus* and *Staphylococcus epidermidis*, than the peptide with L amino acids. The antimicrobial activity of both isoforms of peptide is influenced by their differential sensitivity to bacterial proteases [114-115]. A paragraph dedicated to the antimicrobial peptide, object of this thesis, is reported below.

Branched AMPs

As already mentioned before, the use of peptides as therapeutic agents has been partially limited by their short half-life *in vivo*. Because peptides are mainly broken down by proteases and peptidases, peptide stability is the bottleneck in the development of new peptide-based drugs. The concept of Multiple Antigen Peptide (MAP) is referred to a synthesis of bioactive peptides in a branched form where a peptidyl core of radially branched lysine residues binds covalently more copies of the linear sequence of the peptide. In this way, one lysine could allow synthesis of two-branched peptide, three lysines could give rise to a tetra-branched peptide and so on (Figure 7).

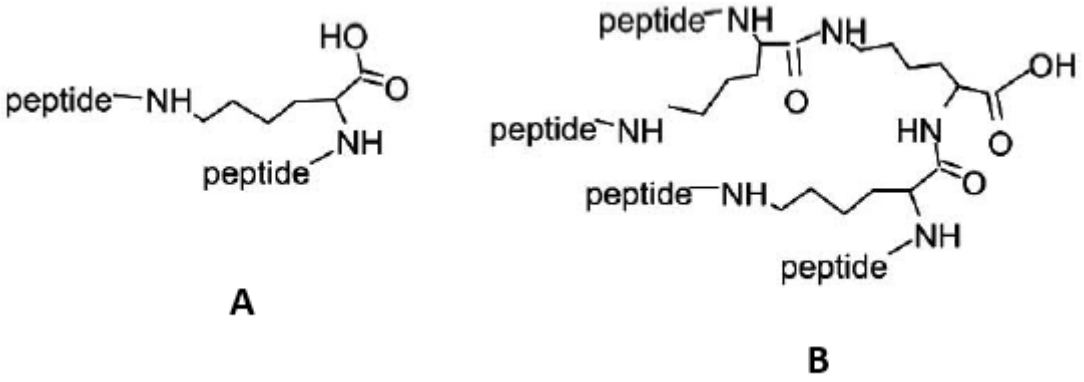

Figure 7. *General structure of A) two-branched peptide synthesized on a one lysine scaffold, and B) tetra-branched peptide synthesized on a three lysine scaffold [117]*

The solid phase synthesis of branched peptides was first described by Tam in the 80s [116] and it is based on the concept of using trifunctional amino acids to construct branched peptide-based molecules that he named MAP. The first idea was to use these molecules to obtain synthetic vaccines, even if different applications followed this first application. It is now widely known that bioactive peptides become more resistant to the proteolytic activity of plasma and serum enzymes when synthetized in a MAP form. Furthermore, peptide biological activity can even be enhanced by multimeric binding. Monomeric peptides are cleaved very rapidly by peptidases that cut them into inactive peptides. This is the mechanism by which they are inactivated. Peptidases acting on small peptides are mainly Zn metallopeptidases and their catalytic site is located in a deep channel to which only small peptides have access. The steric hindrance of branched peptides may limit their access to the cleavage site, lengthening the peptide half-life, with clear advantages for their use as drug. In addition, the *in vitro* and *in vivo* enhanced efficacy of branched peptides is generally ascribed to their multimeric nature, which provides a greater number of interactions compared to the corresponding monomeric form [114; 117-118].

TOXICITY OF AMPs

Toxicity, together with instability and short half-life *in vivo*, is one of the major challenges that need to be overcome for the application of AMPs in clinical usage. *In vitro* and *in vivo* toxicity evaluation is an essential step in the development of potential new drugs [119]. Several tests and indices are required in both *in vitro* and *in vivo* to study and determine the

level of toxicity of AMP. Among these, the EC_{50} value is the peptide concentration causing the 50% of cell death *in vitro*, or LD_{50} is the dose required to kill half the animal in an *in vivo* experiment [120].

One of the most effects caused by AMPs is haemolysis. The main theory used to explain the haemolysis mechanism postulates that the cationic and amphiphilic structures of AMPs are the basis for their haemolytic effect, with an additional influence of peptide length, special amino acids and helicity of the peptide chain. Similar to the membrane-breaking of pathogens, natural AMPs with cationic charges can interact with negative ions on the surface of the erythrocyte membrane, and then form oligomers to destroy cells [121-122]. Just for the reason that the antimicrobial mechanism also determines a certain level of toxicity, the therapeutic window of many AMPs is particularly narrow. In order to overcome this issue, many strategies have been adopted. In the following section one the strategy based on the encapsulation of AMPs into biocompatible nanocarriers are detailed, with the aim to reduce the toxicity maintaining the efficacy.

Another well-known adverse effect of AMPs is its renal toxicity *in vivo*. The nephrotoxicity of peptides already used in clinics, such as Vancomycin [123] or Polymyxin [124], is widely reported in the literature. Acute kidney injury (AKI) occurs in up to 50%-60% of patients receiving Polymyxin and this aspect is the major dose-limiting adverse effect of the polymyxins [125]. The plasma concentration of peptide associated with increased risk of AKI overlaps those required for antibacterial effect, and therefore, the therapeutic window is narrow. [126] From studies conducted in cell lines and *in vivo* preclinical models, it is clear that the AMPs in general have the potential to be toxic to renal tubular cells. The cellular mechanisms involved include oxidative stress, apoptosis (via mitochondrial, death receptor, and endoplasmic reticulum pathways), cell cycle arrest, and autophagy [127-129]. The presentation of data relating to the safety pharmacology of the antimicrobial peptide SET-M33 is precisely the topic of this thesis which, in line with what has just been said and with many other AMPs, shows a certain level of nephrotoxicity in different animal models [130-131].

CHALLENGE AND STRATEGY IN AMPs-BASED DRUG DELIVERY

Antibiotics are commonly administered through systemic routes due to the advantage of reaching broadly distributed pathogenic bacteria. As an alternative, they could be locally administered, especially when achieving a high drug concentration at the infection site is critical. Local antimicrobial treatment has recently gained increasing attention, owing largely to its benefit of minimizing drug systemic exposure and potentially reducing resistance development [132]. As a result, a variety of biomaterials and medical devices have been custom-designed to enable the localized administration of antibiotics. This customization enhances the feasibility and preference for local treatment in addressing diverse infections. [133]. Despite the progress that has been made, the local antimicrobial delivery approach still faces various complications, including the drug clearance mechanisms upon administration and the diffusion barriers within the local environment that preclude drug molecules from reaching bacteria. Last but not least, the local toxicity of some compounds that cause adverse effects following administration of the drug. All these aspects reduce the therapeutic efficacy of an antimicrobial molecule [134].

This scenario is even more complicated in patients affected by some pathologies, like cystic fibrosis (CF) (Figure 8) [133]. CF is one the more common life-shortening genetic disorders of Caucasians caused by mutations in the CF transmembrane conductance regulator (CFTR). CFTR is expressed in epithelia throughout the body, and affects secretory functions in a number of organs, including the lungs, liver, gut and sweat glands. In the lungs, defective CFTR reduces the epithelium sodium channel (ENaC) function leading to an altered fluid and electrolyte composition of airway secretions [135]. This condition predisposes CF patients to recurrent/persistent bacterial infections and neutrophil-dominated endobronchial chronic inflammation, which are still considered the primary cause of bronchiectasis, respiratory failure and consequent death in patients affected by CF [136]. The use of AMPs in lung infections, when administered by aerosol, can be impaired by mucus and other pathological factors generally present in bronchi and lungs infected by bacterial pathogens. In fact, important determinants of the clinical outcomes of inhaled medicines are the concentration/persistency of the drug at lung level, as well as the ability to overcome airway extracellular and cellular barriers [137]. Indeed, while the mucus barrier may strongly limit the amount of drug reaching the target, the way to the target is even more complicated for inhaled antimicrobial agents due to the biofilm-like mode of growth adopted

by some bacteria. Thus, optimal inhalable formulations should be able not only to deliver the intact drug in lung, but also to shield its interactions with lung environment [138]. For these reasons, there is a current need to improve the biopharmaceutical properties of existing compounds. Recent advanced in nanotechnology, particularly the design of novel nanoparticles (NPs) as controlled drug delivery system, have supposed a promising alternative impact in the general medicine, specifically in the antimicrobial therapy [139].

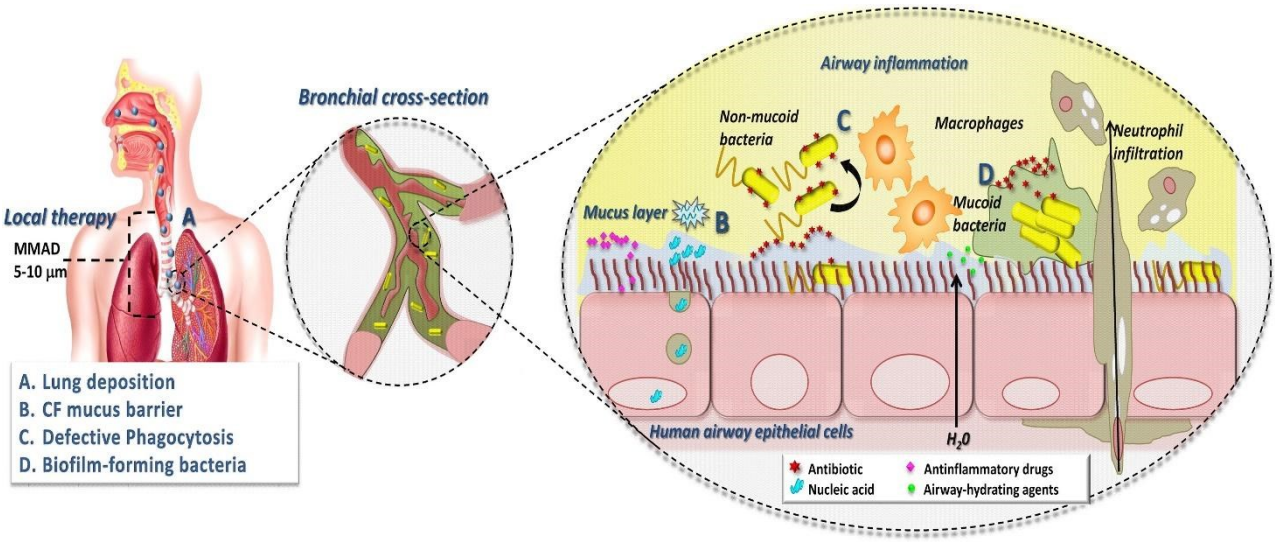

Figure 8. *Anatomical/biological barriers imposed by CF lung to the most widely investigated inhaled drugs [133].*

NANOPARTICLES

Nanomedicine represents a well-known approach initially related to the development of nanomaterials with particular therapeutic properties [139-140]. Further investigation of nanotechnology in pharmaceutical application results in an important improvement of drug delivery system.

NPs, a controlled drug delivery system with a diameter of 1-1000 nanometers (nm) and a polymeric core, may offer remarkable improvements in the biopharmaceutical properties of antibacterial agents. Notably, they can provide an enhancement of drug solubility, modulation of drug release and delivery, promotion of stealth for immune evasion, targeting of antibacterial molecules to desired organs and tissues and increase the retention time in-situ, as well as the simultaneous delivery of multiple drugs [141].

NPs can be characterized on the basis of the size, the morphology and the surface properties. The size and morphology are predominantly investigated using microscopic technique like atomic force microscopy (AFM) scanning electron microscopy (SEM) and transmission electron microscopy (TEM). As regards the surface properties, hydrophobicity and surface charge are two of the main important surface properties of nanoparticles [142]. Zeta potential (ζ) represents an analytical technique used for the determination of surface charge of NPs in colloidal solutions. Normally zeta potential values are in the range of +100 mV to -100 mV. Knowing the magnitude of zeta potential represents a useful information of the colloidal stability and to predict the particles behaviour. It was reported that zeta potential with values >30 mV indicates stability, while with a value <30 mV the particles are subjected to agglomeration or instability [143].

NPs are also classified in polymeric, inorganic and lipid-based. Each class of nanoparticle includes multiple subclasses. Each class has numerous broad advantages and disadvantages regarding cargo, delivery and patient response, schematically represented in Figure 9 [144].

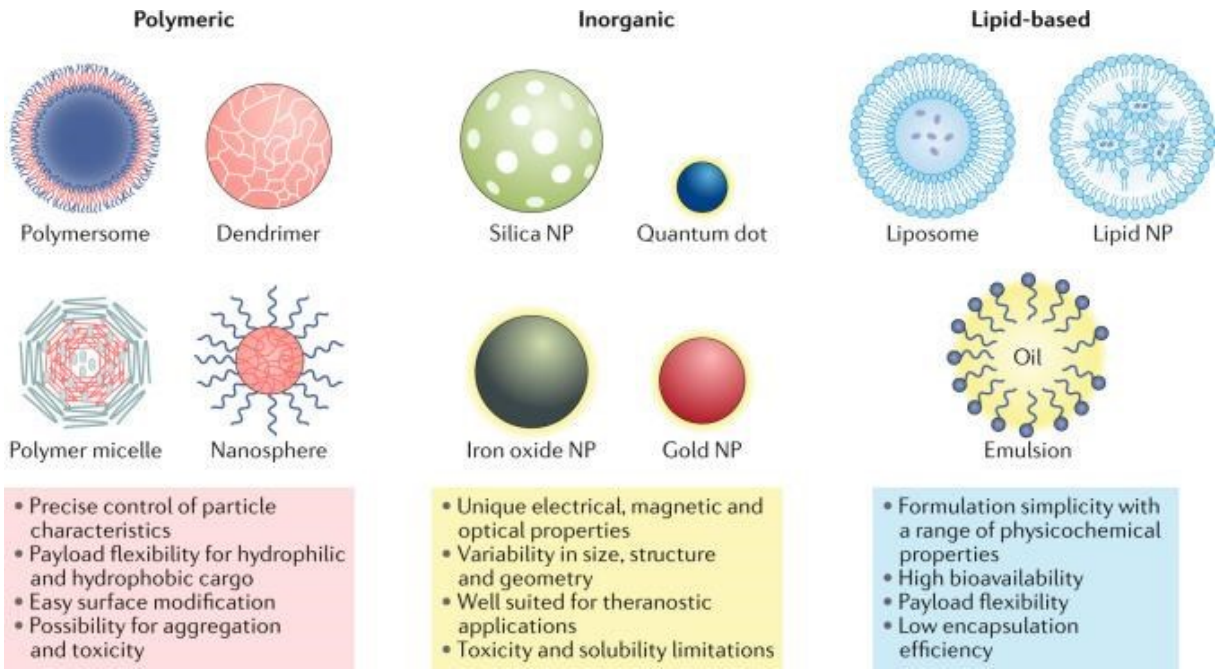

Figure 9. *Classes of NPs. Each class of nanoparticle (NP) features multiple subclasses, with some of the most common highlighted here. Each class has numerous broad advantages and disadvantages regarding cargo, delivery and patient response [144].*

Lipid-based NPs are most typically spherical platforms comprising at least one lipid bilayer enveloping at least one internal aqueous compartment and include various subset structures. As a delivery system, lipid-based NPs provide some advantages including formulation simplicity, self-assembly, biocompatibility, high bioavailability, the possibility to control various physicochemical properties to modulate their biological characteristics. For these reasons, lipid-based NPs are the most common class of nanomedicines approved by FDA [145]. Oncology is the field in which this type of delivery system is most used. VYXEOS, for example, is a liposomal drug marked by Jazz Pharmaceutical approved by FDA in 2017 for the treatment of adults with two types of acute myeloid leukemia (AML) [146].
Inorganic materials such as gold, iron and silica have been used to synthesize nanostructured materials for various drug delivery and imaging applications. These inorganic NPs are precisely formulated and can be engineered to have a wide variety of sizes, structures and geometries. Gold NPs (AuNPs) are the most well studied, but iron oxide NPs represent the majority of FDA-approved inorganic nanomedicines. They are predominantly used in iron-replacement nanoparticle therapies, like Injectafer® approved by FDA in 2013 for the intravenously treatment of Iron Deficiency Anemia (IDA) [145].
For the polymeric NPs, several biodegradable polymers, including poly(lactic acid) (PLA), poly(lactic-co-glycolic acid) (PLGA), poly(caprolactone) (PCL), and poly(cyanoacrylate) (PCA) have been used for the hydrophobic core of the polymers [147]. Nowadays, poly(lactic-co-glycolic acid) (PLGA) is the most used polymer, an aliphatic polymer with a polyester structure that is formed by copolymerization of polylactic acid (PLA) and polyglycolic acid (PGA). PLGA has several interesting properties such as controlled and sustained release, low cytotoxicity, long-standing biomedical applications, biocompatibility with tissues and cells, prolonged residence time and targeted delivery [148]. Because of these characteristics, it received approval from the US Food and Drug Administration (FDA) as well as the European Medicines Quality Agency (EMA) as a superior drug carrier [149]. The polymers are available with different molecular weight and copolymer compositions. The degradation time usually depends on the molecular weight and copolymer ratio. It is possible to obtain different forms of PLGA by using different ratio of monomers, for example, PLGA 50:50 corresponds to a copolymer in which the composition is 50% lactic acid and 50% glycolic acid. PLGA nanoparticles can be prepared by different methods of preparation, like emulsification-diffusion, solvent emulsion-evaporation and nanoprecipitation method [148].

To be used as a drug delivery system, the NPs must persist in the human body avoiding the degradation. The particles are recognized from the body as foreign. The presence of the reticuloendothelial system (RES) determines the elimination of these particles from the bloodstream and takes them into the liver or the spleen. In particular, the binding of opsonin proteins to nanoparticles leads to attachment of opsonized particles to macrophages and consequently to their internalization by phagocytosis. In order to overcome these limitations, nanoparticles have to be not recognizable from the RES through surface modifications. To this purpose, nanoparticles can be coated by molecules that provide them a hydrophilic layer at the surface. The most common strategy for surface modification is the use of polyethylene glycol (PEG) which is a non-ionic, hydrophilic polymer whit excellent biocompatibility. Investigations have been proved that the "PEGylation" increases nanoparticles plasma half-life [150-151].

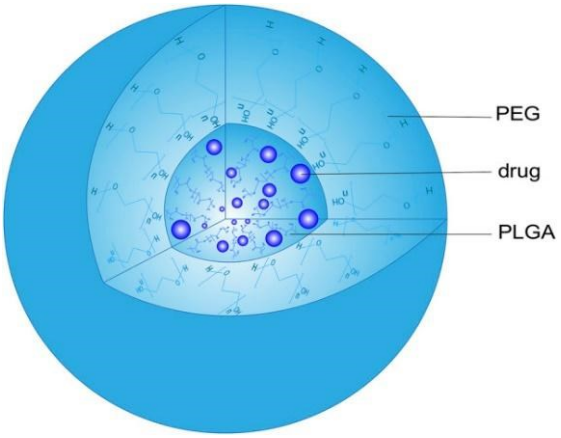

Figure 10. *Structure of a PEG-PLGA nanoparticle. PEG, polyethylene glycol; PLGA, poly (lactic acid-co-glycolic acid) [151].*

PULMONARY DELIVERY OF NANOPARTICLES

The administration of drugs through the inhalation route is highly recommended for the treatment of pulmonary infection, in particular in dangerous lung condition called chronic obstructive pulmonary disease (COPD) or in CF-affected patients [149]. The systemic treatment of a lung disease mainly uses antibiotics, anti-inflammatory, antioxidant, and corticosteroid drugs, but the process of application requires higher doses and caused serious adverse effects [152]. The main advantages of inhaled drugs are the high drug levels in airways, limited systemic toxicity, fast onset of action, no drug inactivation before reaching

the target organ, direct drug activation on target site and the possibility of a home therapy [133]. However, the drug inhalation has some disadvantages, like uncertainty about the drug dose that reached target side, some local side effects and the risk of microbial contamination of the inhaler as a consequent of a wrong cleaning procedure [153]. Considering all these aspects, nanoparticles represent an excellent delivery system for aerosols [154]. Inhalable particles need to find out a delicate balance, being small enough for lung deposition yet sufficiently large for the effective dosage form delivery while avoiding clearance by macrophages. The 1-2μm size allows macrophages to efficiently phagocytose, but particles smaller than 200 nm are taken up less effectively. Although particles below 1 μm are typically exhaled upon inhalation, an engineered nano-sized carriers hold promise for precisely targeting drugs to specific lung tissues, offering a potential opportunity for more effective penetration of extracellular barriers [133; 154-155].

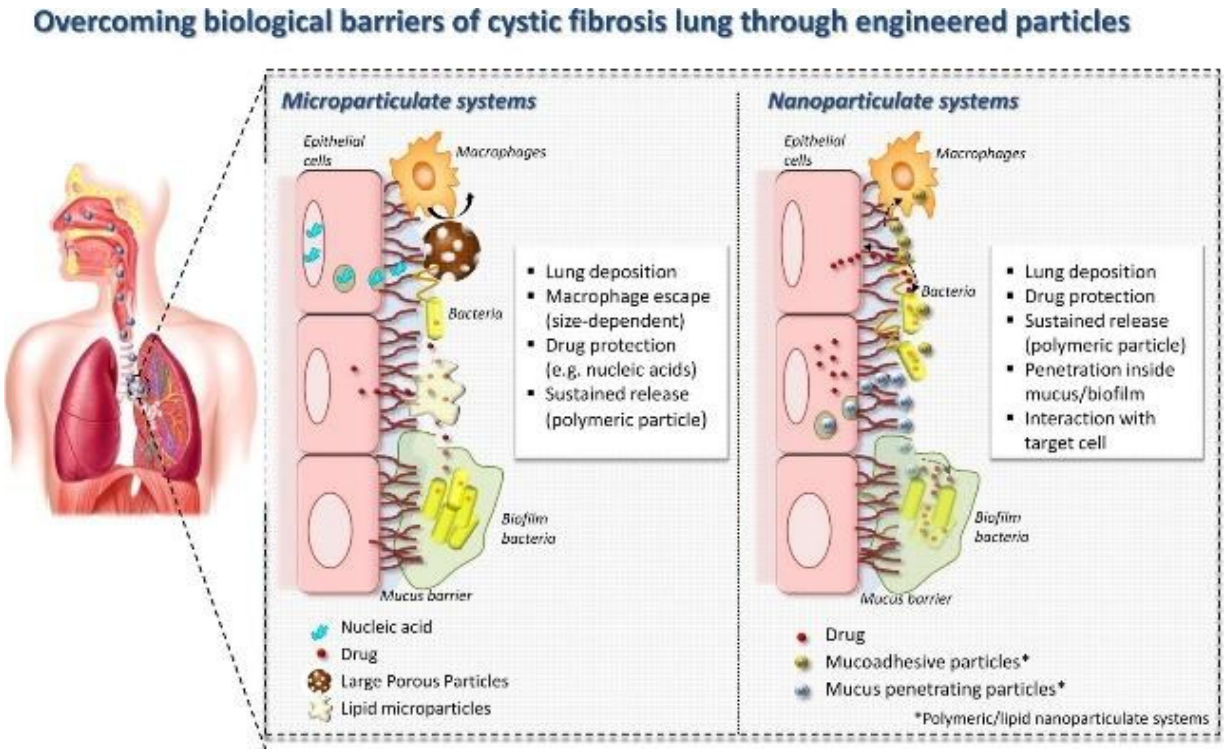

Figure 11. *Inhalable drug-loaded particles engineered for a pulmonary delivery [133].*

NANOPARTICLES FOR AMPs DELIVERY

NPs have been widely investigated for the delivery of various antimicrobial agents, like AMPs, and efficacy in treating different types of infections has been reported [156]. Different strategies by which NPs can improve antibacterial therapy efficacy have already been described [157-158]. Current advanced in the use of inorganic nanoparticles for AMPs delivery involve essentially the development of silver nanoparticles (AgNPs) and gold nanoparticles (AuNPs), as well as silicon derivates nano-system [156; 159]. Teixeira *et al.* detailed the recent studies on inorganic NPs for AMPs delivery [156]. Among these, the photoluminescent gold nanodots (AuND) were functionalized with an antimicrobial peptide, surfactin (SFT), for application in wound infection treatment [160]. Salouti *et al.* reported the synergistic antibacterial effect of plant peptide MBP-1 and AgNPs on infected wounds caused by *S. aureus* [161].

Besides, the development of polymeric nanoparticles for AMPs delivery could offer an excellent technological strategy to improve drug bioavailability and safety, avoiding drug chemical end enzymatic degradation, prevent aggregation, enhancing controlled release. Chitosan NPs (CS-NPs) are particularly interesting as the broad spectrum of antibacterial activity of Chitosan (CS) is well known and reported in literature, offering the possibility of synergistic activity with an antimicrobial molecule like an AMP [162]. Many recent studies report the use of CS-based nanostructures as a promising delivery system of AMPs.

Piras *et al.* reported two studies, one about the development of a nanoparticle model with commercially available CS loaded with lysozyme as an antimicrobial protein drug model [163]; in the other one evidenced the antibacterial action against several strains of *S. epidermidis* of a CS-nanocarrier with Temporin B [164]. Cerchiara *et al.* studied a CS-based nanoparticle for colon delivery of Vancomycin with an antibacterial activity against *S. aureus* [165]. D'Angelo *et al.* designed and developed a poly(lactic-co-glycolic acid) (PLGA) nanoparticles containing colistin (Col), by emulsion/solvent diffusion technique. The Col-loaded NPs were found to kill *P. aeruginosa* biofilm and to display a prolonged efficacy in biofilm eradication compared to the free Col, in a model of lung infection [166]. The same nanocarrier system is used for the encapsulation of two other antimicrobial peptides derived by frog skin, Esculentin-1a and its derivate [167]. The prolonged efficacy against bacterial infections caused by *P. aeruginosa* was demonstrated both *in vitro* and *in vivo* studies,

highlighting this system as promising therapeutic approach for local treatment of lung infectious diseases [168].

THE ANTIMICROBIAL PEPTIDE SET-M33

The antimicrobial peptide SET-M33 is a synthetic molecule obtained several years ago by improving a phage library-derived peptide [169]. A 10-mer peptide phage library was panned against entire *E. coli* cells, selecting a non-natural sequence that showed high antimicrobial activity against Gram-negative bacteria [170]. The best peptide variant was obtained through several optimization (KKIRVRLSA) and it is synthesized in the branched form, in which four identical peptide sequences were synthesized and linked by a lysine core (Figure 12). It showed an increased resistance to proteases, improving half-life with respect to corresponding monomeric sequences [117; 171].

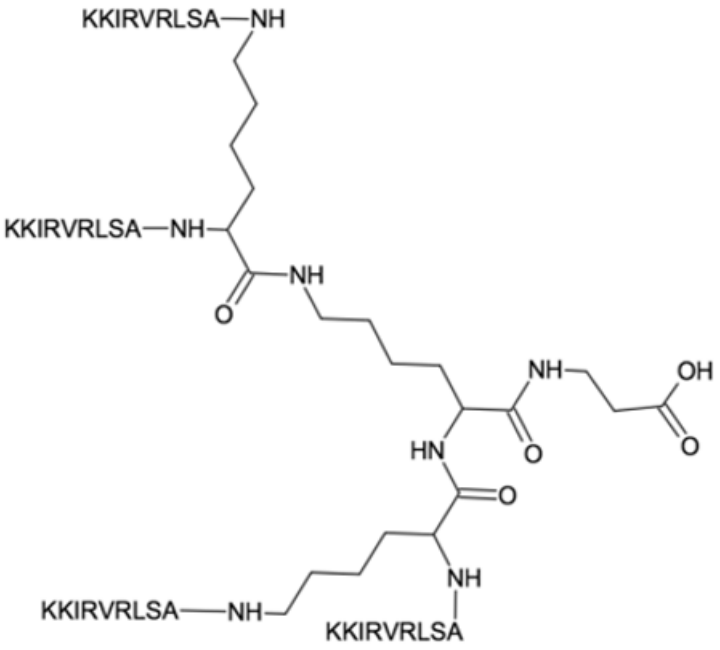

Figure 12. *Structure of SET-M33. Proportion between peptide sequences and lysine core is not respected*

The mechanism of action of SET-M33 is based into two steps: 1) it binds with high affinity the bacterial LPS [172] and LTA [112] 2) it disrupts the bacterial membranes as shown by

scanning electron microscopy (SEM) [173] (Figure 13). Furthermore, NMR investigation has demonstrated that the peptide can stabilize as a regular α-helix shape [173], which impairs cells functions as it gets embedded in the outer membrane surface of the bacterium.

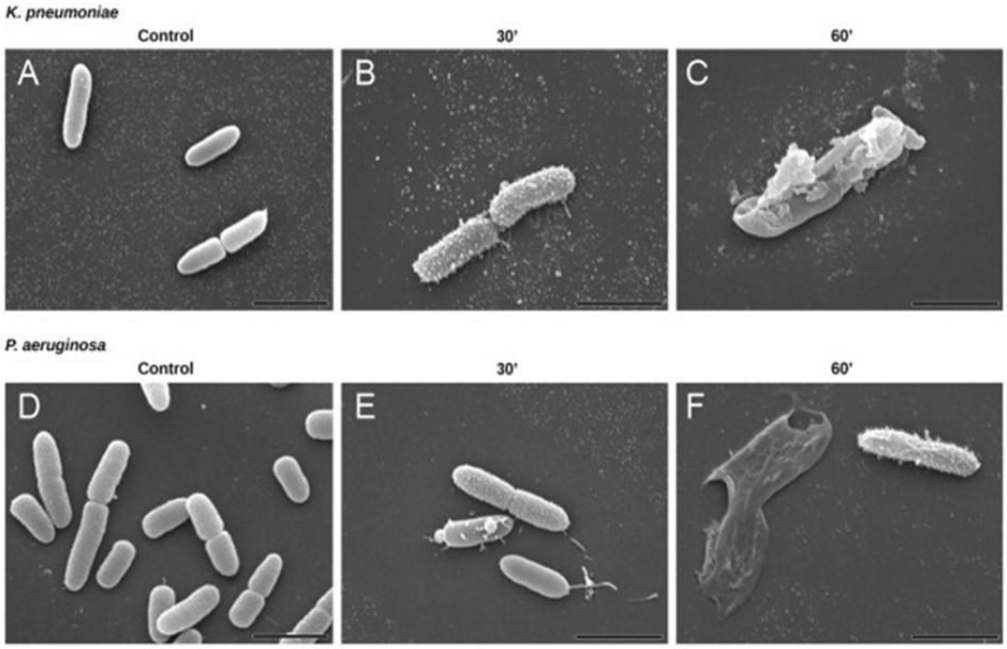

Figure 13. *Scanning electron micrographs (SEM) of K. pneumoniae and P. aeruginosa. SEM micrographs of A) and D) untreated K. pneumonia and P. aeruginosa; B) and E) K. pneumonia and P. aeruginosa after 30 min incubation with SET-M33 at MIC; C) and F) K. pneumonia and P. aeruginosa after 60 min incubation with SET-M33 at MIC [173]*

The peptide has been characterized by a high antimicrobial activity against a panel of multi-drug resistant (MDR) Gram-negative species, including clinical isolates of *P. aeruginosa* from CF patients. This aspect has increased the interest of this molecule as a new drug for this disease, where inflammation triggered by chronic bacterial infection is a major element of disease progression [169].

SET-M33 has shown concentration-dependent bactericidal activity against MDR clinical isolates, including colistin-resistant pathogens, like *P. aeruginosa* and *K. pneumoniae*. Specifically, it showed a MIC90 below 1.5 μM and 3 μM for *P. aeruginosa* and *K. pneumoniae*, respectively [174]. SET-M33 was also very active *in vitro* against other Gram-negative clinical isolates, including MDR strains of *A. baumannii* and *E. coli* [114].

As several others antimicrobial peptides, SET-M33 as well shows a certain degree of toxicity for eukaryotic cells *in vitro*. as human bronchial epithelial cells (16HBE14o- from healthy and CFBE41o- from CF patients) [171; 173].

In terms of its therapeutic power *in vivo*, SET-M33 was tested in models of sepsis, pneumonia and skin infections caused by *P. aeruginosa*. To evaluate the antimicrobial activity *in vivo* in a sepsis model, neutropenic mice were injected intraperitoneally (i.p.) with a lethal amount of *P. aeruginosa* PAO1. They were then treated twice intravenously (i.v.) with SET-M33 at 5mg/Kg. Strong therapeutic activity was evident, obtaining survivals of 60% and 80% with SET-M33 or SET-M33-PEG, respectively (Figure 14) [174].

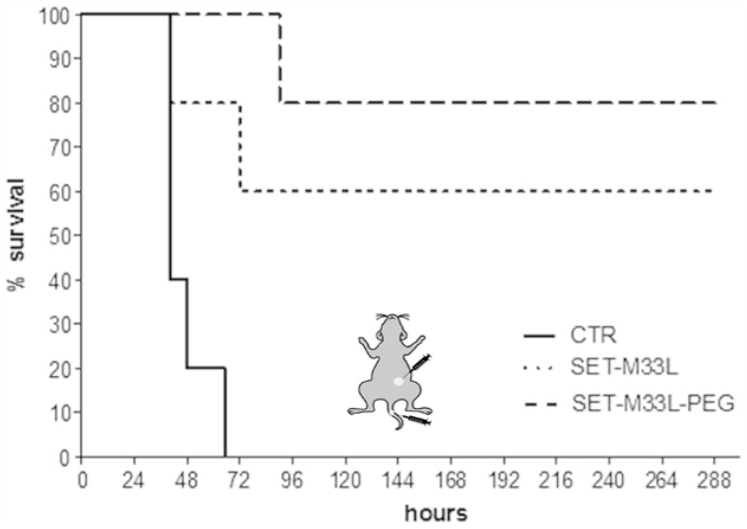

Figure 14. *In vivo antibacterial activity of SET-M33 peptide in sepsis animal model. 10 BALB/c neutropenic mice/group were injected i.p. with a lethal amount of P. aeruginosa PAO-1 and then treated twice i.v. with SET-M33 or SET-M33-PEG (5 mg/Kg), 24 and 72 hours post-infection. p < 0.02. Percentage survival (y-axis) is plotted as a function of time (x-axis) [174].*

In the *in-vivo* lung infection model, animals were injected intratracheally (i.t.) with a lethal amount of *P. aeruginosa* PAO1. Animals were treated i.v. with 5 mg/Kg of SET-M33 or SET-M33-PEG, 1 and 16 hours post-infection. The control group (CTR) only received vehicle. The survival was monitored for 10 days. 40% and 60% survival for SET-M33 and SET-M33-PEG, respectively, was observed (Figure 15 A). In a different model, animals were infected in the same way and treated with SET-M33 at 5mg/Kg, but after 12 hours animals were sacrificed and the lungs collected for CFU counts. 80% of CFU reduction was observed, confirming the strong antibacterial activity of the peptide (Figure 15 B) [174].

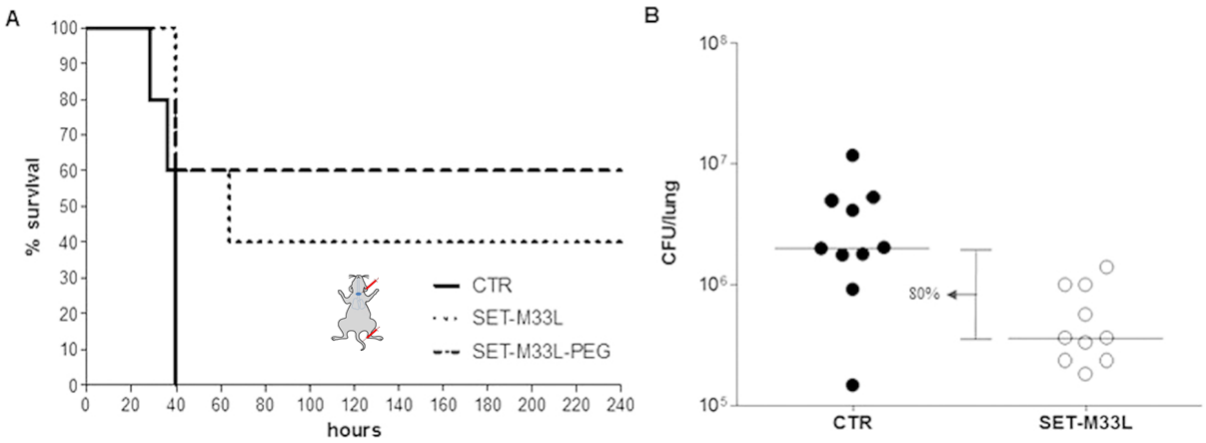

Figure 15. *In vivo antibacterial activity of SET-M33 and SET-M33-PEG peptides in lung infection. (A) Survival of neutropenic BALB/c mice after peptide treatment. All animals were injected i.t. with a lethal amount of P. aeruginosa PAO1. One group of animals was treated i.v. with 5 mg/Kg SET-M33 and one group with 5 mg/Kg SET-M33-PEG, 1 and 16 hours post-infection. The control group (CTR) only received vehicle. The groups are indicated as described in the internal legend. Percentage survival (y-axis) is plotted as a function of time (x-axis); p < 0.05. (B) Scatter plots representing the CFUs/lung (y-axis) in treated and untreated non-neutropenic mice (each circle corresponds to one mice). All animals were injected i.t. with P. aeruginosa PAO1. One group was treated i.t. with a single 5 mg/Kg dose of SET-M33 (white circles). The control group only received vehicle (black circles). The horizontal lines represent the median and the difference between medians is indicated as a percentage. p = 0.05. There were 10 mice/group [174].*

In the skin infection model experiments, 5 neutropenic mice per group (BALB/c) were infected on abraded skin with *P. aeruginosa* P1242 and then treated every day with 10 mg/mL SET-M33-lotion or drug-free-lotion (CTR). One-day post-infection the treatment produced a significant reduction of bacteria, in term of photon flux emitted. The effect is even more evident 2-days after the bacteria challenge (Figure 16) [174].

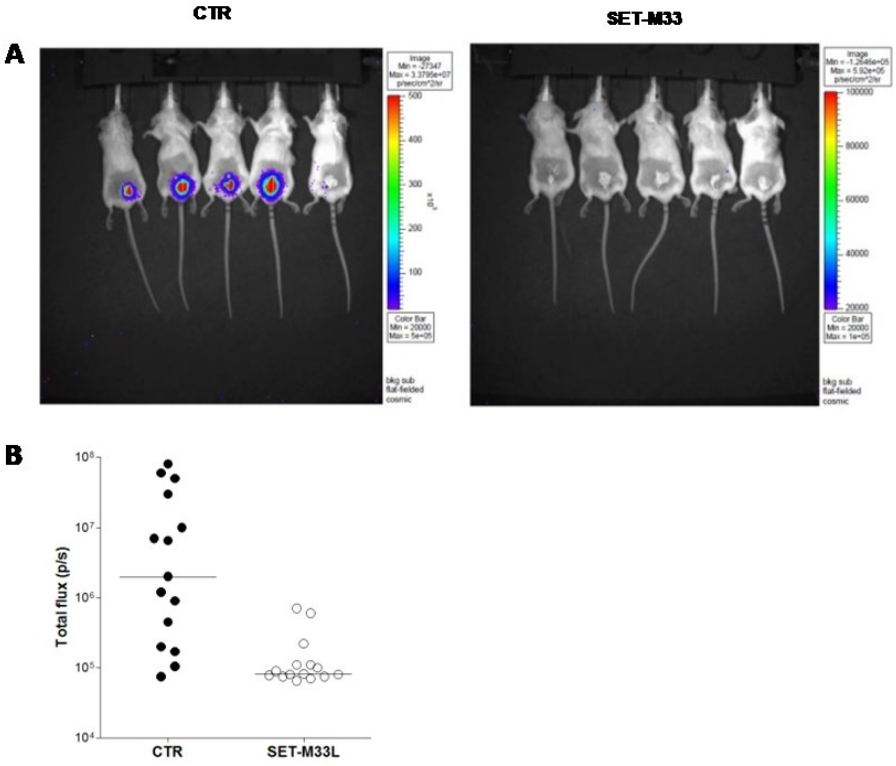

Figure 16. *In vivo antibacterial activity of SET-M33 peptide in skin infection. 15 neutropenic mice per group (BALB/c) were infected on abraded skin with P. aeruginosa P1242 and then treated every day with 10 mg/ml SET-M33-lotion (SET-M33) or with SET-M33 free-lotion (CTR). (A) Example of images of five animals at day 2. (B) Scatter plots representing the photon flux per second (p/s) emitted by bacteria at day 2 from all mice (each circle corresponds to one animal). The horizontal lines indicate the median value. $p < 0.03$ [174]*

Furthermore, SET-M33 was evaluated *in vitro* and *in vivo* for its anti-inflammatory response to LPS from different clinical bacteria which are responsible of lung infections caused by *P. aeruginosa*, *K. pneumoniae* and *E. coli*. Previously studies have demonstrated the ability of SET-M33 to decrease TNF-α production *in vitro* in cell stimulated by LPS from *P.aeruginosa* and *K. pneumoniae* [169]. The anti-inflammatory activity of SET-M33 was analysed in terms of reduced gene expression in murine macrophages of a number of cytokines, enzymes, and signal transduction factors involved in inflammation triggered by LPS from *P. aeruginosa*, *K. pneumonia* and *E. coli*. The results showed that the peptide SET-M33 is able to reduce the expression of many pro-inflammatory cytokines, growth and stimulating factors and the major intracellular signal transduction agent (NF-kB) [175]. Different *in vitro* and *in vivo* experimental techniques were used and all of them confirmed that the peptide is able to neutralize LPS. Gene and protein expression experiments showed

how the peptide inhibited the expression of various pro-inflammatory genes in macrophages (RAW264.7) and bronchial cells (IB3-1) from a CF patient through LPS neutralization [175]. *In vivo* experiments demonstrated that, after being nebulized directly into the lungs of mice previously challenged with LPS from *P. aeruginosa*, SET-M33 led to a significant reduction in TNF-α [175].

It is also described an immunomodulatory activity of SET-M33 in stimulating cell migration of keratinocytes in wound healing experiments *in vitro*, demonstrating that the cells treated with the peptide promote wound closure more rapidly than untreated cells [175].

An evaluation of toxicity *in vivo* in a murine model was done comparing SET-M33 with colistin [174]. In this case, mice were injected i.v. with different concentrations of SET-M33, SET-M33-PEG or colistin, and then monitored for 4 days after inoculation. Overall, SET-M33, in both forms, proved to be much less toxic than colistin [174].

A preliminary pharmacokinetic and bio-distribution analysis showed that the peptide is excreted mainly via urine [174].

A back-up molecule of SET-M33 peptide has been studied. It has been synthetized in a dimeric form (SET-M33DIM), where 2 peptide sequences are linked by a lysine core [176]. SET-M33DIM confirmed the strong antibacterial and anti-inflammatory activity, but showed a very low toxicity compared with results of the tetra-branched form. The dimeric forma of the peptide was studied *in vitro*, *ex vivo* and *in vivo* experiments [176]. At the same time, the peptide isomer consisting of D-amino acids has been synthetized [114-115], displayed a strong antibacterial and anti-inflammatory activity against Gram-positive bacteria, as *S. aureus*, *Staphylococcus saprophyticus* and *Enterococcus faecalis* [115]. Eventually, the SET-M33 peptide has been encapsulated into dextran-nanoparticles, creating a nanosystem that improved lung residence time of the peptide administered via aerosol. This results have to be considered among the aims of the development of a new therapeutic option for patient suffering from recurrent infections, that will benefit from high local doses of persistent antimicrobial [177].

AIM OF THE PROJECT

SET-M33 is an antimicrobial synthetic peptide patented by SetLance srl, a biopharmaceutical company based in Siena, and synthesized in the laboratories of the University of Siena. It has been already characterized for several aspects, like efficacy (sepsis, lung infections, skin infections), toxicity, bio-distribution, excretion, selection of resistances, gene toxicity, mechanism of action, immunomodulatory activity and time-kill concentrations.

The aim of my Ph.D. project is to continue the pre-clinical development of the SET-M33 antimicrobial peptide. In particular, this thesis is focused on three main studies, reported below:

1) Study 1: *in vivo* efficacy and toxicity of SET-M33 in a murine model of endotoxin-induced pulmonary inflammation;

2) Study 2: Safety evaluations of SET-M33 administered intravenously in rats and dogs;

3) Study 3: Inhalable polymeric nanoparticles for pulmonary delivery of SET-M33: antibacterial activity and *in vitro* and *in vivo* toxicity.

MATERIALS AND METHODS

STUDY 1: *IN VIVO* EFFICACY AND TOXICITY OF SET-M33 IN A MURINE MODEL OF ENDOTOXIN-INDUCED PULMONARY INFLAMMATION

SET-M33 PEPTIDE

Peptide with a purity of 96% as declared by the producer (Polypeptide, Strasbourg, France) was used for all tests of the Study 1. The formulations were prepared under sterile conditions by dissolving the powder in water at appropriate concentrations and then sterile filtering with a 0.22 μm polyvinylidenefluoride (PVDF) filtration unit. Dose formulations of SET-M33 and water were analyzed to confirm that the dose formulations prepared were homogeneous and that the SET-M33 concentrations administered were appropriate under the study conditions. The analytical method validated at the Testing Facility involved dilution of SET-M33 dose formulation samples in 100% water followed by quantification using high performance liquid chromatography with ultraviolet detection (HPLC-UV).

ANIMALS AND EXPERIMENTAL PROCEDURES

Crl:CD-1(ICR) mice and male BALB/c mice were used for the toxicity and efficacy studies, respectively. All animals were supplied by Charles River Ltd. (Margate, UK). After 10 days of acclimation prior to the first day of dosing, the animals were randomized into study groups, identified and allocated into monitored cages.

For the toxicity study, administration was by inhalation—snout-only exposure using a specific inhalation exposure system for mice.

*INHALATION EXPOSURE SYSTEM: t*he inhalation exposure system for mice used in the toxicity study is owned by Covance CRS LLC (now Labcorp Drug Development), Huntingdon, Cambridgeshire UK, the CRO where the experiments were performed. The system provided the determinations of achieved concentration of the peptide during the study and the particle size distribution. This is schematically represented in Figure 17.

Briefly, the components of the system are:

- Exposure system: a flow through snout only chamber, an aluminium alloy construction comprising a base unit, one animal exposure section, a top section and a pre chamber;
- Animal Restraint: a polycarbonate snout-only restraint tube;

- Aerosol Generation: A single Aeroneb (Aerogen) vibrating mesh nebuliser was used per exposure system and a disposable clinical syringe driven by a syringe pump;
- Inlet Airflow: from in-house compressed air system - breathing quality. Flow rate of 16 L/minute
- Extract Airflow: drawn by in-house vacuum system, filtered locally. Flow rate: 17 L/minute
- Airflow Monitoring: high quality tapered tube flowmeters, calibrated daily. In-line flowmeters monitored continuously

Mice were exposed to an atmosphere containing SET-M33. Different doses were achieved by varying the concentration of the peptide in the supplied formulation, the rate of formulation delivery to the aerosol generator and the system airflows. Animals were dosed once daily for 7 days. The administration takes 60 minutes each day. The animals under study were acclimatised to the method of restraint for 5 consecutive days immediately preceding their first exposure.

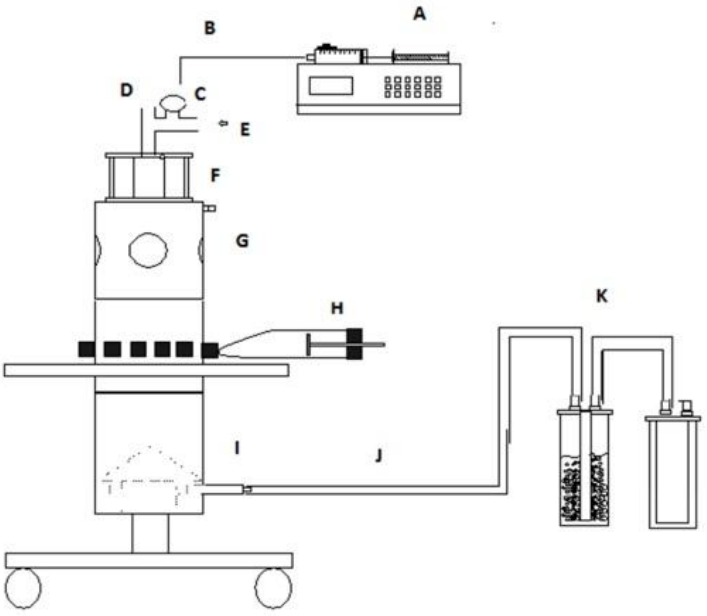

Key

A.	Syringe driver	G.	Inhalation exposure chamber
B.	Feed line	H.	Rodent restraint tube
C.	Nebuliser	I.	Chamber extract
D.	Balance air inlet	J.	Extract tubing
E.	Compressed air inlet	K.	Filtration units
F.	Aerosol conditioning pre-chamber		

Figure 17. *Schematic representation of inhalation exposure system.*

Animals were dosed once daily for 7 days. The duration of the exposure was 60 minutes each day. For the efficacy study, animals were dosed once with vehicle, SET-M33 or budesonide (positive control) intratracheally (i.t.) approximately 30 minutes prior to the beginning of the LPS challenge. Animals were weighed on the day of dosing and a fixed volume of 50 µL was administered (SETM33 at 0.2, 0.8, 2 and mg/mL). They were anaesthetized with a mix of isoflurane/oxygen (administered by inhalation at the following concentrations: 3–4% for induction and 1–3% for maintenance) and secured to an intubation device with a cord around the upper incisors. The tongue was pulled forward and any excess food and/or mucus was removed. A veterinary operating otoscope was inserted into the animal's mouth to illuminate the posterior pharynx and epiglottis. The tip of the dosing device was guided through the vocal cords into the lumen of the trachea. The pipette tip was guided down the trachea and the pipette plunger depressed with firm pressure. After dosing, the animals were removed from the secured position and carefully monitored until full recovery.

For the inflammatory challenge, lipopolysaccharide (LPS) from *E. coli* serotype O26:B6 was used (#L3755, Sigma-Aldrich®, St. Louis, MO, USA). Animals were placed in groups in an acrylic box and 8 mL LPS in 0.9% [w/v] saline was placed in each of two jet nebulizers (Sidestream®, Philips N.V. Amsterdam, The Netherlands). Compressed air at approximately 6 L/min was passed through each nebulizer and the output of the nebulizers directed into the box containing the animals for 30 minutes. On completion of the inflammatory challenge, the mice were returned to their home cage. Budesonide (#B7777, Sigma-Aldrich®) was used as a positive control. It was prepared in 0.1% Tween 80/0.6% NaCl in 0.05 M pH 6.0 phosphate buffered saline.

All animal experiments were approved by the local ethics committee of CRO, where the experiments were performed: Covance CRS LLC (now Labcorp Drug Development), Huntingdon, Cambridgeshire, UK. All experimental procedures during the studies were subject to the provisions of the United Kingdom Animals (Scientific Procedures) Act 1986 Amendment Regulations 2012 (the Act). All methods are reported according to "*Animal Research: Reporting of In Vivo Experiments*" (ARRIVE) guidelines [178]. The number of animals used was the minimum consistent with scientific integrity and regulatory acceptability, considering the welfare of individual animals in relation to the number and extent of procedures to be carried out on each animal.

TOXICITY STUDY BY INHALATION ADMINISTRATION TO CD-1 MICE FOR 1 WEEK

ATMOSPHERE ANALYSIS AND ESTIMATION OF ACHIEVED DOSE

The concentration in the aerosol and the particle size distribution were analysed by ultra-performance liquid chromatography. Briefly, the sample was collected from the filtration units of the aerosol machine, extracted with extraction solvent (0.1% trifluoroacetic acid and 0.05% Tween 80 in water, #302031 and #8.22187, respectively, supplied by Sigma-Aldrich®) and injected into the chromatograph. The chromatograph system was calibrated using an external standard. Peak area data acquired by the data capture software underwent least squares regression analysis and the concentration was calculated. Mass Median Aerosol Diameter (MMAD) and Geometric Standard Deviation (GSD) were calculated by linear regression of the probit of the cumulative percentage, by mass, of particles smaller than the effective cut-off diameter of each stage versus the logarithm of the cut-off diameter of each stage. Particle size was determined by cascade impaction using a Marple 290 series (296 configuration) cascade impactor at a flow rate of 2.0 L/minute.

The estimations of inhaled dose (mg/kg/day) were calculated using the formula reported below [179]:

$$\text{Dose (mg/kg/day)} = \frac{\boldsymbol{C}\ (\boldsymbol{g/L}) \times \boldsymbol{RMV}\ (\boldsymbol{L/min}) \times \boldsymbol{D}\ (\boldsymbol{min})}{\boldsymbol{BW}\ (\boldsymbol{Kg}) \times \mathbf{1000}}$$

where C = aerosol concentration (µg/L)

RMV = respiratory minute volume = 0.608 × BW(Kg)0.852.

D = duration of exposure (60 minutes)

BW = body weight (kg).

NECROSCOPY

Overdose of intraperitoneal pentobarbital sodium (at 50 mg/kg) followed by exsanguination was used for termination. All animals underwent detailed necropsy. A full macroscopic examination of the tissues was performed. Any abnormality in the appearance or size of any organ or tissue was recorded and the required tissue samples preserved in appropriate fixative. The organs were weighed. Tissue samples were routinely preserved in 10% Neutral

Buffered Formalin (except testes and eyes, which were preserved in modified Davidson's fluid Eyes and Davidson's fluid, respectively). Tissue samples were dehydrated, embedded in paraffin wax and sectioned at a nominal four-to-five-micron thickness. For bilateral organs, sections of both organs were prepared. A single section was prepared from each of the remaining tissues required. Sections were stained with haematoxylin and eosin. Each section was examined microscopically. Findings were either reported as "present" or assigned a five-point severity grade: minimal, slight, moderate, marked or severe.

BIOANALYSIS

Blood samples were collected from the jugular vein under isoflurane anaesthesia. Each sample was collected into a polypropylene test tube containing lithium heparin as anticoagulant and centrifuged at 2000 x *g* for 10 minutes at +4 °C. Total concentrations of peptide were determined by a qualified LC-MS/MS method. No specific testing regulations or guidelines were applicable for the plasma sample analysis; however, the analytical procedures followed were based on [180]. All data collection and processing were performed by the data acquisition system associated with the mass spectrometer (PC Analyst V1.6.1 or later). Data processing and quantification were performed using a Watson LIMS V7.2. After analysis, samples were immediately stored at −80 °C.

EFFICACY OF SET-M33 IN A MURINE MODEL OF ENDOTOXIN (LPS)-INDUCED PULMONARY INFLAMMATION

Following confirmation of death, an incision was made in the neck and the muscle layers separated by blunt dissection to isolate the trachea. A small incision was made in the trachea and a tracheal cannula inserted. The cannula was secured in place and the airway was washed with 0.3 mL phosphate buffered saline (PBS). The PBS was left in the airway for approximately 10 seconds while the chest was gently massaged and then removed. This was repeated twice more. In total, three lots of 0.3 mL PBS were used for lung lavage. The BAL fluid from the three lavages was pooled and placed on wet ice until centrifuged. Each BAL sample was centrifuged at 1000× *g* for 10 minutes at approximately 4°C. The cell pellet was resuspended in 0.5 mL PBS and stored on wet ice prior to analysis. A total and differential cell count of the re-suspended BAL cells was performed using the XT-2000iV (Sysmex UK

Ltd., Milton Keynes, UK.). The sample was vortexed for approximately 5 seconds and analyzed. Total and differential cell counts (including neutrophils, lymphocytes, eosinophils and mononuclear cells (includes monocytes and macrophages) are reported as number of cells per animal. BAL cytokines TNF α, IL-6, MIP-1α, KC, MCP-1 and IP-10 were analyzed using a multiplex system following the manufacturer's protocol (#LXSAMSM, Biotechne® Mouse Magnetic Luminex Screening Assay, R&D System, Minneapolis, MN, USA).

STATISTICAL ANALYSIS

For organ weight data in toxicity study, analysis of covariance with Student's *t* test was performed using terminal body weight as covariate [181], unless non-parametric methods were applied. The treatment comparisons were made on adjusted group means in order to allow for differences in body weight that might influence the organ weights. Significant differences between the groups compared were calculated using GraphPad Prism for Windows version 5.03, GraphPad Software, San Diego, CA, USA, and expressed as * $p < 0.05$.

Regarding efficacy study, data were expressed as means ± standard errors of the means. Statistical analysis was used to determine whether there were significant differences in BAL total and differential cell counts and BAL cytokine levels between SET-M33 (0.5, 2 and 5 mg/kg) or budesonide (1 mg/kg)-treated LPS-challenged animals and vehicle-treated LPS-challenged animals. Statistical analysis was also performed to compare vehicle-treated LPS-challenged animals with vehicle-treated saline-challenged animals. Statistical analysis was performed using the Student's *t*-test with GraphPad Prism for Windows version 5.03, GraphPad Software, San Diego, CA, USA. The levels of statistical significance are indicated in the legends of the figures.

STUDY 2: SAFETY EVALUATIONS OF SET-M33 ANTIMICROBIAL PEPTIDE ADMINISTERED INTRAVENOUSLY IN RATS AND DOGS

SET-M33 PEPTIDE PRODUCTION

Peptide with a purity of 97.9% as declared by the producer (Polypeptide, Strasbourg) was used for all tests of the Study 2. The formulations were prepared under sterile conditions by dissolving the powder in the vehicle (0.9% sodium chloride) and then sterile filtering with a 0.22 µm PVDF filtration unit. Dose formulations of SET-M33 and 0.9% sodium chloride for injection were analysed to confirm that the prepared dose formulations were homogeneous and that the administered SET-M33 concentrations were appropriate under the study conditions. The analytical method validated at the Testing Facility involved dilution of SET-M33 dose formulation samples in 100% water followed by quantification using high performance liquid chromatography with ultraviolet detection (HPLC-UV).

ANIMALS

RATS. Sprague Dawley rats were used for the toxicity studies. The animals were supplied by Envigo RMS S.L. All animals were 6-8 weeks old at the start of treatment and were allocated randomly to the treatment groups. The peptide was administered as an intravenous bolus in approximately 50 seconds via the lateral tail vein using a graduated syringe and a 24G (0.55 x 25 mm) needle. The administration volume was 5 mL/kg body weight.

DOGS. Naïve beagle dogs were used for the toxicity studies. The animals were supplied by Marshall US. They were 9-10 months old at the start of treatment with a body-weight range of 9.1-10 kg for the DRF study. They were 6-7 months old at the start of treatment with a body-weight range of 6.6-8.6 kg for males and 5.1-6.5 kg for females for the 4-week toxicity study. The method of administration was an intravenous short infusion with an infusion pump, alternately either into the cephalic or saphenous veins using sterile disposable cannulas and syringes. The volume of the dose of SET-M33 and control in two studies was 2,5 and 5 mL/Kg body weight, respectively.

All experimental protocols were approved by licensing committees from the institutions where the experiments were carried out. All animal experiments were performed in collaboration with the following CROs: Covance CRS LLC (now Labcorp Drug

Development), Huntingdon, Cambridgeshire UK and Somerset, New Jersey USA; AnaPath Research S.A.U., Castellar de Vallès, Barcelona, Spain.

All experimental procedures were carried out in accordance with the following guidelines and regulations: the United Kingdom Animals (Scientific Procedures) Act 1986 Amendment Regulations 2012; USA Animal Welfare Act Regulations: 9 CFR Parts 1 and 2 Final Rules, Federal Register, Volume 54, N. 168, August 31, 1989, pp. 36112-36163 effective October 30, 1989 and 9 CFR Part 3 Animal Welfare Standards; Final Rule, Federal Register, Volume 56, N. 32, February 15, 1991, pp. 6426-6505 effective March 18, 1991; Decret (Decree) 214/1997 of 30 July, Ministry of Agriculture, Livestock and Fishing of the Autonomous Government of Catalonia; Directive 2010/63/EU of the European Parliament and of the Council of 22 September 2010 on the protection of animals used for scientific purposes; Law 5/1995 of 21 June on the protection of animals used for experimentation and other scientific purposes (DOGC 2073, 10.7.1995), Autonomous Government of Catalonia; Law 6/2013 of 11 June, amending Law 32/2007 of 7 November on the care of animals during their exploitation, transport, experimentation and sacrifice, Spain; Real Decreto (Royal Decree) 53/2013 of 1 February 2013, Spain.

All methods are reported in accordance with ARRIVE guidelines [178]. The number of animals used was the minimum consistent with scientific integrity and regulatory acceptability, considering the welfare of individual animals in relation to the number and extent of procedures to be carried out on each animal.

DOSE RANGE FINDING (DRF) IN RATS

A viability/mortality check was recorded at least twice daily. Detailed observation of clinical signs was made daily during dosing.

HAEMATOLOGY. Blood samples were drawn from the retro-orbital plexus of all animals under light isoflurane anaesthesia. Blood was collected into tubes containing EDTA-K_3 as anticoagulant. The following parameters were determined using an ADVIA 120 haematology analyser (Siemens Healthcare): Red blood cell count (RBC), haemoglobin (Hb), haematocrit (Hct), mean corpuscular volume (MCV), mean corpuscular haemoglobin (MCH), mean corpuscular haemoglobin concentration (MCHC), reticulocyte count (absolute and relative) (Retic), platelet count (Plt), total leukocyte count (WBC), neutrophils (N), lymphocytes (L), monocytes (M), eosinophils (E), basophils (B), large unstained cells (LUC).

CLINICAL BIOCHEMISTRY. Blood samples were collected into lithium heparin tubes. The plasma was analysed for the following parameters with a Cobas 6000 analyzer (Roche): glucose (Gluc), urea (Urea), creatinine (Creat), bilirubin, total (Bili), cholesterol, total (Chol), triglycerides (Trig), aspartate aminotransferase (AST), alanine aminotransferase (ALT), creatine kinase (CK), gamma-glutamyl-transferase (gGT), calcium (Ca), inorganic phosphorus (Phos), sodium (Na), potassium (K), chloride (Cl), total protein (total Prot), protein electrophoretogram, albumin (Alb), globulin (calculated from the total protein and Alb%) (Glob), album/globulin ratio (A/G ratio).

URINALYSIS. Urine was collected in specimen vials using a metabolism cage. The following parameters were determined using a Cobas u 411 semi-automated test strip analyser (Roche): specific gravity (SG1), volume (Vol), colour (Col), appearance (App), pH, nitrite (Nite), protein (Prot), glucose (U-Gluc), ketones (Keto), urobilinogen (Urob), bilirubin (Bili), erythrocytes (U-RBC), leukocytes (U-WBC).

NECROSCOPY. Necroscopy was performed after the end of treatment in Phases I and II. Animals were sacrificed by intraperitoneal injection of sodium pentobarbital and immediately exsanguinated. Gross necropsy examination of the cranial, thoracic and abdominal cavities, major organs and injection site was performed on Phase I animals. A full necropsy was performed on Phase II animals, including examination of the external surface of the body, all orifices, cranial, thoracic and abdominal cavity organs in situ and after evisceration.

BIOANALYTIC AND TOXICOKINETIC STUDY. Blood samples were collected from the retro-orbital plexus of animals under light isoflurane anaesthesia. Blood samples were taken from three males and three females at each extraction time. Sampling times were as follows: Day 1: 5, 15, 30 and 60 minutes after administration. Day 7: pre-dose and 5, 15, 30, 60 minutes and 24 hours after administration. Control animals were bled only once on days 1 and 7 of treatment at 30 minutes after treatment. Each blood sample was collected into a polypropylene test tube containing lithium heparin as anticoagulant and kept in an ice bath until centrifuging (1600 x *g* for 10 minutes at 2-8°C). The plasma from each sample was transferred to a fresh polypropylene test tube, immediately frozen in dry ice and stored at -20°C ±5.

FOUR-WEEK TOXICITY STUDY WITH 2-WEEK RECOVERY PERIOD IN RATS

Viability/mortality was monitored twice daily throughout the study. Detailed clinical signs were evaluated once at pre-test, once/twice daily during the treatment period and on days 1, 8, 10 to 14 of the recovery period. Body weight was monitored once at pre-test, twice weekly during treatment and recovery periods, at termination of treatment and before sacrifice (scheduled animals fasted).

HAEMATOLOGY. Blood samples were extracted from the retro-orbital plexus under light isoflurane anaesthesia. The sample were collected into tubes containing EDTA-K_3 anticoagulant. The following parameters were determined with an Advia 120 haematology analyser (Siemens Healthcare): red blood cell count (RBC), haemoglobin (Hb), haematocrit (Hct), mean corpuscle volume (MCV), red cell volume distribution width (RDW), mean corpuscular haemoglobin (MCH), mean corpuscular haemoglobin concentration (MCHC), haemoglobin concentration distribution width (HDW), reticulocyte count (Retic), platelet (thrombocyte) count (Plt), leukocyte count, total (WBC), neutrophils (N), lymphocytes (L), monocytes (M), eosinophils (E) basophils (B), lrge unstained cells (LUC).

COAGULATION. Blood samples were collected into 3.2% sodium citrate tubes to obtain the plasma. The following parameters were determined using a STA COMPACT Automatic Coagulometer: prothrombin time (SPT), activated partial thromboplastin time (SAPT).

CLINICAL BIOCHEMISTRY. Blood samples were collected into lithium heparin tubes. The following parameters were determined using a Cobas 6000 Analyzer (Roche): glucose (Gluc), urea (Urea), creatinine (Creat), bilirubin, total (Bili), cholesterol, total (Chol), triglycerides (Trig), aspartate aminotransferase (AST), alanine aminotransferase (ALT), alkaline phosphatase (ALP), creatine kinase (CK), gamma-glutamyl-transferase (gGT), calcium (Ca), inorganic phosphorus (Phos), sodium (Na), potassium (K), chloride (Cl), albumin (Alb), globulin (calculated from total protein and Alb%) (Glob), total protein (Total Prot), album/globulin ratio (A/G ratio).

URINALYSIS. Urine was collected overnight into specimen vials (animals were placed in metabolism cages at the end of the working day preceding the day of urine collection). The following parameters were determined using a Cobas u 411 semi-automated test strip analyser (Roche): specific gravity (SG1), protein (Prot), ketones (Keto), volume (Vol),

creatinine (U-Creat), bilirubin (Bili), colour (Col), glucose (U-Gluc), erythrocytes (U-RBC), appearance (App), nitrite (Nite), pH, leukocytes (U-WBC).

NECROSCOPY. All animals underwent necropsy. Descriptions of all macroscopic abnormalities were recorded. Samples of tissues and organs were collected from all animals, weighed and fixed in neutral phosphate-buffered 4% formaldehyde solution (10% formalin). All organ and tissue samples to be examined were processed, embedded, cut and stained with haematoxylin and eosin. Samples were examined by confocal laser microscope (Leica TCS SP8). All images were processed using ImageJ software (NIH).

NEUROLOGICAL TOXICITY IN RATS

Evaluation of SET-M33 neurological toxicity was based on the method described by Irwin [182-183]. On the day prior to dosing, detailed subjective observation of all animals was made to assess the neurobehavioral and physiological state of untreated rats. After subjective observation, rectal temperature was measured and spontaneous locomotor activity was assessed. On the day of dosing, the animals were treated and then returned to their home cages. Detailed subjective observation of the rats was then repeated 5, 30, 90 and 240 minutes after dosing. A further observation was made 24 hours after dosing. During these observations, the following parameters were systematically evaluated for each animal using a standard procedure: lethality, restlessness, apathy, writhing, fighting, stereotyped behaviour, tremor, twitches, convulsions, exophthalmos, abnormal respiration, alertness, startle response, loss of righting reflex, abnormal body carriage, abnormal gait, Straub tail, piloerection, pupil diameter, light-pupil response, touch response, fearfulness, pinna reflex, corneal reflex, catalepsy, passivity, aggressiveness, body tone, grip strength, cutaneous blood flow, cyanosis, ptosis, lacrimation, salivation, pain response, motility impairment, grooming, diarrhoea, vocalization, increased urination. Normal attributes of animals (e.g. alertness, body tone etc.) were subjectively scored as 4; enhancement or depression of these attributes by SET-M33 was scored with higher or lower integers, respectively. Attributes normally absent in animals (e.g. abnormal gait, abnormal respiration, tremors etc.) were subjectively scored from 0 (normal) to 8. At the end of each observation period, the rectal temperature of each animal was measured. Finally, spontaneous locomotor activity was analysed. Each animal was placed in a suitable arena and locomotor activity measured in terms of number of squares crossed in a 2-minute period. Animals were inspected daily from

day 3 to day 7 for appearance of any delayed effects. After the day 7 inspection, the animals were killed humanely by a rising concentration of carbon dioxide. Death was confirmed by dislocation of the neck.

EVALUATION OF RESPIRATORY FUNCTION IN RATS

Whole body, bias flow plethysmography equipment was used [184]. Respiratory parameters (respiratory rate, tidal volume and minute volume) were derived from the changes in pressure associated with the warming and humidification of the air breathed in by the animal. This was monitored by specific probes located in the plethysmograph chambers. Bias flow (room air) was set at approximately 2.5 L/min. On a day prior to the first day of dosing, all animals were habituated to the plethysmographs for approximately 2 hours. The study was run over 4 days and 10 animals (two from each group) were examined each day. On the day of dosing, the animals were placed in the plethysmographs for pre-dose recording (session 1) of respiratory parameters for 60 minutes. Groups of 8 rats were then removed from the chambers and dosed by intravenous bolus injection with vehicle, SET-M33 or positive control. Immediately after dosing, the rats were placed in the whole body plethysmographs, where they could move about freely, to continuously record respiratory parameters for 4 hours post-dose (undisturbed recording). Immediately after the last post-dose recording, the animals were killed humanely by a rising concentration of carbon dioxide. Death was confirmed by dislocation of the neck. Respiratory parameters were reported at the following time points: 0, 30, 60, 90, 120, 150, 180, 210 and 240 minutes. Time 0 coincided with the mean value of the last 20 minutes of data recorded in the 60-minute pre-dose period. All other time points were the mean of 10-minute recordings (an average of every 10 breaths) around each time point. Each post-dose time point was analysed separately by analysis of covariance. Factors in the model were group and day of data collection, with pre-dose values as covariate.

DOSE RANGE FINDING (DRF) IN DOGS

Viability/mortality were recorded at least twice daily. On treatment days, all animals were observed for signs of toxic or pharmacological effects prior to, during and immediately after administration and 1-2 hours post-dose. Injection sites were examined daily during dosing.

For clinical investigation, blood obtained via jugular venepuncture from anaesthetized dogs was used to analyse blood, coagulation and biochemical parameters.

HAEMATOLOGY. A blood sample was collected into tubes containing EDTA-K_3 as anticoagulant and analysed for the following parameters using Advia 120 haematology analyser (Siemens Healthcare): red blood cell count (RBC), haemoglobin (Hb), haematocrit (Hct), mean corpuscular volume (MCV), mean corpuscular haemoglobin (MCH), mean corpuscular haemoglobin concentration (MCHC), platelet count (Plt), total leukocyte count (WBC), reticulocyte count (Retic), neutrophils (N), lymphocytes (L), monocytes (M), eosinophils (E) basophils (B), large unstained cells (LUC).

CLINICAL BIOCHEMISTRY. A blood sample was collected in lithium heparin tubes. The following parameters were determined using Cobas 6000 analyzer (Roche): albumine (Alb), glucose (Gluc), urea (Urea), creatinine (Creat), bilirubin (Bili), cholesterol (Chol), aspartate aminotransferase (AST), alanine aminotransferase (ALT), sodium (Na), potassium (K), chloride (Cl), calcium (Ca), inorganic phosphorus (Phos), total protein (Total Prot), protein electrophoretogram.

URINALYSIS. Urine obtained via a 16-hour overnight collection period was analysed. Urine was collected into ice-chilled containers overnight from pans placed beneath each animal's cage. Urine samples were analysed for the following parameters using Multistix reagent strips, interpreted using a Siemens Clinitek Advantus: specific gravity (SG1), colour (Col), pH, protein (Prot), glucose (U-Gluc), ketones (Keto), urobilinogen (Urob), bilirubin (Bili).

NECROSCOPY. All animals were sacrificed at the end of the treatment period by intravenous injection of sodium pentobarbital. Organs were collected and weighed.

BIOANALYTIC AND TOXICOKINETIC STUDY. Blood samples were taken by direct venepuncture of the jugular vein on days 1 and 7 to determine plasma levels of SET-M33. Sampling times were as follows: Day 1: at 0, 5, 15, 30, 60 and 180 minutes. Day 7: at 0, 5, 15, 30, 60, 180 minutes and 24 hours after administration. Control animals were only bled once on days 1 and 7 of treatment, 1 hour after administration. Blood samples were collected into lithium heparin test tubes and kept in an ice bath until centrifuging (1600x *g* for 10 minutes at 2-8°C). The plasma obtained from each sample was transferred to a fresh polypropylenes test tubes, immediately frozen in dry ice and stored at -20°C ± 5.

FOUR-WEEK TOXICTY STUDY WITH 4-WEEK RECOVERY PERIOD IN DOGS

Animals were observed daily for mortality and signs of severe toxic or pharmacological effects. On treatment days, all animals were observed for signs of toxic or pharmacological effects prior to, during and after administration and 1-2 hours post-dose. Blood obtained via jugular venepuncture from anaesthetized dogs was used to analyse blood, coagulation and clinical chemistry parameters for 5 animals/sex/group pre-test and at termination of dosing and from 2 animals/sex/group at the end of recovery.

HAEMATOLOGY. Blood samples were collected into tubes containing K_3EDTA anticoagulant and analysed for the following using ADVIA 120 Haematology Analyser (Siemens): haemoglobin (Hb), haematocrit (Hct), red blood cell count (RBC), platelet count (Plt), mean corpuscular volume (MCV), mean corpuscular haemoglobin (MCH), mean corpuscular haemoglobin concentration (MCHC), red cell distribution width (RDW), total white blood cell count (WBC), reticulocyte count (Retic), neutrophils (N), lymphocytes (L), eosinophils (E), basophils (B), monocytes (M), large unstained cells (LUC).

COAGULATION. Blood samples were collected into tubes containing sodium citrate anticoagulant and analysed for the following using a Diagnostica Stago Products STA Compact MAX mechanical clot detection system: prothrombin time (SPT), activated partial thromboplastin time (APTT), fibrinogen (FIB).

C*LINICAL BIOCHEMISTRY*. Blood samples were collected into tubes with no anticoagulant, allowed to clot, centrifuged to obtain serum and analysed for the following using ADVIA 1800 Chemistry Analyzer (Siemens): aspartate aminotransferase (AST), alanine aminotransferase (ALT), alkaline phosphatase (ALKP), blood urea nitrogen (BUN), creatinine (Creat), glucose (Glu), cholesterol (Chol), triglycerides (Trig), total protein (Tot Prot), albumin (Alb), total bilirubin (Bili), sodium (Na), potassium (K), chloride (Cl), calcium (Ca), inorganic phosphorus (Phos), gamma-glutamyl transferase (gGT).

URINALYSIS. Urine obtained via a 16-hour overnight collection period was analysed for all animals/sex/group pre-test, at study termination, and at the end of recovery. Urine was collected into ice-chilled containers overnight from pans placed beneath each animal's cage. Urine samples were analysed for the following parameters using Multistix reagent strips, interpreted using a Siemens Clinitek Advantus: pH, protein (Prot), glucose (U-Gluc), ketones (Keto), bilirubin (Bili), appearance (App), specific gravity (SG1), volume (Vol).

NECROSCOPY. Complete macroscopic examination was performed on all animals, including examination of the external surface and all orifices; the external surfaces of the brain and spinal cord; the organs and tissues of the cranial, thoracic, abdominal and pelvic cavities and neck; and the rest of the carcass for macroscopic morphological abnormalities. Necropsy was performed on up to 3 animals/sex/group after treatment for 4 weeks and on 2 animals/sex/group after a 4-week treatment-free recovery period. Organs and tissues were weighed, preserved and examined microscopically. Prior to weighing, organs were carefully dissected and properly trimmed to remove adipose and other contiguous tissue in a uniform manner. Organs were weighed as soon as possible after dissection in order to avoid drying. Paired organs were weighed together. Eyes, optic nerve and testes were initially placed in Modified Davidson's solution and then kept in 10% neutral buffered formalin (NBF). Lungs and urinary bladder were infused with 10% NBF prior to immersion in a larger volume of the same fixative. All other tissues were preserved in 10% NBF.

BIOANALYTICS AND TOXICOKINETICS IN RATS AND DOGS

RATS. Blood samples were drawn from the retro-orbital sinus under light isoflurane anaesthesia for determination of plasma SET-M33 levels. The samples were taken on days 1 and 28 of treatment at the following times: control group: pre-dose and 30 minutes; 5, 9 and 15 mg/kg/day-group: pre-dose, 5, 15, 30, 60 minutes and 24 hours after administration. Blood samples were collected into polypropylene test tubes containing lithium heparin anticoagulant and kept at room temperature for no longer than 60 minutes until centrifuging (1600x *g* for 10 minutes at 2-8°C). The plasma obtained from each sample was transferred to a fresh polypropylene test tubes, immediately frozen in dry ice and stored at -20°C ± 5. Plasma concentrations of SET-M33 were measured by a previously validated LC-MS/MS method. Toxicokinetic parameters were determined for mean plasma concentrations at each dose level and time point, according to the validated method and with WinNonlin software, version 6.3, in the Phoenix Suite version 1.3 (Pharsight Corporation, Mountain View, CA, USA).

DOGS. On days 1 and 28, blood samples were obtained for toxicokinetic determinations from all animals at the following times: Day 1 at the end of infusion and 5, 10, 15, 30, 60 and 180 minutes later; 6 ± 15 minutes and 24 hours ± 30 minutes post-dose; Day 28 at the end

of infusion and 5, 10, 15, 30, 60 and 180 min later; 6 ± 15 minutes and 24 hours ± 30 minutes post-dose. Blood samples were collected into lithium heparin test tubes and kept in an ice bath until centrifuging (1600x *g* for 10 min at 2-8°C). The plasma obtained from each sample was transferred to a fresh polypropylenes test tubes, immediately frozen in dry ice and stored at -20°C ± 5. Bioanalytical samples were analysed by a validated liquid chromatographic mass spectrometric assay. Pharmacokinetic parameters were calculated using the computer program Phoenix WinNonlin version 6.3 (Certara USA, Inc).

STUDY 3: INHALABLE POLYMERIC NANOPARTICLES FOR PULMONARY DELIVERY OF ANTIMICROBIAL PEPTIDE SET-M33: ANTIBACTERIAL ACTIVITY AND TOXICITY *IN VITRO* AND *IN VIVO*

MATERIALS

The poly(lactide-co-glycolide) PLGA (Resomer® RG 502H uncapped PLGA 50:50, inherent viscosity 0.16–0.24 dL/g) was acquired from Boehringer Ingelheim (Ingelheim, Germany). Poly(lactic-co-glycolic acid) copolymer-Rhodamine-B conjugate (Mn 10,000–30,000 Da) (PLGA-Rhod) was purchased from PolyScitech (Akina division, Inc.,West Lafayette, IN, USA). Poly(ethylene glycol) methyl ether-block-poly(lactide-co-glycolide) with PEG average Mn 2000 Da, PLGA Mn 4500 Da and with PEG average Mn 5000 Da, PLGA Mn 7000 Da, diethylenetriaminepentaacetic acid (DTPA), DNA, egg yolk emulsion, poly(Llysine), RPMI amino acid solution and type II mucin from porcine stomach were purchased from Merck-Sigma Aldrich (St. Louis, MO, USA). Bacterial alginate from the fermentation of *Azotobacter vinelandii* or *Pseudomonas mendocina* was purchased from Carbosynth (UK). Methylene chloride and ethanol were supplied by Carlo Erba (Italy). All salts and reagents were of analytical grade or higher.

PEPTIDE PRODUCTION

SET-M33 was produced in tetrabranched form by solid-phase synthesis using standard Fmoc (N-(9-fluorenyl)methoxycarbonyl) chemistry on Fmoc4-Lys2-Lys-_-AlaWang resin with a Syro multiple peptide synthesizer (MultiSynTech, Witten, Germany). Sidechain-protecting groups were 2,2,4,6,7-pentamethyldihydrobenzofuran-5-sulfonyl for Arg, t-butoxycarbonyl for Lys, and t-butyl for Ser. The final product was cleaved from the solid support, deprotected by treatment with TFA containing tri-isopropylsilane and water (95/2.5/2.5), and precipitated with diethyl ether. Crude peptide was purified by reversephase chromatography on a column for medium-scale preparation in linear gradient form for 30 min using 0.1% TFA/water as eluent A and methanol as eluent B. The purified peptide was obtained as trifluoroacetate salts (TFacetate). Exchange from TFacetate (toxic by-product) to acetate form was carried out using a quaternary ammonium resin in acetate

form (AG1-X8, 100–200 mesh, 1.2 meq/mL capacity). The resin-to-peptide ratio was 2000:1. Resin and peptide were stirred for 1 hour, the resin was filtered off and washed extensively, and the peptide was recovered and freeze dried [185]. Final peptide purity and identity were confirmed by reverse-phase chromatography using a Phenomenex Jupiter C18 analytical column (300 Å, 5 mm, 25,064.6 mm) and by mass spectrometry MALDI-TOF/TOF. Rhodamine-labeled peptides were synthesized using Lys-tetramethyl-rhodamine (Lys-TMR) as the first amino acid (SET-M33-Rhod).

QUANTITATIVE ANALYSIS OF SET-M33

SET-M33 was quantified by a RP-HPLC system consisting of a liquid chromatograph (LC-10ADvp), an auto-injector (SIL-10ADvp), a UV–Vis detector (SPD-10Avp) and an integrator (C-R6) (Shimadzu, Japan). The SET-M33 quantitation was performed using a Jupiter 5 µm C18 column (250 x 4.6 mm, 300 Å) (Phenomenex, Torrance, CA, USA) and a mixture of 0.1% (v/v) TFA in water and acetonitrile (77:23 v/v) as the mobile phase. The flow rate was 1 mL/min and the detection wavelength 215 nm. Calibration curves were achieved by plotting peak area versus the concentration of SET-M33 standard solutions in water, and the linearity of the response was verified over the concentration range 1–200 µg/mL ($r^2 \geq 0.999$).

Rhodamine-labeled SET-M33 was quantified by a spectrofluorimetric assay at λ_{ex} = 520 nm and λ_{em} = 580/640 nm using a plate reader (GloMax® Explorer, Promega, Milano, Italy). The linearity of the response was verified over the SET-M33_Rhod concentration range 0.1–100 µg/mL ($r^2 > 0.999$).

NANOPARTICLES PRODUCTION

PEGylated PLGA-based NPs were prepared at a SET-M33 theoretical loading of 4% (4 mg of SET-M33 per 100 mg of NPs) by emulsion/solvent diffusion technique, as previously reported [185-186]. Briefly, 100 µL of SET-M33 aqueous solution (0.4 mg) was emulsified with 1 mL of methylene chloride containing a mixture of PLGA (8 mg) and PEG-conjugated PLGA (2 mg) by vortex mixing (2400 min^{-1}, Heidolph, Schwabach, Germany). Two formulations were produced employing PLGA conjugated with PEG at different molecular weights (2000 and 5000 Da PEG): SET-M33_PEG2000 NPs and SET-M33_PEG5000 NPs, respectively. The obtained emulsion was added to 12.5 mL of ethanol 96% (v/v), allowing

polymer precipitation in the form of NPs. The NP dispersion was then diluted with 12.5 mL of water and kept under magnetic stirring for 10 minutes at room temperature. Afterwards, the organic solvent was evaporated under vacuum at 30°C (Rotavapor®, Heidolph VV 2000, Germany), and the colloidal dispersion of NPs was collected and adjusted with ultrapure water to a final volume of 5 mL. Finally, NPs were isolated by centrifuge at 7000 rcf for 20 minutes at 4°C and dispersed in ultrapure water.

Two NP formulations containing fluorescent probes were obtained by encapsulating SET-M33 conjugated with rhodamine B (SET-M33_Rhod) [172] or by embedding PLGA Rhodamine-B conjugate (PLGA-Rhod) in the polymeric matrix (10% w/w with respect to total PLGA amount) (Figure 18).

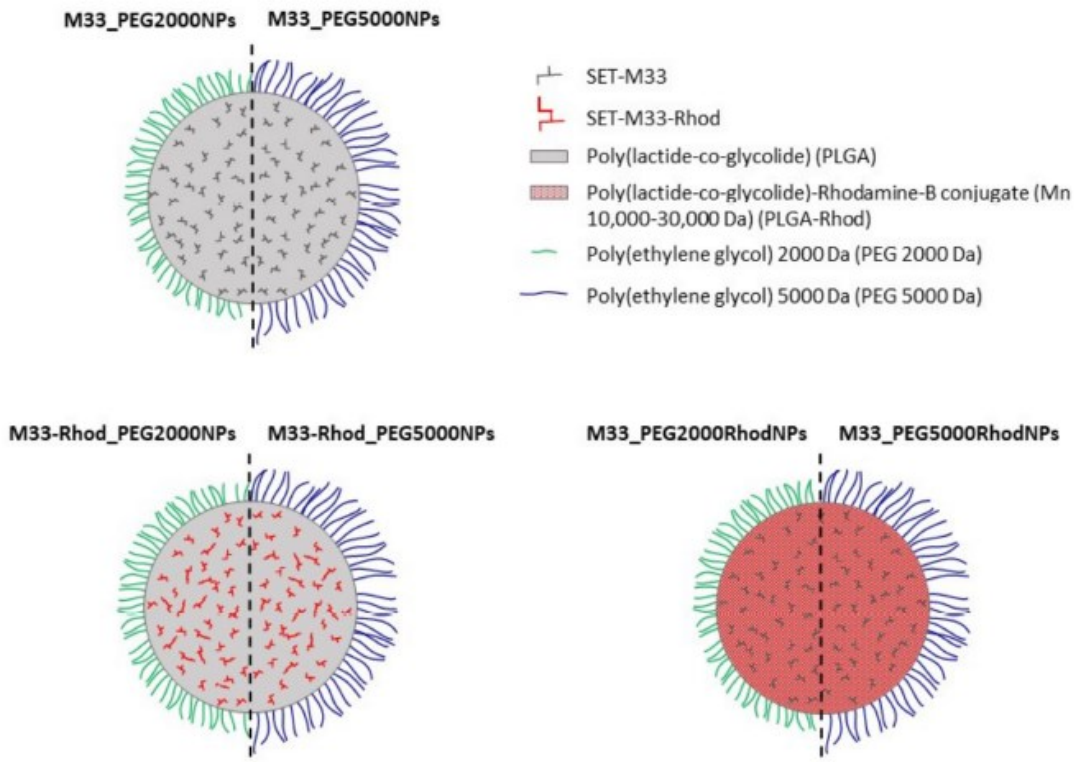

Figure 18. *Diagram of the core–shell structure of SET-M33-loaded PLGA NPs, PLGA NPs containing SET-M33 conjugated with rhodamine (SET-M33_Rhod), and NPs prepared by employing PLGA conjugated with rhodamine (PLGA-Rhod).*

NANOPARTICLES PROPERTIES

The hydrodynamic diameter (DH), polydispersity index (PDI) and zeta potential (ζ potential) of SET-M33-loaded NPs were measured by dynamic light scattering (DLS) and electrophoretic light scattering (ELS) with a Zetasizer Nano ZS (Malvern Instruments Ltd.,

Malvern, UK). The ζ potential of the NP aqueous dispersion was evaluated after appropriate dilution in ultrapure water using an electrophoresis cell at a fixed potential of ±150 mV. The reported results are the mean of three measurements for three different batches (n = 9) ±SD. The NP morphology was evaluated by transmission electron microscopy (TEM) using a FEI Tecnai G2 200 kV S-TWIN microscope equipped with a 4 K camera (Thermo Fisher Scientific, Waltham, MA, USA). Briefly, 10 µL of SET-M33-loaded NP dispersion in water (3 mg/mL) was mounted on 200 mesh copper grids coated with carbon film (Ted Pella Inc., Nanovision, Italy) and dried overnight at room temperature. The actual amount of SET-M33 encapsulated in NPs was evaluated indirectly by measuring the amount of non-encapsulated peptide in the NP dispersion. Briefly, just after production, NPs were collected by centrifugation at 7000 rcf for 20 minutes at 4°C (Hettich Zentrifugen, Universal 16R), and the SET-M33 content in the supernatant was analyzed by RP-HPLC, as described above. The results are reported as actual loading (mg of encapsulated SET-M33 per 100 mg of NPs) and encapsulation efficiency (actual loading/theoretical loading x 100) ± SD from three different batches (n = 6).

The PEG shell on the NP surface was evaluated by measuring fixed aqueous layer thickness (FALT), i.e., by monitoring the influence of the ionic strength of the dispersing medium on NP surface charge, as previously reported [166; 187]. According to the Gouy–Chapmann theory, ζ potential decreases with increasing ionic strength of the dispersion medium. By plotting ln (ζ) against k (k = 3.3 c0.5, where k -1 is the Debye length), a linear regression is obtained, and the thickness of the fixed aqueous layer (expressed in nm) due to the PEG shell is determined from the slope. Unloaded PLGA-based NPs prepared without PEG were tested in the same conditions as the control.

In vitro release kinetic studies were performed by employing NPs containing SET-M33_Rhod in phosphate buffer at pH 7.2 (120 mM NaCl, 2.7 mM KCl, 10 mM phosphate salts, PBS). SET-M33_Rhod-loaded NPs diluted in PBS were incubated at 37 °C and 40 rpm, in a horizontal shaking water bath (ShakeTemp SW 22, Julabo Italia, Italy). At scheduled time intervals, samples were centrifuged at 7000 rcf for 20 minutes at 4 °C to isolate NPs, and to withdraw 0.5 mL of the release medium. The released medium was analyzed by spectrofluorometer at λ_{ex} = 520 nm and λ_{em} = 580/640 nm, as described above. Experiments were run in triplicate, and the results are expressed as the percentage of SET-M33 released from NPs (%) ± SD over time.

IN VITRO AEROSOL PERFORMANCE OF NANOPARTICLES

Aerosolization properties of SET-M33-loaded NPs were evaluated *in vitro* on fluorescently labeled NPs prepared employing PLGA-Rhod (i.e., SET-M33-Rhod_PE2000 NPs and SET-M33-Rhod_PEG5000 NPs) after nebulization through an air jet nebulizer (PARI TurboBOY, PARI GmbH, Starnberg, Germany) or a vibrating mesh nebulizer (Aeroneb® Go, Aerogen Ltd., Galway, Ireland). The aerosolization behaviour of NPs was evaluated using a next generation impactor (NGI) (Copley Scientific, Nottingham, UK), according to the Comité Européen de Normalization standard methodology for nebulizer systems, with sampling at 15 L/min and insertion of a filter in a micro-orifice collector (MOC). Briefly, the nebulizer reservoir was filled with 1 mL of a water dispersion of SET-M33-loaded fluorescent NPs (1 mg/mL). The nebulizer device was connected to the induction port of the NGI and operated at 15 L/min. The aerosol was drawn through the impactor for 5 min until dry. The NPs aerosolized (i.e., remaining inside the nebulizer reservoir, deposited on the seven cups of the NGI and in the induction port) were recovered quantitatively in 0.5 N NaOH. The achieved samples were maintained under magnetic stirring at room temperature for 1 h, and the number of fluorescent NPs in the resulting solutions was quantified by spectrofluorimetric analysis at λ_{ex} = 520 nm and λ_{em} = 580–640 nm (GloMax® Explorer, Promega, Italy). Calibration curves were derived by analyzing serial dilutions of a stock of fluorescent NPs after degradation in 0.5 M NaOH, as described above. Each experiment was run in triplicate.

The experimental mass median aerodynamic diameter (MMADexp) and the geometric standard deviation (GSD) were calculated, according to the European Pharmacopoeia, by plotting the cumulative mass of particles retained in each collection cup (expressed as percent of total mass recovered in the impactor) versus the cut-off diameter of the corresponding stage. At the used flow (15 L/min), the cut-off diameters of the NGI stages were 0.98 μm (Cup 1), 1.36 μm (Cup 2), 2.08 μm (Cup 3), 3.3 μm (Cup 4), 5.39 μm (Cup 5), 8.61 μm (Cup 6), 14.1 μm (Cup 7).

The fine particle fraction (FPF) was calculated by considering the number of NPs deposited on stages 3–7 (MMADexp < 5.39 μm) compared to the initial amount loaded in the nebulizer chamber, while the respirable fraction (RF) was determined by the total amount recovered from the NGI.

IN VITRO NANOPARTICLES INTERACTIONS WITH MUCIN AND BACTERIAL ALGINATES

The interactions of SET-M33-loaded NPs with the main components of mucus and *P. aeruginosa* biofilm extracellular matrix (i.e., mucin and bacterial alginates, BA) were assessed by turbidimetric measurements, as previously described [166-167]. For mucin/NP interactions, a saturated aqueous solution of mucin was made by dispersing an excess of mucin in water (0.08% w/v), under overnight stirring, followed by centrifuging at 6000 rcf and 4°C for 20 minutes and collection of the supernatant. For NP/BA interactions, a BA dispersion in water (1% w/v) was centrifuged at 6000 rcf and 4°C for 15 minutes, and the supernatant was collected. Briefly, 10 µL of SET-M33-loaded NP water dispersion (1 mg) was diluted to 1 mL with the mucin or BA solution and mixed by vortex for 30 seconds; the turbidity was measured at time 0 and after incubation at 37°C for 30 and 60 minutes. The absorbance at an arbitrary unit (650 nm) was recorded by a spectrophotometer. The free SET-M33 in mucin and BA solutions, the mucin and the BA dispersion (without NPs) and the SET-M33-loaded NP dispersions in water were analyzed as controls. Results are expressed as mean absorbance of three replicates at 650 nm ± SD over time. The size of NPs dispersed in mucin and BA was assessed by DLS, as described above. DLS analysis of free SET-M33 in mucin and BA was carried out as a control.

IN VITRO TRANSPORT OF NANOPARTICLES THROUGH ARTIFICIAL CYSTIC FIBROSIS MUCUS AND SIMULATED BACTERIA BIOFILM

The diffusion of fluorescent NPs through artificial CF mucus (AM) and simulated bacteria biofilm (BA) was evaluated using a previous model based on Transwell® multiwall plates [166-167], with some changes. The AM was prepared as previously described [166], by adding 25 µL sterile egg yolk emulsion, 25 mg mucin, 20 mg DNA, 30 µL aqueous DTPA (1 mg/mL), 25 mg NaCl, 11 mg KCl and 100 µL RPMI 1640 to 5 mL water. The BA was a dispersion of bacterial alginates in water (1% w/v), obtained as described previously for NP/BA interactions.

Briefly, 75 µL AM or BA was transferred to Transwells® (6.5 mm; pore size 8 µm; Corning Incorporated, Corning, NY, USA). Then, 25 µL of a NP dispersion in water (20 mg/150 µL) was placed on top of the AM/BA layer, and the wells were inserted into a 24-well plate containing 300 µL acceptor medium per well. Simulated interstitial lung fluid (SILF) and

PBS at pH 7.2 were used as acceptor media for AM and BA diffusion experiments, respectively. SILF was prepared as described by Moss [188], and consisted of 600 mg NaCl, 30 mg KCl, 15.7 mg Na_2HPO_4, 7.1 mg Na_2SO4, 27.8 mg $CaCl_2$, 57.4 mg $NaH_3C_2O_2$, 260.8 mg $NaHCO_3$, 9.8 mg $Na_2H_5C_6O_7$*H_2O and 29.4 mg $MgCl_2$*6 H_2O in 100 mL water. At scheduled time points (from 0 to 6 h), the acceptor medium was sampled and centrifuged at 9000 rcf for 20 minutes at 4°C to isolate NPs. The NP pellet was suspended in 50 µL water, diluted with 450 µL 0.5 N NaOH, and stirred for 1 hour to achieve complete PLGA matrix degradation. The resulting samples were analyzed by spectrofluorimetric analysis at λ_{ex} = 520 nm and λ_{em} = 580–640 nm (GloMax® Explorer, Promega, Italy) to quantify the number of permeated fluorescent NPs. Calibration curves were obtained by analyzing serial dilutions of SET-M33-loaded fluorescent NP standard solutions prepared from a stock of fluorescent NPs degraded in 0.5 M NaOH. The linearity of the response was verified over the concentration range 10–1000 µg/mL ($r \geq 0.999$). Experiments were run in triplicate, and the results are expressed as the percentage of total NPs permeating over time ± SD. The ability of free SET-M33 to diffuse through AM and BA was also evaluated using SET-M33_Rhod. The diffusion test was carried out on free SET-M33_Rhod, and compared to SET-M33-Rhod_PEG2000 NPs and SET-M33-Rhod_PEG5000 NPs. Briefly, 25 µL of a SET-M33_Rhod aqueous solution (4.8 mg/mL), or 25 µL of a SET-M33-Rhod-loaded NP dispersion (20 mg/150 µL corresponding to 4.8 mg/mL of SET-M33_Rhod), was added on top of AM or BA. At scheduled time intervals (from 0 to 6 hours), the acceptor medium (i.e., SILF or PBS) was collected and the amount of SET-M33_Rhod permeated was determined by spectrofluorometer, as described above. In the case of SET-M33_Rhod-loaded NPs, the amount of SET-M33 diffused was evaluated after degradation of permeated NPs in NaOH. Experiments were run in triplicate, and the results are expressed as the percentage of permeated SET-M33_Rhod ± SD.

IN VITRO ANTIBACTERIAL ACTIVITY OF SET-M33_PEG 5000 NPS

P. aeruginosa (ATCC 27853™) was grown at 37°C in Luria Bertani (LB) medium to an optical density (OD) of 0.8 (λ= 590 nm). The bacterial culture was centrifuged at 4000 RPM for 10 minutes at 4°C, washed in PBS, and resuspended in minimal medium E supplemented with 0.2% glucose and 1 µg/mL vitamin B1 (medium E++) [189]. The bacterial culture was then diluted to a concentration of 2 x 10^5 colony forming units (CFU)/mL in medium E++.

SET-M33_PEG5000 NPs were solubilized in medium E++ to final peptide concentrations of 24 μM, 12 μM and 6 μM. In a 96-well plate, 100 μL of bacterial culture was added to 100 μL of NPs loaded with SET-M33 peptide at different concentrations; 100 μL of bacterial culture plus 100 μL of medium E++, and 100 μL of bacterial culture plus 100 μL of unloaded NPs, were used as controls. The plate was incubated at 30 °C. After 24, 48 and 72 hours, an aliquot from each well was withdrawn and plated in an LB agar plate for the bacterial colony count. Statistically significant differences between groups were evaluated by one-way ANOVA with Dunnett's multiple comparison test using GraphPad Prism 5.03 software.

IN VITRO ANTIBIOFILM ACTIVITY OF FREE SET-M33 AND SET-M33_PEG5000 NPS

P. aeruginosa (ATCC 27853™) biofilm was produced using special microtiter plates with lids bearing 96 pegs (Innovotech Inc., Edmonton, AB, Canada), according to a previous procedure [114; 190]. Briefly, 200 μL of the bacterial culture (1 x 10^7 cells/mL) in LB medium was transferred to each well. Plates were sealed with the peg lids, on which biofilm cells can grow, and then placed in a humidified orbital incubator at 35°C for 20 hours under agitation at 100 rpm. After biofilm formation, the peg lids were rinsed twice with PBS to remove planktonic cells, and transferred to a 96-well microtiter challenge plate, each well containing 200 μL of free SET-M33 (peptide concentrations: 24 μM, 12 μM and 6 μM), SET-M33_PEG5000 NPs (peptide concentrations: 24 μM, 12 μM and 6 μM) and unloaded NPs dissolved in minimal medium E supplemented with 0.2% glucose and 1 μg/mL vitamin B1 (medium E++) [189]. Bacteria in complete medium E++ and bacteria incubated with unloaded NPs were used as controls. The plates were incubated at 30°C for 24, 48 and 72 hours. For biomass evaluation, pegs were then washed twice with PBS and fixed in 4% paraformaldehyde (PFA) solution in PBS for 15 minutes at room temperature. Pegs were stained with 0.05% [w/v] crystal violet (CV) solution for 15 minutes. The excess CV was removed by washing the pegs with water. Finally, bound CV was released from pegs using absolute ethanol. The absorbance was measured at 600 nm using a microplate reader (VICTOR® Nivo™ Multimode plate reader, PerkinElmer), and the percentage of biofilm biomass was calculated with respect to the control (100% biofilm biomass). Statistically significant differences between groups were evaluated by one-way ANOVA with Dunnett's multiple comparison test using GraphPad Prism 5.03 software.

CITOTOXICITY OF FREE SET-M33 AND SET-M33_PEG5000 NPS

CFBE41o- and 16HBE14o- cells (obtained by Prof. Dieter Gruenert, University of California San Francisco under specific agreement) were plated at a density of 2.5 x 10^4 per well in 96-well microplates, previously incubated with coating solution (88% LHC basal medium, 10% bovine serum albumin, 30 μg/mL bovine collagen type I and 1% human fibronectin). Free SET-M33 and SET-M33_PEG5000 NPs were diluted in culture medium (Minimum Essential Medium, MEM, with Earle's salts, 10% FBS, 60 μg/mL penicillin, 100 μg/mL streptomycin and 200 μg/mL glutamine) in order to achieve final SET-M33 concentrations from 100 to 3.125 μM, and added 24 hours after plating. Cells were grown for 48 hours at 37 °C under 5% CO2. Viability was assessed with 0.1% [w/v] CV solution. Cells were fixed with 4% PFA-PBS for 15 minutes at room temperature and stained with 0.1% CV solution for 1 hour at room temperature. The cells were then solubilized with 10% acetic acid, and the absorbance was measured at 595 nm using a microplate reader (VICTOR® Nivo™ Multimode plate reader, PerkinElmer). EC_{50} values were calculated by non-linear regression analysis using GraphPad Prism 5.03 software.

IN VIVO ACUTE TOXICITY OF FREE SET-M33 AND SET-M33_PEG5000 NPS

Fifteen female 20 g BALB/c mice (Charles River Ltd.) were used for this toxicity experiment. After an acclimatization period of 4 days, the mice were divided as follows: group 1 (n = 5 mice; free SET-M33 at 10 mg/Kg), group 2 (n = 5 mice; SET-M33-loaded NPs at 10 mg/Kg), group 3 (n = 5 mice; unloaded NPs). The mice were first anesthetized intraperitoneally with Zoletil 50/50 (250 mg tielamine + 250 mg zolazepam) + nerfastin (20 mg xilazine). Then they were placed on specific mouse holders and treated with a single intratracheal (i.t.) administration of free SET-M33 (10 mg/Kg) or SET-M33_PEG5000 NPs (263 mg/Kg, corresponding to 10 mg/Kg of SET-M33) or unloaded NPs (263 mg/Kg) at a volume of 25 μL/mouse. The delivery system used for the i.t. administration was a PennCentury™ dry powder insufflator for mice (FMJ-250, Penn-Century Inc., Wyndmoor, PA, USA) [191-192]. The mice were observed for 96 hours after inoculation. They were weighed every day from arrival to the last day of the experiment. Moribund animals were killed humanely with 3.5% isoflurane and CO2 to avoid unnecessary distress. A toxicity score was assigned as follows:

wiry coat and poor motility = mild signs; very wiry coat, abundant lachrymation and poor motility even under stimulation = manifest signs.

Animal procedures of present study were approved by the Italian Ministry of Health protocol 34/2016-PR of 14 January 2016. All animal experiments complied with the ARRIVE guidelines [178] and were carried out in accordance with EU Directive 2010/63/EU for animal experiments.

RESULTS

STUDY 1: IN VIVO EFFICACY AND TOXICITY OF SET-M33 IN A MURINE MODEL OF ENDOTOXIN-INDUCED PULMONARY INFLAMMATION

TOXICITY STUDY BY INHALATION ADMINISTRATION TO CD-1 MICE FOR A WEEK

In this study we evaluated the toxicity of SET-M33 during a one-week-inhalation study in CD-1 mice. The mice (six males and six females/group) were treated with the peptide at 5 mg/kg/day, 20 mg/kg/day or vehicle only (control) by inhalation every day for 1 week. These doses were selected by preliminary studies on SET-M33 efficacy and toxicity.

ATMOSPHERE ANALYSIS AND ESTIMATION OF ACHIEVED DOSE

An aerosol administration study was performed. Atmosphere analysis, including da-ta on the concentration of peptide achieved in the aerosol, the particle size distribution in the aerosol and the estimated dose of peptide inhaled by the mice is reported in Table 1. The aerosol concentrations achieved were 87% and 117% of the target concentrations (Table 1), and the estimated inhaled doses achieved were 97% and 116% of the target doses for animals treated at 5 and 20 mg/kg/day, respectively. The mass median aerodynamic diameter (MMAD) of the droplets was slightly below for the lower dose and within the ideal range (1–3 μm) of a repeated dose inhalation study for the higher dose. For technical details and the formula used to calculate the estimated inhaled dose, see Material and Methods.

Table 1. *Atmosphere analysis and estimated inhaled dose of SET-M33 peptide achieved at 5 and 20 mg/kg/day inhaled by CD-1 mice.*

Concentration (μg/L)			Particle Size		Dose (mg/kg/Day)	
Target	Achieved		MMAD (μm)	σg	Target	Estimated Achieved Inhaled
	Mean	SD				
79	68.5	17.8	0.8	2.3	5	4.34
318	371	25.4	1.4	2.5	20	23.1

Abbreviation: SD = Standard deviation; MMAD = Mass Median Aerodynamic Diameters; σg = geometric standard deviation.

From now on throughout the article, the doses administered will be indicated as 4.34 mg/kg/day and 23.1 mg/kg/day.

CLINICAL OBSERVATIONS

During the administration period, the animals were inspected visually at least twice daily for evidence of ill health or reaction to treatment. Clinical condition, body weight, food consumption, organ weight, macropathology, histopathology and toxicokinetic were observed. The weight of each animal was recorded twice during the study and before necropsy.

There were no mortalities. Clinical signs in animals given 23.1 mg/kg/day were noted after the first dose. These included decreased activity, unsteadiness, cold to touch, partially closed eyelids, tremor, piloerection, hunched posture, splayed limbs and irregular breathing. The incidence and duration of the signs lessened as the study progressed. Regarding body weight, in males dosed at 23.1 mg/kg/day, group mean body weight loss (–2.2%) exceeded the loss seen in the control group (–0.32%) over days 1–8. In females, mean body weight loss was slightly less (–2.65%) than that of the control group (–4.8%). Group mean food consumption in males at 23.1 mg/kg/day was slightly less than controls (–16%). A similar effect was not seen in females. There were no effects on body weight or food consumption in animals dosed with 4.34 mg/kg/day. There was no restriction on diet supply. The weight of food supplied to each cage was recorded for the week before the treatment started and for each week throughout the study.

NECROSCOPY

In animals dosed with 23.1 mg/kg/day, group mean body weight adjusted lung and bronchi weight was higher than the controls in males and females (+5.6% and +25.61%, respectively), group mean body weight adjusted liver weight was lower than the concurrent controls in males (* $p < 0.05$) and females (–11.6% and –13.37%, respectively) and group mean body weight adjusted kidney weight was statistically significantly (* $p < 0.05$) lower than the control for males (–12.94%). In animals dosed with 4.34 mg/kg/day, group mean

body weight adjusted lung and bronchi weight was higher than the control (+5.9% and +12% for male and females, respectively).

Interstitial and granulomatous inflammation associated with perivascular infiltrate of inflammatory cells and/or alveolar inflammation was seen in the lungs of animals given 23.1 mg/kg/day, with fibrosis of the alveolar ducts in one female. Minimal interstitial inflammation was seen in two females on 4.34 mg/kg/day. Atrophy/degeneration of the olfactory epithelium and minimal-to-marked inflammatory exudate was seen in the nose/turbinates of all treated animals. In one male on 23.1 mg/kg/day, the exudate was haemorrhagic. These changes were generally associated with an increase in eosinophilic globules in the olfactory and respiratory epithelium and inflammatory cell infiltrate in the lamina propria. Minimal squamous metaplasia of the respiratory epithelium was seen in the larynx of animals on 4.34 or 23.1 mg/kg/day and was associated with minimal inflammatory cell infiltrate in most animals on 23.1 mg/kg/day and three males on 4.34 mg/kg/day. Loss of respiratory epithelial cilia at the tracheal bifurcation was observed in animals on 23.1 mg/kg/day. Macroscopically enlarged tracheobronchial lymph nodes were seen in two females on 23.1 mg/kg/day. The above changes were considered adverse only at 23.1 mg/kg/day. A summary of all these findings is reported in Table 2.

BIOANALYSIS

Blood samples were obtained from 2 animals/group/sex at day 7, immediately and 23 hours after dosing. Plasma concentrations of SET-M33 were only quantifiable in 1 out of 2 males (20.3 ng/mL) and both females (17.7 and 23.1 ng/mL) immediately after dosing at an achieved inhaled dose of 23.1 mg/kg. No quantifiable levels of the peptide were detected.

Table 2. *SET-M33-related findings in the lungs, nose/turbinates, larynx and tracheal bifurcation in CD-1 mice after treatment with inhaled peptide at 0, 4.34 and 23.1 mg/kg/day for 1 week. The findings were assigned a severity grade: minimal, slight, moderate, marked or severe.*

		Male			Female		
		0 mg/Kg/day	**4.34 mg/Kg/day**	**23.1 mg/Kg/day**	**0 mg/Kg/day**	**4.34 mg/Kg/day**	**23.1 mg/Kg/day**
SET-M33-related findings in the lungs							
Inflammation, interstitial	Minimal	0	0	1	1	2	4
	Slight	0	0	4	0	0	2
	Total	0	0	5	1	2	6
Inflammation, granulomatous	Minimal	0	0	2	0	0	3
	Slight	0	0	3	0	0	0
	Total	0	0	5	0	0	3
Infiltrate, inflammatory cell, perivascular	Minimal	0	0	2	0	1	1
	Slight	0	0	0	0	0	1
	Total	0	0	2	0	1	2
Inflammation, alveolar ducts	Minimal	0	0	2	1	0	2
	Total	0	0	2	1	0	2
Fibrosis, alveolar ducts	Minimal	0	0	0	0	0	1
	Total	0	0	0	0	0	1
SET-M33-related findings in the nose/turbinates							
Atrophy/degeneration, olfactory epithelium	Minimal	0	2	1	1	4	0
	Slight	0	4	5	0	2	3
	Moderate	0	0	0	0	0	3
	Total	0	6	6	1	6	6
Inflammatory exudate	Minimal	0	4	0	0	0	2
	Slight	0	0	2	0	0	0
	Moderate	0	0	3	0	0	3
	Marked	0	0	0	0	0	1
	Total	0	4	5	0	0	6
Eosinophilic globules, olfactory epithelium	Minimal	0	6	3	0	6	3
	Total	0	6	3	0	6	3
Eosinophilic globules, respiratory epithelium	Minimal	0	3	3	0	6	2
	Total	0	3	3	0	6	2
Infiltrate, inflammatory cell, lamina propria	Minimal	0	1	2	0	3	2
	Slight	0	1	0	0	2	2

	Moderate	0	0	0	0	0	1
	Total	0	2	2	0	5	5
Haemorrhage	Moderate	0	0	1	0	0	0
	Total	0	0	1	0	0	0
SET-M33-related findings in the larynx							
Squamous metaplasia	Minimal	0	4	6	0	6	6
	Total	0	4	6	0	6	6
Infiltrate, inflammatory cell	Minimal	0	3	4	0	0	5
	Total	0	3	4	0	0	5
SET-M33-related findings at the tracheal bifurcation							
Loss of cilia, point of bifurcation	Minimal	0	0	2	1	0	3
	Total	0	0	2	1	0	3

EFFICACY OF SET-M33 ON ENDOTOXIN (LPS)-INDUCED LUNG INFLAMMATION

Vehicle (0.9% saline solution) or 0.5, 2, 5 mg/kg SET-M33 or 1 mg/kg budesonide (positive control) was administered intratracheally to male BALB/c mice (10 animals/group) approximately 30 min prior to saline or the LPS challenge (0.5 mg/mL). Budesonide is a corticosteroid drug administered clinically by inhalation to reduce inflammation of the lungs in cases of acute asthma [38]. The animals were sacrificed 4 hours after the LPS challenge, and bronchoalveolar lavage (BAL) was performed. Total and differential cell counts were carried out in the BAL fluid recovered from the mice, and levels of cytokines IL 6, IP-10, KC, MCP-1, MIP-1α and TNF-α were quantified in BAL supernatant. There were no mortalities. Clinical signs showed dose dependency in severity and onset. All animals in groups dosed at 2 and 5 mg/kg showed clinical signs (piloerection and labored breathing) 1 hour post-dose (immediately after the challenge); however clinical signs did not improve before termination. Group dosed at 0.5mg/kg/day showed no clinical signs during the experimental procedures.

TOTAL AND DIFFERENTIAL CELL COUNTS IN BAL

The LPS challenge resulted in a statistically significant increase in the BAL total cell count, neutrophils, eosinophils and lymphocytes and a significant decrease in mononuclear cells compared with vehicle-treated saline-challenged mice (Figure 19). Intratracheal administration of SET-M33 at 0.5 and 2 mg/kg produced a statistically significant decrease in the BAL total cell count (Figure 19 A), neutrophils (Figure 19 B) and lymphocytes (Figure 19 E), a significant increase in mononuclear cells (Figure 19 D) and no significant effect on eosinophils (Figure 19 C) compared with the vehicle-treated LPS-challenged mice. SET-M33 at 5 mg/kg produced a statistically significant decrease in neutrophils (Figure 19 B), a significant increase in mononuclear cells (Figure 19 D) and no significant effect on the BAL total cell count (Figure 19 A), lymphocytes (Figure 19 E) and eosinophils (Figure 19 C) compared with vehicle-treated LPS-challenged mice. The maximum inhibition of neutrophil cell infiltrate was recorded at all three doses of SET-M33 (Figure 19 B), which resulted in an equivalent to steroid efficacy, but a dose-dependent increase in BAL mononuclear cells

(macrophages) was recorded after the administration of SET-M33 (0.5, 2 and 5 mg/kg) (Figure 19 D). Budesonide at 1 mg/kg produced a significant decrease in neutrophils (Figure 19 B) and a marked decrease in the BAL total cell count, which did not quite reach statistical significance with respect to vehicle-treated LPS-challenged mice (Figure 19 A).

BAL CYTOKINE LEVELS

The LPS challenge resulted in a statistically significant increase in the BAL concentrations of IL-6, IP-10, KC, MCP-1, MIP-1α and TNF-α compared with vehicle-treated saline-challenged mice (Figure 20). SET-M33 at 0.5 mg/kg produced significant inhibition of IP-10 (Figure 20 B), MCP-1 (Figure 20 D) and MIP-1α (Figure 20 E) and no significant effect on IL-6 (Figure 20 A), KC (Figure 20 C) or TNF-α (Figure 20 F). The same was found for SET-M33 at 2 mg/kg (Figure 20 A–E) except that TNF-α was significantly inhibited (Figure 20 F). SET-M33 at 5 mg/kg produced significant inhibition of five cytokines (IP-10, KC, MCP-1, MIP-1α and TNF-α; Figure 20 B–F), and a significant increase in IL-6 (Figure 20 A). The inhibitory effect of SET-M33 on pro-inflammatory cytokines was clearly dose-dependent for KC, TNF-α and MIP-1α (Figure 20 C, E, F). Inhibition of IP-10 and MCP-1 after administration of SET-M33 at all doses was similar to that recorded after budesonide. SET-M33 administration at 5 mg/kg proved more effective than steroid (budesonide 1 mg/kg) in inhibiting MIP-1α and TNF-α. Budesonide 1 mg/kg significantly inhibited all the cytokines tested.

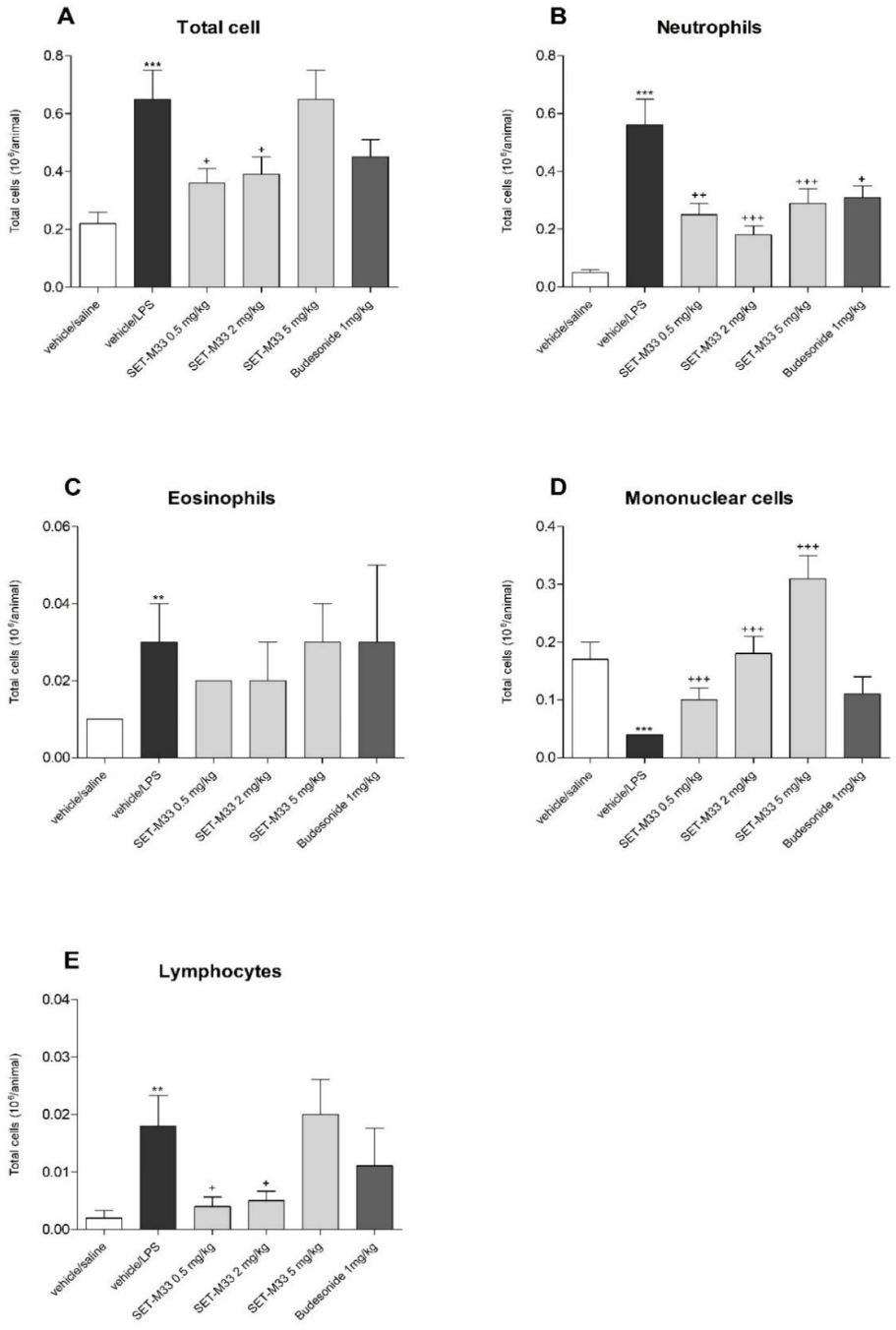

Figure 19. *Effect of vehicle, SET-M33 (0.5, 2 and 5 mg/kg) and budesonide (1 mg/kg) on BAL total cell (A), neutrophils (B), eosinophils (C), mononuclear cells (D) and lymphocytes (E) (group mean values ± s.e.m.) in LPS-induced lung inflammation. Significant differences between groups are indicated as follows: *** $p < 0.001$ and ** $p < 0.01$ Vehicle/LPS versus Vehicle/Saline; +++ $p < 0.001$, ++ $p < 0.01$ and + $p < 0.05$ drug-treated groups versus Vehicle/LPS. Groups were compared by the Student's t test. The graphs were plotted using GraphPad Prism for Windows version 5.03, GraphPad Software, San Diego, California, USA.*

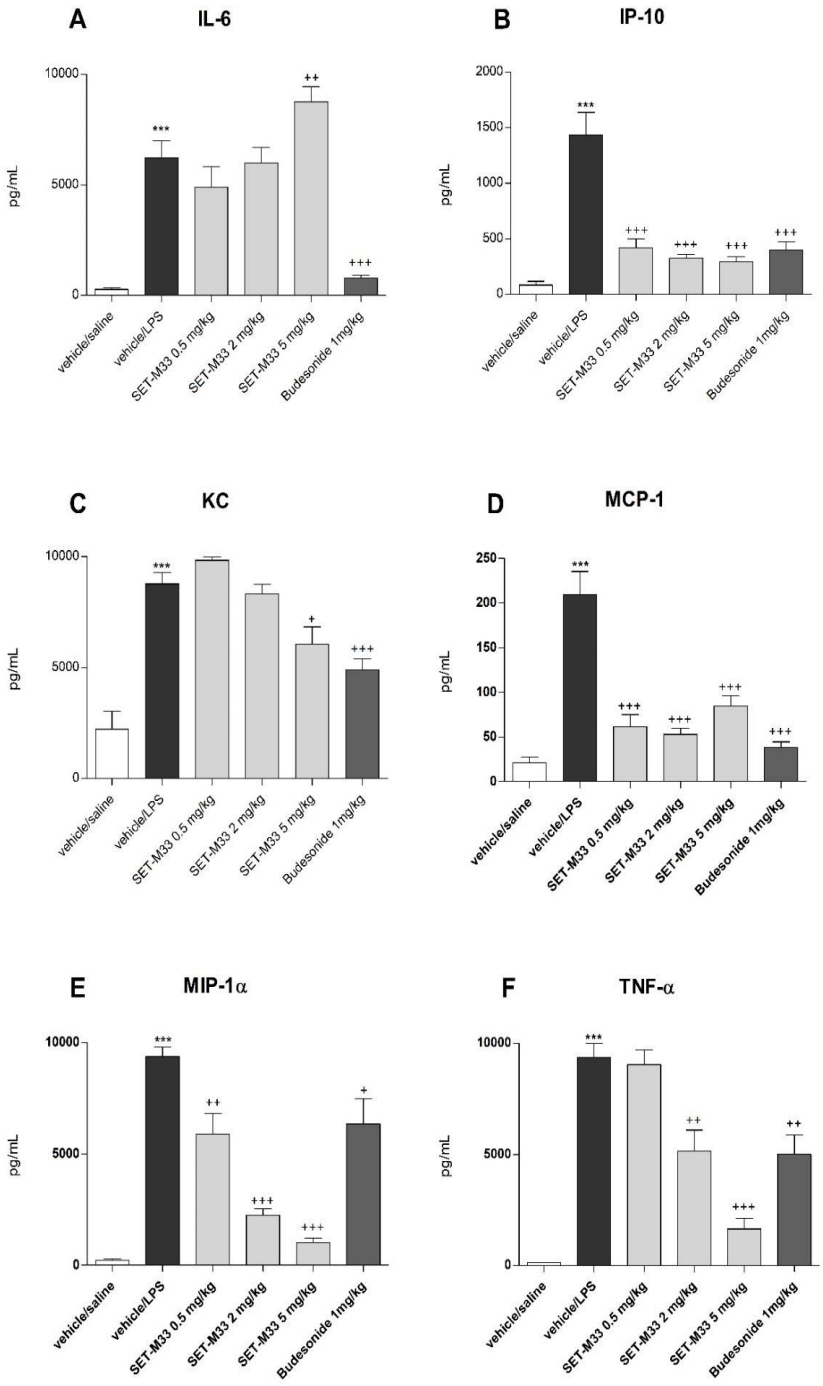

Figure 20. *Effect of vehicle, SET-M33 (0.5, 2 and 5 mg/kg) and budesonide (1 mg/kg) on BAL levels of cytokines IL-6 (A), IP-10 (B), KC (C), MPC-1 (D), MIP-1α (E) and TNF-α (F) (group mean values ± s.e.m.) in LPS-induced lung inflammation. Significant differences between groups are indicated as follows: *** $p < 0.001$ Vehicle/ LPS versus Vehicle/Saline; +++ $p < 0.001$, ++ $p < 0.01$ and + $p < 0.05$ drug-treated groups versus Vehicle/LPS. Groups were compared by the Student's t test. The graphs were plotted using GraphPad Prism for Windows version 5.03, GraphPad Software, San Diego, California USA.*

STUDY 2: SAFETY EVALUATIONS OF SET-M33 ANTIMICROBIAL PEPTIDE ADMINISTERED INTRAVENOUSLY IN RATS AND DOGS

DOSE RANGE FINDING (DRF) IN RATS

The purpose of this study was to determine the DRF of SET-M33 peptide when administered by intravenous bolus to Sprague Dawley rats. In order to identify a starting point for DRF, in Phase I of this study the peptide was administered once daily for 3 days at a constant dose of 20 mg/kg/day to six animals (three males and three females). Detailed observations were made daily during dosing: decreased or increased activity, circling, slow breathing, partially closed eyelids, swollen eyelids, abnormal uncoordinated gait, reduced body tone and hunched posture were observed in treated animals in the first 5 minutes. No clinical signs were recorded in any animal 20-60 minutes after administration. Body weight of all animals in Phase I remained constant or decreased slightly during treatment.

Phase II, where 10 animals/group (5 males and 5 females) were used, included a control group and two dose groups (10 mg/kg/day and 20 mg/kg/day), that were injected once daily for seven days. Moderate clinical signs, such as partially closed eyelids, not perfectly coordinate gait and hunched posture, were observed at 10 mg/kg/day. At 20 mg/kg/day, additional clinical signs, including decreased activity, irregular and/or slow breathing, piloerection, partially closed eyelids, abnormal uncoordinated gait, reduced body tone and hunched posture, were observed during the 7 days. The mean body weight of males treated with 10 and 20 mg/kg/day declined slightly (6% and 5% less than control group, respectively). Female body weight was unaffected by treatment. All animals survived both phases.

CLINICAL LABORATORY INVESTIGATIONS

Clinical haematology, biochemistry and urinalysis parameters were evaluated in animals in Phase II at the end of the treatment period. A complete list of parameters is reported in Materials and Methods. Administration of SET-M33 at 10 and 20 mg/kg/day for 7 days caused a statistically significant decrease of reticulocytes in males and females. SET-M33

caused a significant dose-related increase in creatinine levels in both sexes at 10 and 20 mg/kg/day and a significant increase in urea levels in both sexes at 20 mg/kg/day. There were significant differences in other parameters, such as glucose (males at 10 and 20 mg/kg/day), cholesterol (males at 20 mg/kg/day), triglycerides (females at 20 mg/kg/day), electrolytes, total protein and albumin (males at 20 mg/kg/day). Increased urine volume and lower specific gravity compared to the control group was recorded in both sexes at both doses. Differences were statistically significant for specific gravity in all cases and for volume in females at 20 mg/kg/day. Group mean values (± standard deviation) of significant changes are reported in Table 3.

Table 3. *Group mean values of significant changes obtained in haematology, clinical biochemistry and urinalysis tests (group mean values ± standard deviation) in male and female rats treated intravenously once daily for seven days with 0 (vehicle=0.9% saline solution), 10 and 20 mg/kg/day of SET-M33 peptide.*
*Abbreviations: Retic = reticulocyte count (absolute and relative), Creat = creatinine, Gluc = glucose, Chol = total cholesterol, Trig = triglycerides, Na = sodium, K = potassium, Cl = chloride, Ca = calcium, Phos = inorganic phosphorus, Total Prot = total protein, Alb = albumin, SG1 = specific gravity, Vol = volume. Significant differences between peptide vs control groups are expressed at 5% (*p<0.05) or 1% (**p<0.01) level. For statistical analysis, Dunnett, Shirley or Williams tests were used.*

Sex	Dose (mg/kg/day)	HAEMATOLOGY		CLINICAL BIOCHEMISTRY												URINALYSIS	
		Retic ($x10^{12}$/L)	**Retic (%)**	**Urea (mmol/L)**	**Creat (µmol/L)**	**Gluc (mmol/L)**	**Chol (mmol/L)**	**Trig (mmol/L)**	**Na (mmol/L)**	**K (mmol/L)**	**Cl (mmol/L)**	**Ca (mmol/L)**	**Phos (mmol/L)**	**Total Prot (g/L)**	**Alb (g/L)**	**SG1**	**Vol (mL)**
Male	0	0.112 ±0.0088	1.46 ±0.131	4.82 ±0.537	24 ±1.9	12.58 ±1.155	2.49 ±0.213	0.81 ±0.16	134 ±1.1	4.4 ±0.26	93 ±1.2	2.48 ±2.48	2.51 ±0.106	55 ±1.2	30 ±1.8	1.0299 ±0.006	7 ±1.8
	10	0.037** ±0.007	0.46** ±0.1	5.46 ±0.756	41** ±2.9	8.73** ±1.741	2.79 ±0.29	0.73 ±0.139	136** ±1.3	4.0* ±0.18	96** ±1.3	2.38** ±0.036	2.31** ±0.098	57 ±1.2	31 ±1	1.0163** ±0.0044	11 ±4.5
	20	0.027** ±0.007	0.33** ±0.096	8.52** ±1.286	62** ±3.3	7.64** ±0.650	3.46** ±0.325	0.85 ±0.183	136** ±0.4	4.1* ±0.29	96** ±0.6	2.54* ±0.033	2.26** ±0.081	62** ±1.3	34** ±1.6	1.0197** ±0.0043	13 ±7.6
Female	0	0.086 ±0.0109	1.14 ±0.179	4.77 ±1.894	27 ±2.4	8.31 ±1.051	2.52 ±0.448	0.57 ±0.213	137 ±1.2	3.8 ±0.24	97 ±1.5	2.44 ±0.073	1.92 ±0.138	57 ±4	35 ±1.9	1.0328 ±0.0173	5 ±3
	10	0.065 ±0.0266	0.85 ±0.323	5.79 ±0.971	46** ±6	7.57 ±0.884	2.99 ±0.241	0.75 ±0.127	136 ±1.1	3.6 ±0.21	97 ±1.1	2.46 ±0.079	1.96 ±0.187	61 ±2.8	34 ±1.5	1.0154* ±0.0079	18 ±8.4
	20	0.043** ±0.008	0.57** ±0.143	7.63* ±1.941	57** ±9.7	7.15 ±1.529	3.09 ±0.574	0.93* ±0.213	136 ±0.5	3.6 ±0.36	97 ±2	2.5 ±0.54	2.05 ±0.26	60 ±3	33 ±0.9	1.0142* ±0.0045	20* ±14.8

NECROSCOPY

A gross necroscopy examination was performed on Phase I animals. A full necroscopy was performed on all Phase II animals. Organs were collected and weighed. No treatment-related findings were recorded at the end of Phase I. After Phase II, pale kidneys were observed in one female at 10 mg/kg/day and two females at 20 mg/kg/day. Dilated pelvis was observed in one male at 10 mg/kg/day. Higher kidney weight was recorded in both sexes at 20 mg/kg/day (26% and 36% increase with respect to the control group for males and females, respectively). A statistically significant dose-related decrease in heart weight was recorded in treated males compared to the control group. Prostate, seminal vesicles and coagulating gland weight from males dosed at 20 mg/kg/day was significantly lower than in the control group; no differences were recorded in the weight of the testes.

BIOANALYTIC AND TOXICOKINETIC STUDY

SET-M33 concentration was determined after administration by intravenous bolus for 7 days at 10 mg/kg/day and 20 mg/kg/day. Exposure parameters (AUC_t and C_{max}) were compared in order to evaluate dose-dependency, accumulation ratio and sex-related differences. On day 1, SET-M33 profiles showed quantifiable concentrations until 1 hour post-dose and on day 7, until 0.5-1 hours for 10 mg/kg/day and up to 24 hours for 20 mg/kg/day. Mean plasma levels of SET-M33 increased in parallel with dose in males and females. Mean time to maximum concentrations (t_{max}) were observed immediately after administration, 5 minutes post-dose for both periods (days 1 and 7) and sexes, coherently with intravenous bolus administration. On day 1, mean AUC_t and C_{max} values for the low vs high dose were close to the theoretical ratio of 2 (values: 2.2 for AUC_t and 2.4 to 2.7 for C_{max}). On day 7, mean AUC_t and C_{max} values for the low vs high dose were higher than the theoretical ratio of 2 (values: 9.8-14.0 for AUC_t and 2.8-7.2 for C_{max}). At 20 mg/kg, exposure to SET-M33 was higher on day 7 than on day 1, whereas no accumulation or low accumulation was observed at 10 mg/kg. Mean SET-M33 exposures were comparable for males and females in all groups and on days 1 and 7 (data not shown)

FOUR-WEEK TOXICITY STUDY WITH 2-WEEK RECOVERY PERIOD IN RATS

The purpose of this study was to evaluate the toxic effects of SET-M33 when administered intravenously to Sprague Dawley rats for 4 weeks. Recovery was evaluated during a 14-day drug-free period. The peptide was administered once a day at three dose levels at 5, 9 and 15 mg/kg/day, and the control group was treated with the vehicle (10 males and 10 females per group which were sacrificed after four weeks for clinical and necroscopy analyses; 5 males and 5 females for the control and 15 mg/kg/day groups which were sacrificed after the 2 weeks recovery period). The higher dose was selected on the basis of the DRF study (above) in which evident toxicity was recorded at the dose of 20 mg/kg. The efficacy dose in mouse is 5 mg/kg [174]. The lowest dose of this test is approximately twice the equivalent efficacy dose in rat (using body surface area) and the intermediate dose is approximately the geometric mean of the other two.

Mortality was only recorded at 15 mg/kg/day. One male died on day 8 and one male and one female were euthanized for animal welfare reasons on days 6 and 10 of the recovery period, respectively, after showing various clinical signs (hunched back, abnormal gait and pallor) and weight loss of 14% and 11%, respectively. SET-M33-related effects consisting of decreased motor activity, irregular breathing, piloerection, closed or partially closed eyelids, abnormal gait and hunched back were recorded in animals treated at 15 mg/kg/day just after administration for the whole treatment period (as in the DRF study above). From day 8 of recovery onwards, hunched back and pallor were observed in animals treated at 15 mg/kg/day. Among animals that had to be sacrificed for welfare reasons, abnormal gait, partially closed eyelids (the male) and decreased motor activity and piloerection (the female) were also recorded from day 3 onwards. Effects on body weight were observed mainly in males during the treatment period. During the recovery period, body-weight loss (between 2% and 14% based on individual values) was recorded in some animals dosed at 15 mg/kg/day.

CLINICAL LABORATORY INVESTIGATIONS

Blood, coagulation, biochemistry and urinalysis parameters were evaluated at the end of treatment and at the end of recovery. A complete list of parameters can be found in Materials and Methods. A dose-related decrease in red blood parameters (haematocrit, haemoglobin, red blood cells and reticulocyte count) was noted in males and females at all dose levels, but was most pronounced at 15 mg/kg/day. Differences in other parameters, such as mean corpuscular haemoglobin (MCH), mean corpuscular haemoglobin concentration (MCHC), mean corpuscular volume (MCV) and haemoglobin concentration distribution width (HDW) were also observed, mainly at doses of 9 and 15 mg/kg/day. A significant increase in white blood cells (WBC), mainly due to an increase in lymphocyte and large unstained cell (LUC) count was recorded at 15 mg/kg/day, in both sexes. Platelet count was significantly higher than in the control group at all doses in males and females. Differences were dose-related. A slight increase in prothrombin time (SPT) and a decrease in activated partial thromboplastin time (SAPT) were recorded in both sexes at 9 and 15 mg/kg/day (Table 4). The effects on red blood cell parameters were not reversible after 2 weeks of recovery, whereas the effect on lymphocyte count seemed to be reversible, as no significant differences compared to control were recorded in males or females (Table 4). A significant dose-related increase in alkaline phosphatase was recorded at all dose levels in animals treated at 9 and 15 mg/kg/day. Increased gamma-glutamyl-transferase (gGT) was also observed in females at 9 and 15 mg/kg/day. A sharp dose-related effect on urea and creatinine was recorded at all doses, being statistically significant in all cases except in females at 9 mg/kg/day. Urea levels were more than 4 times control group values at 15 mg/kg/day. Creatinine values were more than 6 times control group values at 15 mg/kg/day. A significant decrease in albumin levels (and in total protein levels in males) was observed at 15 mg/kg/day (Table 4bis). Differences in alkaline phosphatase, gGT (mainly in females), bilirubin, urea and creatinine values had not reversed after two weeks of recovery.

A higher dose-related volume of urine than in the control group was observed at all doses. The specific gravity recorded in all SET-M33-treated groups was lower than in controls. Differences were statistically significant except for volume in females at 5 mg/kg/day. Creatinine levels lower than in controls were recorded at all doses. Differences were dose-related in females. The protein levels recorded in males from all SET-M33-treated groups

were significantly lower than in controls. Statistically significant differences in glucose increase were found in animals treated at 15 mg/kg/day. Differences observed at the end of treatment persisted at the end of the recovery period. Group mean values of significant changes are reported in Table 4 and Table 4(bis).

Table 4. *Major changes obtained in haematology and coagulation measurements (group mean values ± standard deviation) in male and female rats treated intravenously for 4 weeks and 2 weeks of recovery period with 0 (vehicle= 0.9% saline solution), 5, 9 and 15 mg/kg/day of SET-M33 peptide. Abbreviations: Hct = haematocrit, Hb = haemoglobin, RBC = erythrocyte count, Retic = reticulocyte count (absolute and relative), MCH = mean corpuscular haemoglobin, MCHC = mean corpuscular haemoglobin concentration, MCV = mean corpuscular volume, WBC = leukocyte count, total, HDW = haemoglobin concentration distribution width, L = lymphocytes, LUC = large unstained cells, Plt = platelet (thrombocyte) count, SPT = prothrombin time, SAPT = activated partial thromboplastin time. Significant differences between peptide vs control groups were expressed at the 5% (*p<0.05) or 1% (**p<0.01) level. For statistical analysis, Dunnett, Shirley' Williams, Wilcoxon and t-tests were used.*

Sex	Dose (mg/kg/day)	HAEMATOLOGY AND COAGULATION WEEK 4 OF TREATMENT - GROUP MEAN VALUES														
		Hct (L/L)	Hb (g/dL)	RBC ($x10^{12}$/L)	Retic ($x10^{12}$/L)	Retic (%)	MCH (pg)	MCHC (g/dL)	MCV (fL)	WBC ($x10^{9}$/L)	HDW (g/dL)	L ($x10^{9}$/L)	LUC ($x10^{9}$/L)	Plt ($x10^{9}$/L)	SPT (sec)	SAPT (sec)
Male	0	0.454 ±0.0145	15.3 ±0.45	8.49 ±0.32	0.139 ±0.0233	1.64 ±0.253	18.00 ±0.49	33.70 ±0.71	53.50 ±0.79	10.00 ±1.761	2.94 ±0.097	8.67 ±1.283	0.08 ±0.022	779 ±143.1	23.0 ±6.54	37.6 ±5.65
	5	0.401** ±0.0198	13.5** ±0.48	7.55** ±0.306	0.152 ±0.0283	2.00* ±0.352	17.90 ±0.38	33.80 ±0.76	53.00 ±1.15	10.76 ±1.713	3.21** ±0.126	9.73 ±1.418	0.08 ±0.027	917* ±95.4	21.8 ±0.82	36.5 ±6.18
	9	0.348** ±0.0275	11.9** ±0.84	6.81** ±0.538	0.076** ±0.0292	1.10** ±0.357	17.40* ±0.39	34.20 ±0.73	51.0** ±1.71	11.36 ±2.206	3.30** ±0.174	10.30 ±2.104	0.10 ±0.049	923* ±148.7	24.1** ±0.68	31.6* ±5.31
	15	0.311** ±0.0158	10.7** ±0.58	6.15** ±0.322	0.037** ±0.0091	0.60** ±0.160	17.50* ±0.47	34.6** ±0.50	50.50** ±0.77	13.51** ±2.506	3.23** ±0.151	12.35** ±2.216	0.14** ±0.053	961** ±130.1	24.5** ±1.05	31.9* ±5.11
Female	0	0.416 ±0.0133	14.1 ±0.47	7.62 ±0.23	0.176 ±0.0445	2.31 ±0.52	18.50 ±0.40	33.80 ±0.73	54.70 ±1.64	7.30 ±2.064	2.76 ±0.096	6.25 ±2.013	0.05 ±0.023	853 ±204.900	21.9 ±1.150	37.0 ±5.260
	5	0.382** ±0.0127	12.9** ±0.46	7.11** ±0.291	0.180 ±0.0473	2.55 ±0.712	18.20 ±0.40	33.90 ±0.43	53.70 ±0.91	7.11 ±0.596	2.92 ±0.127	6.31 ±0.710	0.05 ±0.011	1004* ±115.600	21.9 ±0.660	33.1 ±5.900
	9	0.352** ±0.0199	12.0** ±0.48	6.61** ±0.358	0.112** ±0.0462	1.69* ±0.646	18.10 ±0.43	34.00 ±0.80	53.30* ±0.76	9.15 ±2.982	3.34** ±0.189	7.91 ±2.475	0.08** ±0.038	1075** ±136.70	23.6** ±1.00	26.7** ±3.890
	15	0.284** ±0.0223	9.7** ±0.75	5.44** ±0.488	0.060** ±0.0162	1.12** ±0.345	17.9** ±0.48	34.20 ±0.33	52.3** ±1.44	10.34** ±1.917	2.99** ±0.199	9.22** ±1.713	0.09** ±0.019	1250** ±181.00	23.3** ±1.270	25.6** ±5.910
Sex	**Dose (mg/kg/day)**	**HAEMATOLOGY AND COAGULATION WEEK 2 OF RECOVERY - GROUP MEAN VALUES**														
		Hct (L/L)	**Hb (g/dL)**	**RBC ($x10^{12}$/L)**	**Retic ($x10^{12}$/L)**	**Retic (%)**	**MCH (pg)**	**MCHC (g/dL)**	**MCV (fL)**	**WBC ($x10^{9}$/L)**	**HDW (g/dL)**	**L ($x10^{9}$/L)**	**LUC ($x10^{9}$/L)**	**Plt ($x10^{9}$/L)**	**SPT (sec)**	**SAPT (sec)**
Male	0	0.450 ±0.0136	15.2 ±0.4	8.73 ±0.359	0.122 ±0.0091	1.40 ±0.13	17.4 ±0.61	33.8 ±0.74	51.6 ±0.8	9.86 ±1.818	3.03 ±0.075	8.39 ±1.371	0.08 ±0.026	722 ±58.2	21.5 ±0.63	20.3 ±3.44
	15	0.262** ±0.0197	9.5** ±0.55	5.36** ±0.37	0.061* ±0.412	1.16 ±0.797	17.7 ±0.47	36.1** ±0.98	49.0 ±2.37	6.84* ±1.913	3.25* ±0.16	6.12 ±1.655	0.05 ±0.034	919* ±169.1	21.1 ±0.67	13.3* ±3.41
Female	0	0.431 ±0.0097	15 ±0.29	8.04 ±0.097	0.083 ±0.0311	1.03 ±0.385	18.7 ±0.29	34.9 ±0.31	53.6 ±1.07	7.47 ±1.792	2.64 ±0.102	6.16 ±1.375	0.06 ±0.014	819 ±135	22.4 ±0.33	20.4 ±1.8
	15	0.268** ±0.0087	9.3** ±0.34	5.31** ±0.139	0.063 ±0.0254	1.17 ±0.458	17.5** ±0.62	34.7 ±0.5	50.6** ±1.15	7.89 ±1.712	3.04** ±0.167	6.58 ±1.708	0.05 ±0.018	1208** ±106.8	22.9 ±0.79	16.8* ±1.37

Table 4. (bis) *Major changes in biochemical and urine parameters (group mean values ± standard deviation) in male and female rats treated intravenously for 4 weeks, followed by a 2-week recovery period with 0 (vehicle= 0.9% saline solution), 5, 9 and 15 mg/kg/day of SET-M33 peptide. Abbreviations: ALP = alkaline phosphatase, gGT = gamma-glutamyl-transferase, Creat = Creatinine, Na = sodium, Cl = chloride, Ca = calcium, Phos = inorganic phosphorus, Total Prot = total protein, Alb = albumin, SG1 = specific gravity, Vol = volume, Prot = protein, U-Creat = creatinine, U-Gluc = glucose. Significant differences between peptide vs control groups were expressed at the 5% (*p<0.05) or 1% (**p<0.01) level. For statistical analysis the Dunnett, Shirley, Williams, Wilcoxon and t-tests were used.*

Sex	Dose (mg/kg/day)	BIOCHEMISTRY WEEK 4 OF TREATMENT - GROUP MEAN VALUES										URINALYSIS WEEK 4 OF TREATMENT - GROUP MEAN VALUES				
		ALP (U/L)	gGT (U/L)	Urea (µmol/L)	Creat (µmol/L)	Na (mmol/L)	Cl (mmol/L)	Ca (mmol/L)	Phos (mmol/L)	Total Prot (g/L)	Alb (g/L)	SG1	Vol (mL)	Prot (g/L)	U-Creat (µmol/L)	U-Gluc (mmol/L)
Male	0	130 ±19.5	0 ±0.0	4.91 ±0.501	23 ±2.5	138 ±3.1	98 ±1.7	2.46 ±0.095	2.08 ±0.18	58 ±3.4	39 ±2.7	1.051 ±0.0194	5 ±2.2	2.51 ±1.123	12902 ±5527.3	4.31 ±2.798
	5	160** ±16.8	0 ±0.2	6.97* ±0.554	47* ±4.5	134* ±2.3	98 ±1.5	2.34* ±0.06	1.97 ±0.309	56 ±2.4	38 ±1.8	1.0214** ±0.0063	10** ±4	1.04** ±0.336	4027** ±1766.3	1.52 ±0.676
	9	187** ±28.8	0* ±0.3	11.64** ±3.171	97** ±22.8	134* ±2.4	103** ±2.2	2.13** ±0.088	2.26 ±0.393	52** ±3.3	37 ±4.4	1.0302** ±0.0219	15** ±11.3	1.54** ±1.24	4267** ±3748.6	11.22 ±14.93
	15	196** ±27.8	1** ±0.3	21.16** ±7.736	156** ±59.9	138 ±3.2	107** ±3.2	2.11** ±0.167	2.83** ±0.324	54** ±3.5	36* ±2.4	1.0182** ±0.003	26** ±11.9	0.94** ±0.402	1324** ±352.0	39.10** ±13.323
Female	0	98 ±13.7	0 ±0.0	5.91 ±0.963	31 ±3.2	134 ±1.9	97 ±1.6	2.41 ±0.066	1.84 ±0.179	56 ±3.0	41 ±3.4	1.036 ±0.0076	6 ±1.9	0.33 ±0.186	6205 ±1731.9	1.68 ±0.431
	5	111 ±14.6	0 ±0.1	6.32 ±1.258	40 ±5.8	134 ±2.2	100* ±1.6	2.33 ±0.067	1.45** ±0.201	58 ±2.7	42 ±2.2	1.0203** ±0.0072	13 ±4.4	0.30 ±0.271	2969** ±1365.2	1.00 ±0.642
	9	134** ±12.6	0 ±0.4	9.81** ±2.224	80** ±15	135 ±1.9	104** ±2.0	2.36 ±0.095	1.49 ±0.415	58 ±4.7	39 ±3.2	1.0173** ±0.0063	20* ±12	0.34 ±0.184	1654** ±667.2	7.77 ±11.212
	15	119** ±18.0	2** ±0.5	28.57** ±15.12	190** ±76.6	136 ±9.8	102** ±8.6	2.33 ±0.127	2.52* ±0.757	55 ±2.8	36** ±2.7	1.0175** ±0.0046	34** ±13.7	0.76** ±0.489	985** ±428.7	43.03** ±14.984
Sex	**Dose (mg/kg/day)**	**BIOCHEMISTRY WEEK 2 OF RECOVERY - GROUP MEAN VALUES**										**URINALYSIS WEEK 2 OF RECOVERY - GROUP MEAN VALUES**				
		ALP U/L	gGT U/L	Urea µmol/L	Creat µmol/L	Na mmol/L	Cl mmol/L	Ca mmol/L	Phos mmol/L	Total Prot g/L	Alb g/L	SG1	Vol mL	Prot g/L	U-Creat µmol/L	U-Gluc mmol/L
Male	0	122 ±10.9	0 ±0.0	6.07 ±0.61	24 ±1.1	139 ±0.8	99 ±0.7	2.6 ±0.043	1.96 ±0.122	62 ±1.6	40 ±1.4	1.0394 ±0.0302	7 ±3.2	1.65 ±1.52	11288 ±8063.3	3.38 ±4.649
	15	208** ±53.1	0 ±0.8	46.64* ±30.424	235* ±101.4	145* ±5.9	104 ±5.7	2.19** ±0.154	2.83 ±1.37	61 ±4.4	42 ±3.3	1.0131* ±0.0004	34** ±7.5	0.35* ±0.132	1339* ±134.3	27.05** ±5.353
Female	0	105 ±22.1	0 ±0.0	5.73 ±0.558	30 ±2.0	140 ±0.7	101 ±1.3	2.64 ±0.048	1.65 ±0.267	64 ±1.4	44 ±2.7	1.0508 ±0.0238	5 ±2.8	0.78 ±0.516	11012 ±4985.4	2.9 ±1.896
	15	146* ±30.0	1* ±0.8	34.83** ±16.358	179** ±63.2	143 ±4.3	103* ±1.4	2.45** ±0.054	2.04 ±0.616	63 ±2.0	43 ±1.4	1.0130* ±0.0005	34** ±4.7	0.29 ±0.206	1089* ±71.3	34.76** ±6.659

NECROSCOPY

Necroscopy and histopathological examinations were performed at the end of treatment and at the end of the recovery period. Macroscopic changes were recorded in the kidneys (pale coloration and a reddened medullary area in almost all males and females from groups on 9 and 15 mg/kg/day) and bladder (distended in a few males of all treated groups). These findings were also recorded at the end of the recovery period affecting all animals dose at 15 mg/kg/day (pale coloration of the kidneys) or one male (distended urinary bladder). The mean weight of the kidneys, liver and spleen was significantly higher with respect to control group in both sexes at all dose levels. At the end of the recovery period the mean weight of the spleen (both sexes) and the mean weight of the kidneys and ovaries (females) from animals treated at 15 mg/kg/day were still higher with respect to control group. The microscopic examination revealed that all treated animals at 15mg/Kg/day showed a severe nephropathy. Furthermore, a SET-M33-related findings were found in femorotibial growth plate, brain, duodenum and ovaries (doses of 15 and 9 mg/kg), and in bone marrow, heart, uterine cervix and vagina and mammary glands (dose of 15 mg/kg). In particular, both in the femur and sternum of 3 out of 5 males and 2 out of 5 females treated at 15 mg/kg/day, a minimal to slight increase in adipocytes was observed in the bone marrow, compared with concurrent controls. 1 out of 5 animal treated at 15 mg/kg/day showed cervical and vaginal epithelial atrophy compared to controls. For 15 mg/kg/day group, the changes observed in the kidneys, bone marrow, uterine cervix and vagina were not reversible (Figure 21), while the rest of the findings were fully (femorotibial growth plate and duodenum) or partially recovered (heart, ovaries and mammary glands) after two weeks of recovery period.

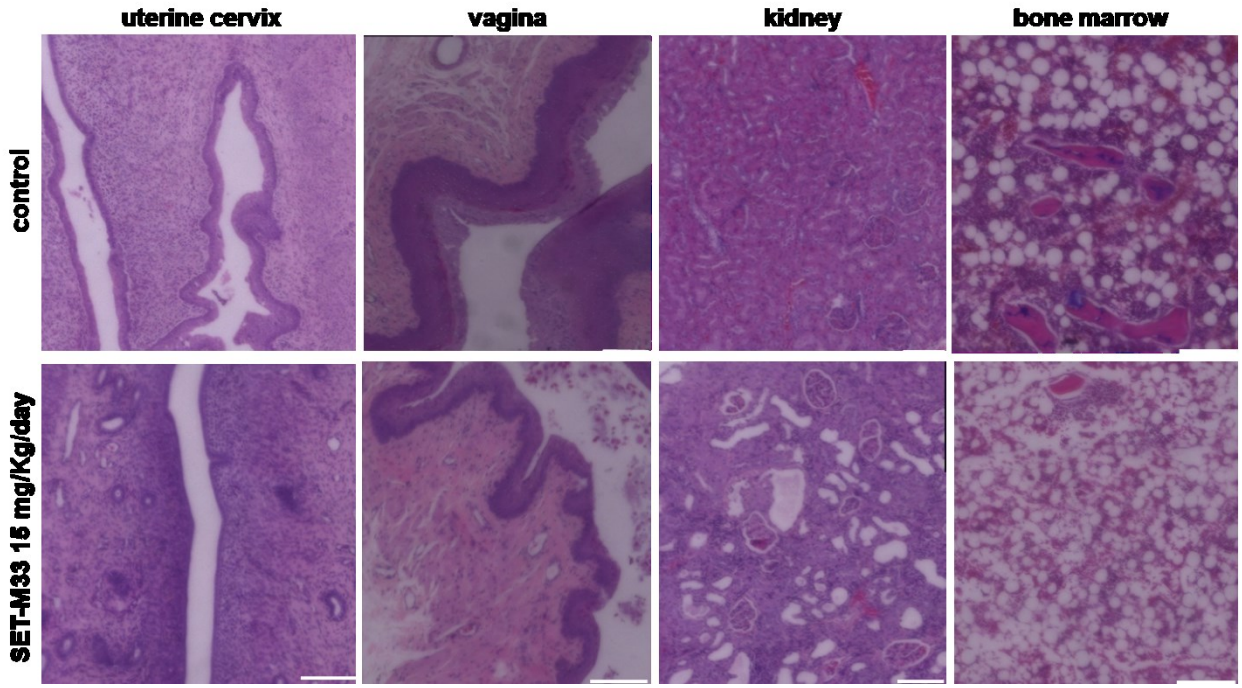

Figure 21. *Histological sections of tissues collected after 2-week recovery period of rats treated with vehicle (panels above) and SET-M33 at 15 mg/Kg/day for 28 days (panels below). In the animals treated with SET-M33 the following findings resulted evident: atrophy of the epithelial surface in uterine cervix and vagina; parenchymal degenerations in the kidney; increase of adipocytes in the femur bone marrow. Scale bars (white lines) correspond to 100 µm. Samples were examined by confocal laser microscope (Leica TCS SP8). All images were processed using ImageJ software (NIH).*

NEUROLOGICAL TOXICITY IN RATS

The purpose of this study was to evaluate the neurological side-effects of SET-M33 following a single intravenous injection of 5, 9 and 15 mg/kg and vehicle (6 animals/group). The study was based on subjective observation of central nervous system effects on general behaviour (Irwin test), combined with objective evaluation of body temperature and locomotor activity in male rats [182-183]. Effects on body weight were also assessed. Again the dose levels were selected on the basis of the DRF study reported above.

SET-M33 did not cause any adverse clinical signs during detailed observations at 5, 30, 90, 240 minutes and 24 hours post-dose. Animals were also inspected daily from day 3 to day 7 for any delayed effects. The list of parameters and observations considered in the Irwin test can be found in Materials and Methods. No delayed effects of toxicity and no mortality were recorded up to day 7.

Pre-dose group mean body temperatures were similar across groups. A single intravenous injection of SET-M33 at doses of 5, 9 and 15 mg/kg had no significant effects on body temperature when compared with control animals. Actually, significantly lower body temperatures were recorded 5 minutes post-dose in the 9 and 15 mg/kg SET-M33-treated groups compared with control animals (* $p<0.05$, ** $p<0.01$). However, since the group mean values were only 0.4-0.6 C° lower than the vehicle-treated control group, this cannot be considered biologically noteworthy (Table 5).

Pre-dose group mean locomotor activity was relatively similar across all groups. SET-M33 at doses of 5 and 9 mg/kg did not cause any effect on locomotor activity when compared with control animals. The 15 mg/kg dose caused a small transient reduction in locomotor activity at 5 minutes post-dose. However, since this effect subsided by 30 minutes and only occurred at a single time point, it was not considered to be adverse or dose-limiting (Table 5).

No statistically significant effects on body weight were recorded at any dose. Small weight losses (approximately 2-3%) were recorded in the 9 and 15 mg/kg treated groups at 24 h, compared with the weights of the previous day (not significant with respect to the control group), and were followed by increases on day 3. As these effects were very transient and small in magnitude, they were not considered adverse (Table 5).

No other adverse effects were observed for any other neurological parameter listed in Material and Methods.

Table 5. *Effects of intravenous bolus injection of SET-M33 at 0 (vehicle = 0.9% saline solution), 5, 9 and 15 mg/kg on body temperature, locomotor activity and body weight in male rats (group mean values ± standard deviation).*
 # number of times the rats entered a new square in the arena
*Statistical significance compared with vehicle: * p<0.05, ** p<0.01. The results of each treated group were compared with those of the vehicle-treated control group by analysis of variance and Williams test.*

DOSE (mg/kg)	Group mean body temperature (°C ± sd) at time post-dose:						Group mean locomotor activity (# ± sd) at time post-dose:						Group mean bodyweight (g ± sd) on day:			
	Pre-dose	5 minutes	30 minutes	90 minutes	240 minutes	24 hours	Pre-dose	5 minutes	30 minutes	90 minutes	240 minutes	24 hours	1	2	3	7
0	37.3 ±0.26	38 ±0.36	37.4 ±0.25	37.1 ±0.45	36.6 ±0.41	36.9 ±0.38	44.8 ±6.77	39.3 ±10.46	28.8 ±10.38	27.8 ±5.64	16 ±7.29	35 ±8.65	204.5 ±6.72	206 ±8.79	210.7 ±9.07	229 ±12.03
5	37.5 ±0.31	37.9 ±0.27	37.2 ±0.51	36.9 ±0.29	36.9 ±0.48	37.1 ±0.51	37.8 ±9.56	30.7 ±6.56	26.5 ±7.12	24.2 ±6.71	22.5 ±5.05	30 ±15.02	207.2 ±2.79	209 ±3.22	215.8 ±3.87	236.5 ±8.17
9	37.5 ±0.34	37.6* ±0.31	37.3 ±0.43	36.9 ±0.35	36.7 ±0.41	36.8 ±0.79	38.2 ±7.73	32.5 ±5.96	27 ±9.34	21.3 ±12.65	22.5 ±12.82	28.3 ±12.82	204.8 ±4.92	201.2 ±4.36	209.5 ±3.39	229.5 ±5.01
15	37.2 ±0.51	37.4** ±0.29	36.9 ±0.41	36.9 ±0.24	36.7 ±0.31	36.9 ±0.5	38.3 ±4.08	22.2** ±9.5	29 ±5.8	20.7 ±8.02	18.5 ±8.17	25.5 ±10.21	206 ±5.93	200.3 ±6.92	209.7 ±7.58	227 ±8.34

EVALUATION OF RESPIRATORY FUNCTION IN RATS

The possible side-effects of SET-M33 on respiratory function were evaluated after administration of the peptide as a single intravenous bolus at doses of 5, 9 and 15 mg/kg with vehicle (8 animals/group). Respiratory rate, tidal volume and minute volume were assessed. As in the case of neurological toxicity and the 4-week toxicity study, again the dose levels were selected on the basis DRF (above). Baclofen, a muscle relaxer and antispasmodic used to treat muscle pain, spasms and stiffness in people with multiple sclerosis or spinal cord injury or disease, was used as positive control. It was administered as a single intravenous injection at a dose of 15 mg/kg.

SET-M33 did not produce any statistically significant adverse effects on respiratory rate, tidal volume or minute volume with respect to control animals, except for a statistically significant increase in minute volume recorded at 30 minutes post-dose at 15 mg/kg. However, since this effect subsided by 60 minutes post-dose and only occurred at a single time point, it was not considered to be adverse or dose-limiting. Baclofen produced sharp, statistically significant increases in tidal volume and minute volume, which were accompanied by a sharp, statistically significant decrease in respiratory rate, compared with vehicle-treated control animals (Figure 22). At 30 minutes the group treated at 15 mg/kg had significantly higher minute volume than the vehicle control (p=0.019, Williams' test). At 30 and 60 minutes the group treated with the Baclofen had significantly higher minute volume than the vehicle control ($p \leq 0.014$, t-test). At all post-dose time points the group treated with Baclofen had significantly higher tidal volume than the vehicle control ($p<0.001$, t-test). At 30, 60, 90, 120, 150, 180 and 240 minutes the group treated with Baclofen had significantly lower respiration rate than the vehicle control ($p \leq 0.031$, t-test)

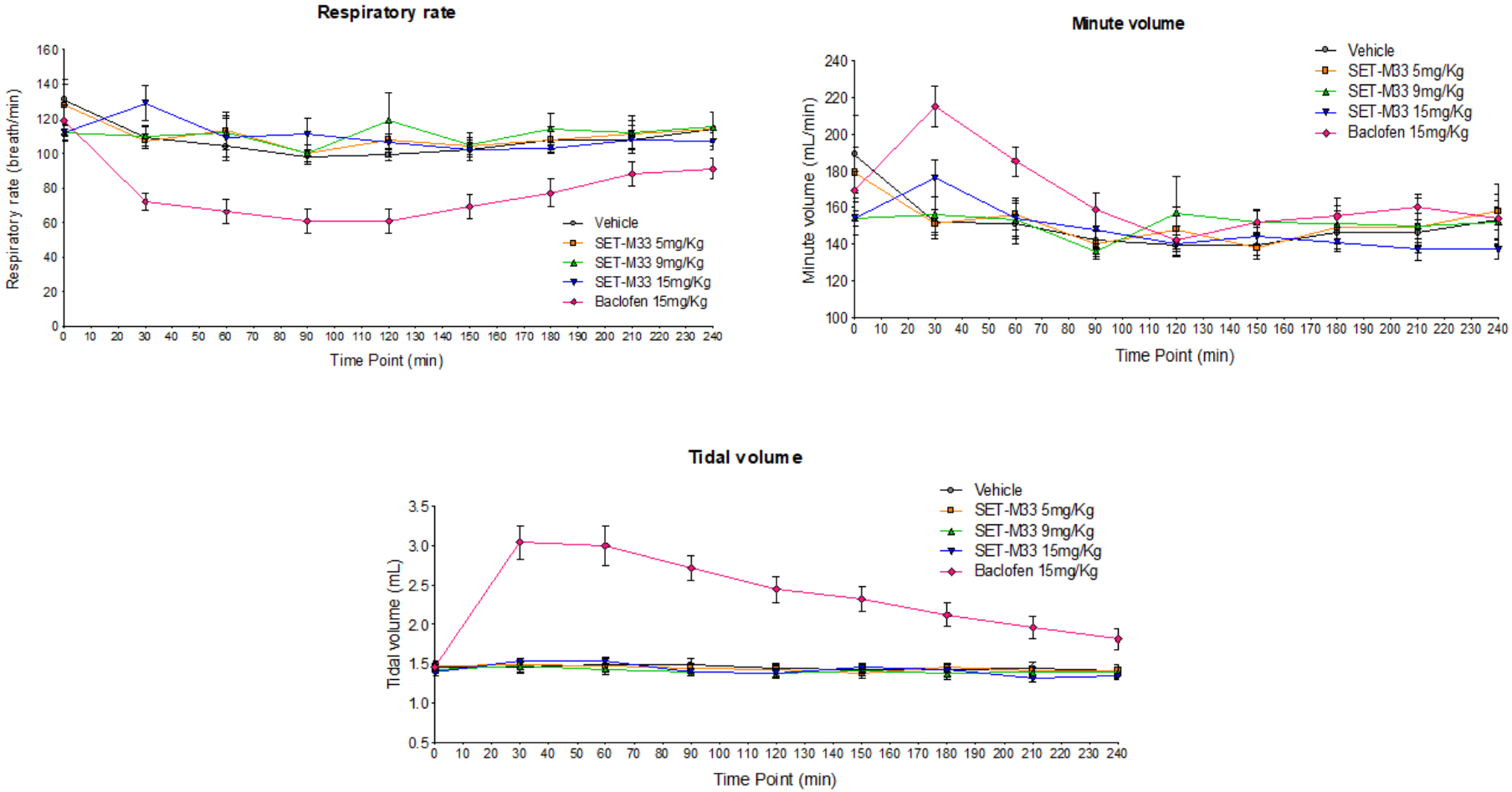

Figure 22. *Effects of intravenous injection of SET-M33 at 0 (vehicle), 5, 9 and 15 mg/kg on respiratory rate (breaths/min ± sem), tidal volume (mL ± sem) and minute volume (mL/min ± sem) in rats. Baclofen at 15 mg/day was used as positive control. Abbreviations: sem = standard error of mean. Symbols (triangle, circle, rhombus or square) indicate a group mean respiratory parameter. The bar represents the standard error. The graphs were obtained using GraphPad Prism for Windows version 5.03, GraphPad Software, San Diego, California USA, www.graphpad.com. The groups treated with SET-M33 peptide were compared to vehicle using Williams' test. The comparison between positive control and vehicle were made using two-tailed t-test based on the error mean square from the analysis of covariance.*

DOSE RANGE FINDING (DRF) IN DOGS

The purpose of this study was to conduct DRF for SET-M33 administered by short intravenous infusion (30 minutes) to beagle dogs at 4.0 and 8.0 mg/kg/day (7-day treatment period). Two animals served as control group (one male, one female), and four animals were assigned to treated groups (two males, two females). The doses were determined by a preliminary study not reported here.

The following clinical signs were reported: tremors were occasionally recorded in a male treated at 4 mg/kg (on days 4 and 5 of administration), and in a male and a female treated at 8 mg/kg (on days 5 of administration). In the males treated at 8 mg/kg, vomit was observed in the box on days 1 (both animals) and 3 (one dog). A 9.4% loss of body weight with respect to day 1 was recorded at the end of treatment in one animal of the 8 mg/kg/day group. No noteworthy effects on body weight were observed in the other dogs. All animals survived the scheduled period.

CLINICAL LABORATORY INVESTIGATIONS

Blood, coagulation, biochemical and urine parameters were evaluated pre-test and on completion of treatment. The complete list of parameters evaluated is reported in Materials and Methods. Increased urea and creatinine levels were recorded in males and females on 8 mg/kg/day (67% and 74% higher than pre-test values for males, and 26% and 21% higher than pre-test values for females, respectively). No noteworthy effects on blood and coagulation parameters were recorded. Group mean values of significant changes are reported in Table 6.

Table 6. *Major differences of urea and creatinine in clinical biochemistry values (group mean values ± standard deviation) in beagle dogs treated with intravenous 30 minutes-short infusion of SET-M33 at 0 (vehicle=0.9% saline solution), 4.0 and 8.0 mg/kg/day (7-day treatment period)***.** *Statistical analysis was not performed due to the small number of animals*

Sex	Dose (mg/kg/day)	Urea (nmol/L)		Creatinine (µmol/L)	
		Pre-dose	End of treatment	Pre-dose	End of treatment
Male	0	5.15	4.58	79	58
	4.0	4.31 ±0.849	4.92 ±0.035	84 ±18.4	77 ±2.8
	8.0	4.26 ±0.064	7.64 ±0.191	66 ±4.2	115 ±25.5
Female	0	4.57	5.2	58	58
	4.0	3.76 ±0.156	4.76 ±0.021	69 ±17.7	79 ±2.8
	8.0	6.29 ±2.15	7.94 ±0.099	85 ±23.3	103 ±0

NECROSCOPY

A full necropsy was performed in all animals. Organs were collected and weighed. No noteworthy changes in organ weight were reported for the doses tested, except for lower weight of the thymus in males on doses of 4 and 8 mg/kg/day (66 and 76% less than control, respectively).

BIOANALYTIC AND TOXICOKINETIC STUDY

Concentrations of SET-M33 in dog plasma samples and the main toxicokinetic parameters were determined. The exposure parameters (AUC_t and C_{max}) were compared to evaluate dose-dependency, accumulation ratio and sex-related differences. Overall, on day 1, SET-M33 profiles observed at doses of 4 and 8 mg/kg/day showed quantifiable concentrations until 3.5 hours after starting the infusion. In addition, one male on 8 mg/kg/day showed quantifiable concentrations at day 7 up to 24.5 hours after the start of infusion. Mean SET-M33 plasma levels increased in parallel in males and females. Mean time to maximum SET-M33 concentration (t_{max}) was after the end of infusion for both periods (days 1 and 7) and sexes, i.e. 30 minutes post-dose, coherently with intravenous administration. On day 1 and 7, mean AUC_t and C_{max} values for the low *vs* high dose were close to the theoretical ratio of 2. No accumulation or low accumulation was observed at 4 and 8 mg/kg after 7 days. Mean SET-M33 exposures were comparable for males and females in all groups on days 1 and 7,

with a male/female ratios ranging from 0.3 to 1.3 for C_{max} and from 0.4 to 1.3 for AUC_t (data not shown).

FOUR-WEEK TOXICITY STUDY WITH 4-WEEK RECOVERY PERIOD IN DOGS

Beagle dogs (5/sex/group) were dosed by intravenous infusion once daily for 1 hour with 0 (0.9% sodium chloride for injection), 0.5, 1.5 or 4.0 mg/kg/day SET-M33 for four consecutive weeks. The doses were selected in the dog DRF study (above). The dose of 4 mg/kg/day was selected as the highest dose without macroscopic side effects in the DRF study, and was used to evaluate renal toxicity and its reversibility. The dose of 0.5 mg/kg/day was selected as the lowest dose, about one order of magnitude less than the highest dose. The dose of 1.5 mg/kg/day was selected as an approximately median mid-dose. On completion of 4 weeks of infusion, three animals/sex/group were euthanized and necropsied and the remaining two animals/sex/group were held for a 4-week drug free recovery period after which they were euthanized and necropsied. Blood samples were obtained from all animals on days 1 and 28 for toxicokinetic analysis.

All animals survived until their scheduled termination and there were no noteworthy peptide-related clinical signs.

CLINICAL LABORATORY INVESTIGATIONS

Blood, coagulation, biochemical and urine parameters were evaluated. A complete list of parameters is reported in Materials and Methods. There were no SET-M33-related blood or coagulation changes at the end of treatment or in the 4-week recovery period. SET-M33-related biochemical changes at all doses in both sexes included increases in blood urea nitrogen (BUN; 25% to 64% higher than pre-test) and creatinine (14% to 50% higher than pre-test) in individual animals (data not show). The magnitude of these changes was generally similar across all dose groups. These increases were correlated with minimal renal tubule degeneration/regeneration at 1.5 mg/kg/day and 4 mg/kg/day in males and at 4.0 mg/kg/day in females and minimal interstitial cell infiltrate in both sexes at a dose of 4.0 mg/kg/day. There were no SET-M33-related biochemical changes at any dose after 4-week recovery, indicating complete recovery of the changes detected at the end of dosing. There were no SET-M33-related urine changes at 0.5 or 1.5 mg/kg/day. There were decreases in

urine specific gravity and urine creatinine concentrations with respect to individual pre-test values in individual animals on 4.0 mg/kg/day. These changes were more prominent in females and suggest more dilute urine, possibly associated with a lower concentrating ability of the kidneys. There were no SET-M33-related urine changes at any dose after the 4-week recovery period.

NECROSCOPY

Higher SET-M33-related kidney weights (absolute and relative to body and brain weight) were observed in both sexes at a dose of 4.0 mg/kg/day. These higher weights were correlated microscopically with minimal tubule degeneration/regeneration and minimal interstitial cell infiltrates. There were no other SET-M33-related organ weight changes (Table 7). There were no organ weight changes at recovery sacrifice, or macroscopic findings at terminal and recovery necroscopy. SET-M33-related microscopic findings were observed in kidneys at doses of 1.5 mg/kg/day and 4 mg/kg/day and at infusion sites at all doses. The kidney findings included minimal tubule degeneration/regeneration at 1.5 mg/kg/day and 4 mg/kg/day in males, and at 4.0 mg/kg/day in females, and minimal interstitial cell infiltrate in both sexes at a dose of 4.0 mg/kg/day. Degeneration featured vacuolation, cell sloughing and/or tinctorial change, and regeneration was characterized by increased basophilia, nuclear crowding and/or increased mitoses of cortical tubule epithelial cells. Regenerative changes were typically more pronounced than degenerative changes. SET-M33-related microscopic findings in kidney were correlated with higher kidney weights (absolute and relative to body and brain weight) and elevated BUN and creatinine in both sexes at 4.0 mg/kg/day. SET-M33-related findings were observed at all four infusion sites (different site each week) in both sexes at all doses and included vascular thrombi (minimal to high), vascular/perivascular inflammation (minimal to moderate), hypertrophy/hyperplasia of the tunica intima or tunica media (minimal to slight), and/or vascular/perivascular haemorrhage (minimal to moderate). The other SET-M33-related microscopic findings in kidney and at infusion sites were considered non-adverse due to the magnitude of the changes (minimal to moderate) and/or a lack of correlations suggesting functional impairment. After the 4-week recovery period, kidney interstitial infiltrates cleared completely and tubule degeneration/regeneration resolved almost completely. At the infusion sites, there was complete recovery from vascular/perivascular inflammation

and tunica intima hypertrophy/hyperplasia with partial recovery from vascular thrombi and hypertrophy/hyperplasia of the tunica media. Minimal regeneration of cortical tubule epithelial cells, observed in the kidneys of 1 female at a dose of 4.0 mg/kg/day, was considered to be due to a repair process, and a slight thrombus observed at the infusion site (saphenous vein) of another female was also in line with ongoing repair. In addition, slight tunica media hypertrophy/hyperplasia of the left cephalic vein was observed in one male (Table 7). Slight tunica media hypertrophy/hyperplasia of the left cephalic vein was observed in 1 male at a dose of 4.0 mg/kg/day.

As a final result of this toxicological study, the no-observed-adverse-effect-level (NOAEL) of SET-M33 was determined to be 0.5 mg/kg/day

Table 7. *SET-M33-related changes in beagle dogs dosed with the peptide at 0 (vehicle=0.9% saline solution), 0.5, 1.5 and 4.0 mg/kg/day for 28 days and after 4-week recovery. For kidney weight changes statistical analysis was not performed due to the small number of animals*

			Male				Female			
			0 mg/kg/day	0.5 mg/kg/day	1.5 mg/kg/day	4.0 mg/kg/day	0 mg/kg/day	0.5 mg/kg/day	1.5 mg/kg/day	4.0 mg/kg/day
Kidney weight changes (% difference relative to controls)										
Kidney	Absolute weight (%)			-	-	8.63		-	-	15.16
	vs. body weight (%)			-	-	11.47		-	-	9.56
	vs. brain weight (%)			-	-	9.80		-	-	13.59
SET-M33-related findings in the kidney after 28-days dosing and after the 4-week recovery period										
4-week dosing	Degeneration/ Regeneration, tubules	Minimal	0	2	3	0	0	0	0	2
	Infiltrate, interstitium	Minimal	0	0	1	0	0	0	0	1
4-week recovery period	Regeneration, tubules	Minimal	0	0	0	0	0	0	0	1
SET-M33-related findings at infusion site after 28-days dosing and after the 4-week recovery period (combined incidence from all four sites)										
4-week dosing	Thrombus, blood vessels	Minimal	0	1	0	0	0	0	0	0
		Slight	0	0	0	2	0	1	0	0
		Moderate	0	0	0	5	0	0	1	5
		High	0	0	0	1	0	0	0	0
		Total	0	1	0	8	0	1	1	5
	Inflammation, vascular/perivascular	Minimal	0	2	3	0	1	0	1	1
		Slight	0	1	2	0	0	0	1	4
		Moderate	0	0	0	0	0	0	0	1
		Total	0	3	5	0	1	0	2	6
	Hypertrophy/hyperplasia, tunica intima	Minimal	0	0	0	0	1	0	0	0
		Slight	0	1	1	0	0	0	0	0
		Total	0	1	1	0	1	0	0	0
	Hypertrophy/hyperplasia, tunica media	Minimal	0	0	0	1	0	0	0	0
		Slight	0	2	0	2	0	0	1	0
		Total	0	2	0	3	0	0	1	0
	Haemorrhage, vascular/perivascular	Minimal	0	1	1	0	2	1	3	2
		Slight	0	1	0	1	2	1	0	3
		Moderate	0	0	0	0	0	0	1	0
		Total	0	2	1	1	4	2	4	5
4-week recovery period	Thrombus, blood vessels	Slight	0	0	0	0	0	0	0	1
		Total	0	0	0	0	0	0	0	1
	Hypertrophy/hyperplasia, tunica media	Slight	0	0	0	1	0	0	0	0
		Total	0	0	0	1	0	0	0	0

BIOANALYTICS AND TOXICOKINETICS IN RATS AND DOGS

Unlike similar tests reported in DRF studies, here SET-M33 was administered for a prolonged period (4 weeks instead of 1 week) and at doses previously selected by DRF. In order to better relate the toxicokinetics data (presented below) with SET-M33 activity we report, as examples, the following SET-M33 MIC values: MIC50 and MIC90 for *P. aeruginosa* are 1.4 μM; MIC50 and MIC90 for *K. pneumoniae* are 1.4 μM and 2.8 μM, respectively [174].

RATS

SET-M33 was administered intravenously as a slow bolus to Sprague Dawley rats once daily for 4 weeks at 0 (vehicle only), 5, 9 and 15 mg/kg/day (control group 3 animals/sex, treated groups 6 animals/sex). Blood samples were taken on day 1 and day 28. The SET-M33 profiles showed quantifiable concentrations until 1 hour post-dose at days 1 and 28. Mean plasma SET-M33 exposures were higher for females than males at day 28, while no differences were observed at day 1. Mean plasma SET-M33 exposure increased in parallel with dose in males and females. Males and (especially) females showed higher exposure levels at day 28 than day 1 (Figure 23). Mean time to maximum plasma SET-M33 concentration (t_{max}) was 5 minutes post-dose for both times and sexes as expected for intravenous bolus administration. On day 1, mean AUC_{0-t} and C_{max} values for the low vs intermediate and high doses were close to the theoretical ratios of 1.8 and 3 (2 and 2.9-3.2 for AUC_{0-t}, and 1.7-2 and 2.7 for C_{max}). On day 28, female intermediate dose AUC_{0-t} ratio was 1.7 times the theoretical ratio. The results suggest accumulation of SET-M33 in all dose groups in males and especially in females. This accumulation does not seem due to the repeated dose, since no steady state was reached (Table 8).

Table 8. *Pharmacokinetic parameters of SET-M33 on day 1 and day 28 of 4 weeks of daily intravenous (slow bolus) administration to male and female rats at 5, 9 and 15 mg/kg/day (group mean values). Abbreviations: Cmax= maximum plasma concentrations; tmax = time at which Cmax occurred; AUCo-t= area under the curve from zero to last quantifiable sampling time. Statistical analysis is not applicable to these experiments.*

Time	Parameters	Units	5 mg/kg/day		9 mg/kg/day		15 mg/kg/day	
			Male	Female	Male	Female	Male	Female
Day 1	t_{max}	minutes	5	5	5	5	5	5
	C_{max}	ng/mL	2227	2107	4563	3503	6043	5727
	AUC_{0-t}	ng · h/mL	692	663	1433	1152	2236	1944
Day 28	t_{max}	minutes	5	5	5	5	5	5
	C_{max}	ng/mL	3017	4103	5890	12387	8170	13567
	AUC_{0-t}	ng · h/mL	938	1218	1819	3558	2734	4111

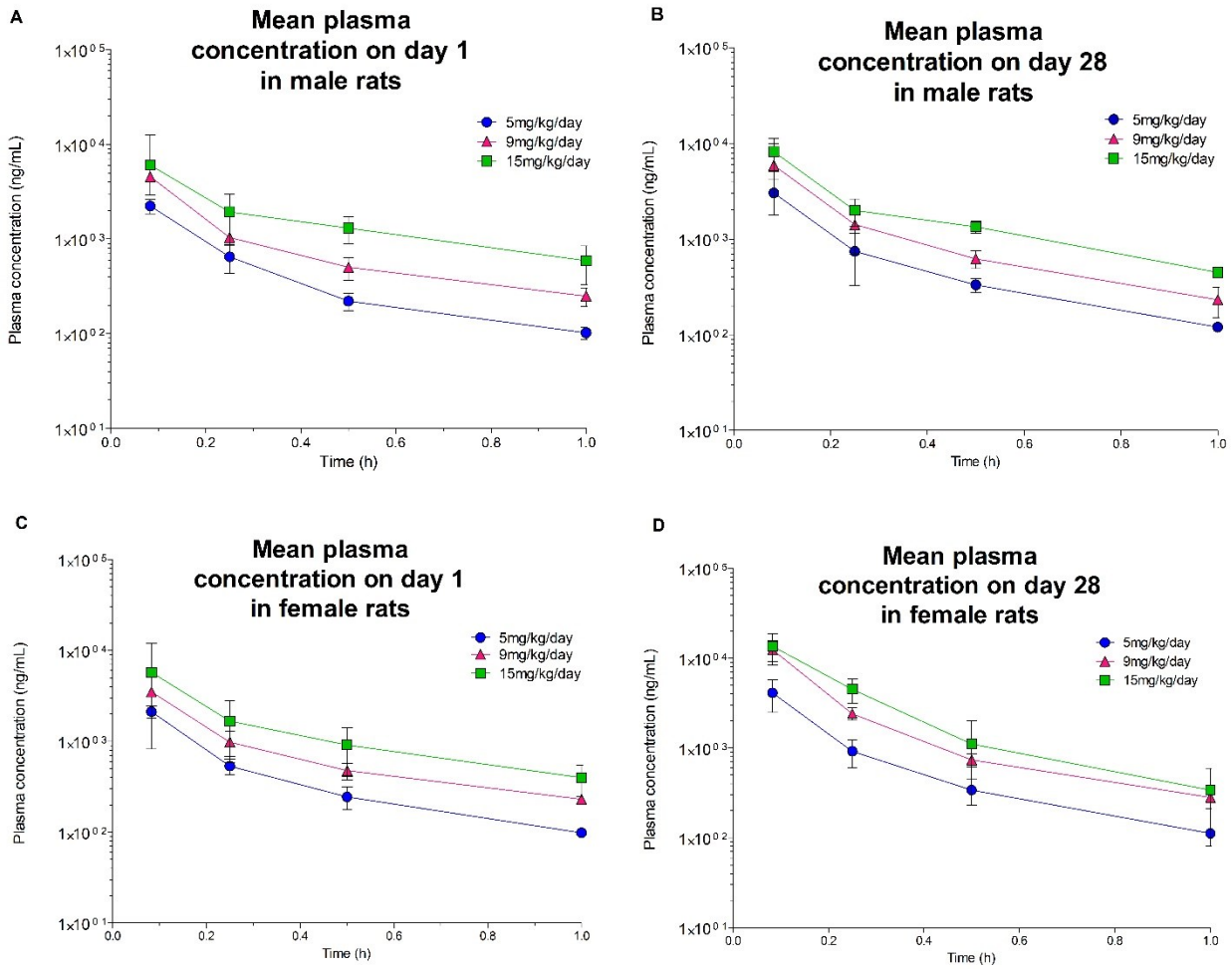

Figure 23. *Mean plasma concentrations of SET-M33 on day 1 (A and C) and day 28 (B and D) of 4 weeks of daily intravenous (slow bolus) administration to male (A and B) and female (C and D) rats at 5, 9 and 15 mg/kg/day. Symbols (circle, triangle or square) indicate a group mean value. Bars represent the standard deviation. The graphs were plotted using GraphPad Prism for Windows version 5.03, GraphPad Software, San Diego, California USA, www.graphpad.com.*

DOGS

Plasma concentrations and the main toxicokinetic parameters of SET-M33 in plasma samples were determined in beagle dogs after intravenous administration of SET-M33 by daily 1-hour-infusion at 0.5, 1.5 or 4.0 mg/kg/day or only vehicle for 4 weeks (5 animals/group/sex). Blood samples were taken on day 1 and day 28.

Mean plasma concentration-time profiles showed higher values for all doses at day 28 (Figure 24). Maximum plasma concentrations (C_{max}) of SET-M33, their times of occurrence (T_{max}) and the areas under the plasma SET-M33 concentration-time curves within a 24-hour dosing interval (AUC_{0-24}) on day 1 and day 28 are shown in Table 9, where the mean C_{max} and AUC_{0-24} for the group are shown with standard deviations in brackets. The time when the maximum plasma concentration occurred (T_{max}) was at the end of the 1-hour infusion in all animals, as expected for this route of administration. Plasma concentrations of SET-M33 at 24 hours post-dose were below the limit of quantification (<20.0 ng/mL) in all animals at all dose levels on day 1 and day 28 (not shown).

The systemic exposure (C_{max} and AUC_{0-24}) of dogs to SET-M33 increased with increasing dose over the dose range 0.5 to 4.0 mg/kg/day on day 1 and day 28. Excluding C_{max} values in males, the C_{max} and AUC_{0-24} values at the highest dose (4.0 mg/kg/day) were approximately 2.1 times higher than those predicted in the case of a linear relationship (not shown). The C_{max} and AUC_{0-24} values of SET-M33 in female dogs were similar to the indices of exposure in males at the two lower dose levels, but were approximately 1.6 times higher than those of males at the highest dose level (Figure 25). After repeated doses (day 28), C_{max} and AUC_{0-24} values of SET-M33 were generally higher than those after a single dose (day 1) (Figure 24). The accumulation ratios, based on C_{max} and AUC_{0-24} values, were generally greater than one, indicating that systemic exposure to SET-M33 was higher after repeated administrations than after a single dose (not shown). However, since plasma concentrations of SET-M33 were below the limit of quantification 24 hours post-dose in all animals, these results indicate that SET-M33 has time-dependent kinetics.

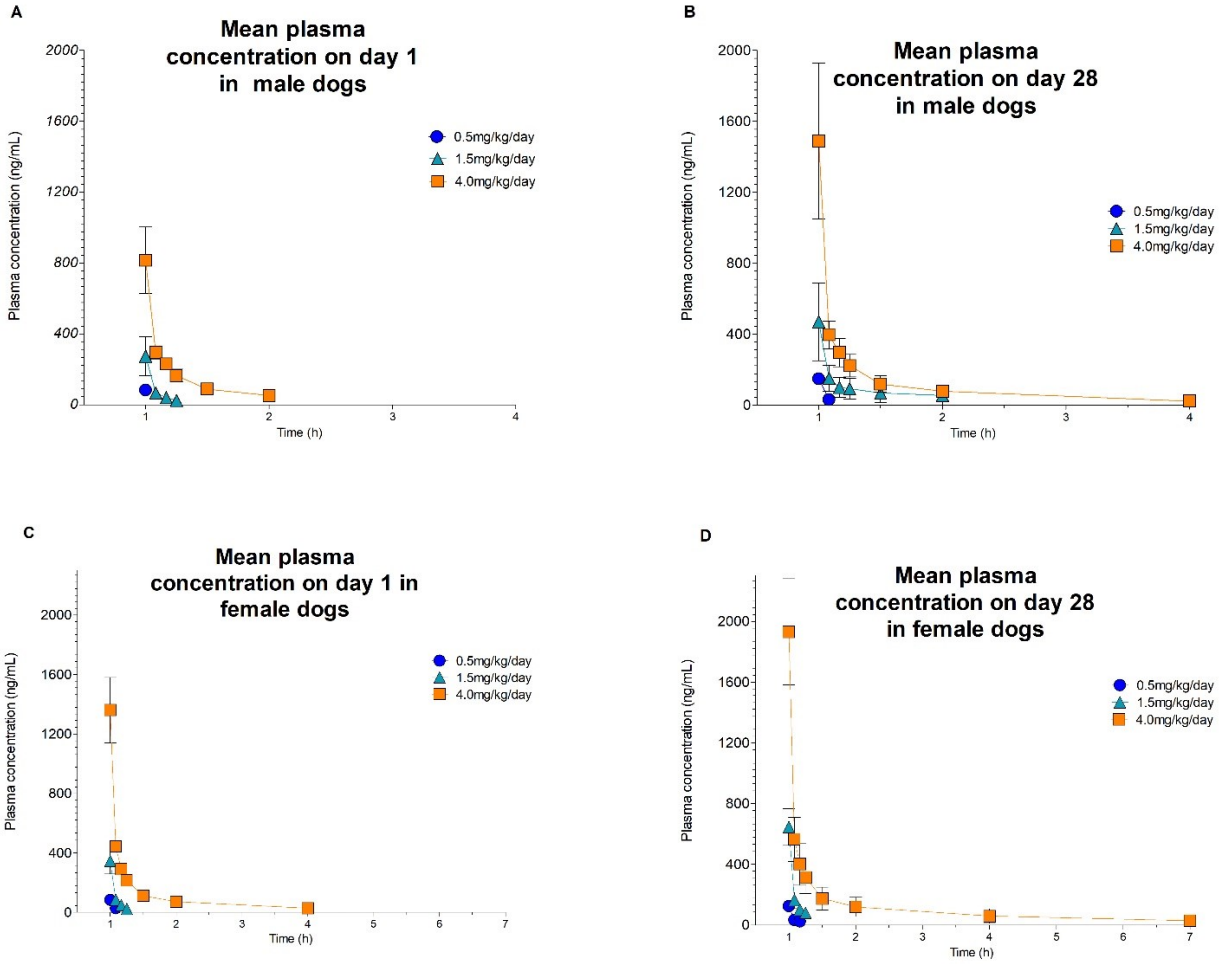

Figure 24. *Mean plasma concentrations of SET-M33 on day 1 (A and C) and day 28 (B and D) of 4 weeks of daily intravenous (infusion) administration to male (A and B) and female (C and D) dogs at 0.5, 1.5 and 4.0 mg/kg/day. Symbols (circle, triangle or square) indicate a group mean value. Bars represent standard deviations. The graphs were plotted using GraphPad Prism for Windows version 5.03, GraphPad Software, San Diego, California USA, www.graphpad.com.*

Table 9. *Pharmacokinetic parameters of SET-M33 on day 1 and day 28 of 4 weeks of daily intravenous (infusion) administration to male and female beagle dogs at 0.5, 1.5 and 4.0 mg/kg/day (group mean values ± standard deviation of Cmax and AUC0-24). Abbreviations: AUC0-24 = area under the plasma concentration-time curve in 24-hour dosing intervals; Cmax= maximum plasma concentrations; EOI = end of infusion; tlast = time point of the last quantifiable plasma concentration; tmax = time at which Cmax occurred. Statistical analysis is not applicable to these experiments.*

Time	Parameters	Units	0.5 mg/kg/day		1.5 mg/kg/day		4 mg/kg/day	
			Male	Female	Male	Female	Male	Female
Day 1	t_{max}	minutes	EOI	EOI	EOI	EOI	EOI	EOI
	t_{last}	minutes	EOI	5	15	15	60	180
	C_{max}	ng/mL	82.4 ±22.4	82.8 ±19.1	274 ±110	345 ±87	816 ±188	1360 ±220
	AUC_{0-24}	ng · h/mL	42.2 ±13.3	45.6 ±10.4	157 ±60	196 ±48	569 ±99	991 ±161
Day 28	t_{max}	minutes	EOI	EOI	EOI	EOI	EOI	EOI
	t_{last}	minutes	10	10	60	60	180	360
	C_{max}	ng/mL	149 ±16	125 ±35	470 ±218	645 ±121	1490 ±440	1930 ±350
	AUC_{0-24}	ng · h/mL	83.0 ±9.8	76.5 ±25.2	416 ±209	402 ±104	1050 ±150	1550 ±450

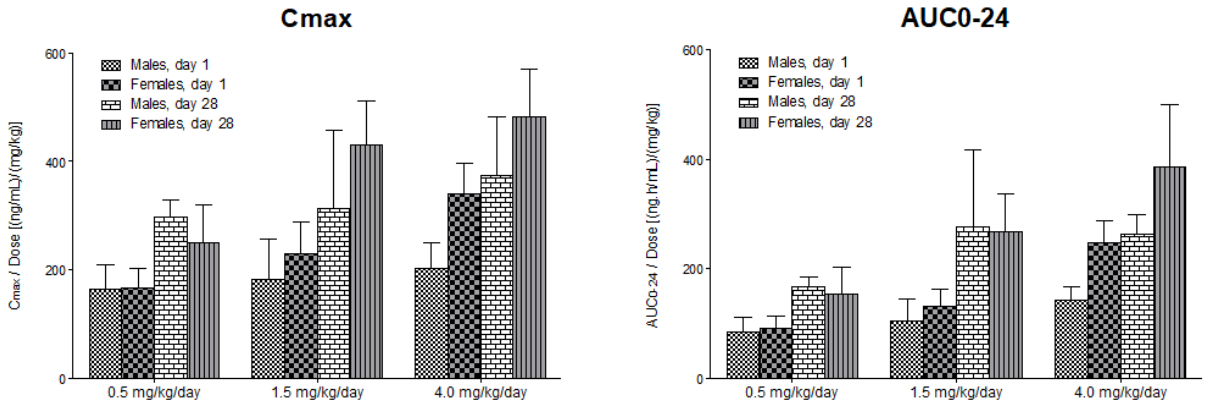

Figure 25. *Mean maximum plasma concentrations (Cmax) of SET-M33 and mean areas under the plasma concentration-time curves (AUC0-24), on day 1 and day 28 of 4 weeks of daily intravenous (infusion) administration of SET-M33 to beagle dogs at 0.5, 1.5 and 4.0 mg/kg/day. Abbreviations: AUC0-24 = area under the plasma concentration-time curve in 24-hour dosing intervals; Cmax= maximum plasma concentrations. Columns and bars represent group mean values and standard deviations, respectively. The graphs were plotted using GraphPad Prism for Windows version 5.03, GraphPad Software, San Diego, California USA, www.graphpad.com. Statistical analysis is not applicable to these experiments.*

STUDY 3: INHALABLE POLYMERIC NANOPARTICLES FOR PULMONARY DELIVERY OF ANTIMICROBIAL PEPTIDE SET-M33: ANTIBACTERIAL ACTIVITY AND TOXICITY *IN VITRO* AND *IN VIVO*

SET-M33 AND SET-M33_Rhod PEPTIDE PRODUCTION

The peptide SET-M33 was produced on a solid support in tetrabranched form using Fmoc chemistry. The SET-M33_Rhod were synthesized in the same way using Lys-tetramethyl-rhodamine (Lys-TMR) as the first amino acid. Both synthesis and purification process resulted in more than 95% pure product, as shown by analytical reverse phase chromatography on a Jupiter C18 column (Figure 26 A, C) and by mass spectrometry (MS) that have shown a single peak corresponding to the molecular mass of the tetrabranched peptide SET-M33 (4683) and SET-M33_Rhod (5754.504) (Figure 26 B, D)

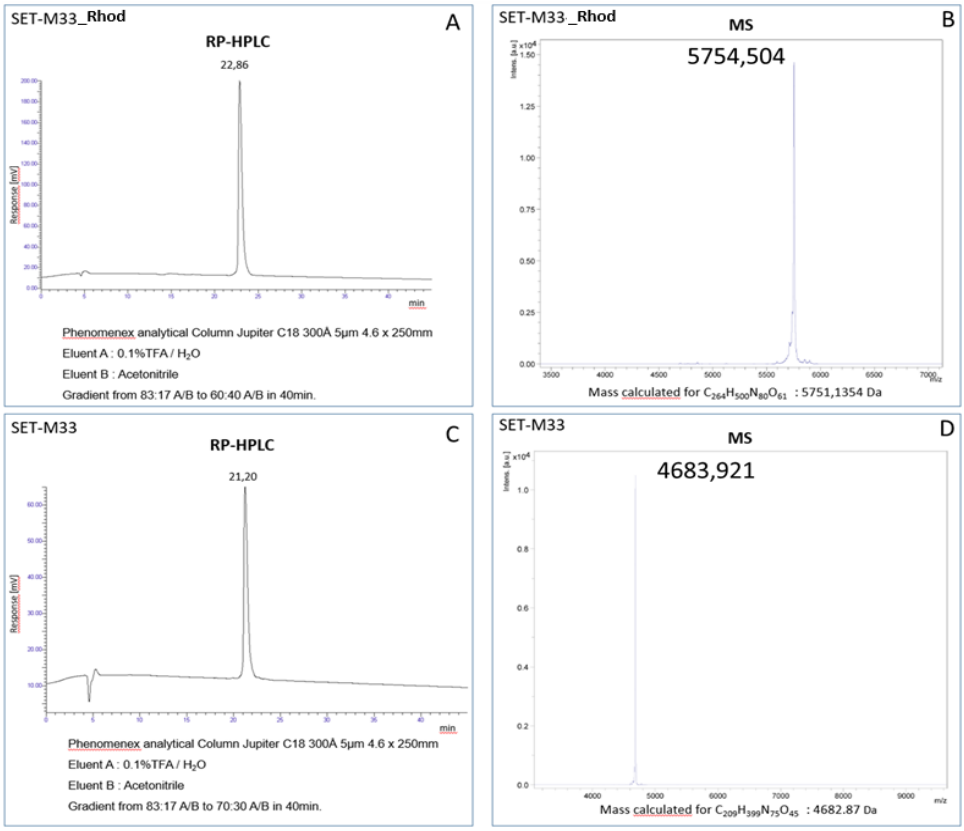

Figure 26. *HPLC and Mass Spectrometry (MS) profiles of SET-M33 conjugated with tetramethyl-rhodamine (SET-M33_Rhod) and free SET-M33. A and C, reverse phase HPLC profiles of SET-M33_Rhod (A) and SET-M33 (C) with test method (below) and retention times (above the peaks). B and D, MS profiles of SET-M33_Rhod (B) and SET-M33 (D) with the indication of revealed (above the main peak) and calculated MW (below the graph).*

SET-M33-LOADED NANOPARTICLE PROPERTIES

Two different formulations of PEGylated PLGA-based NPs containing SET-M33 were prepared by a modified emulsion/solvent diffusion technique employing PLGA conjugated with PEG 2000 Da or 5000 Da. The hydrodynamic diameter (DH), polydispersity index (PDI) and zeta potential (ζ potential) of SET-M33-loaded NPs were determined by DLS and ELS, as described above, and the results are reported in Table 10.

Table 10. *Overall properties (hydrodynamic diameter - DH, polydispersity index - PDI, ζ potential, en-capsulation efficiency -EE and actual loading - AL) of SET-M33-loaded PLGA NPs.*

Formulation	D_H (nm) ± SD	PDI (mean) ± SD	ζ potential (mV) ± SD	EE (%) ±SD	AL (mg SET-M33/100 mg NPs) ± SD
M33_PEG2000 NPs	208.8 ± 1.5	0.141 ± 0.020	-18.4 ± 0.7	93.9 ± 1.25	3.793 ± 0.045
M33_PEG5000 NPs	185.7 ± 1.8	0.09 ± 0.044	-18.87 ± 0.6	85.9 ± 4.63	3.557 ± 0.159

DH= Hydrodynamic diameter; PDI= Polydispersity index; EE= Encapsulation efficiency, calculated as actual loading/theoretical loading x 100; AL= Actual loading.

Both NP formulations showed a DH close to 200 nm, sufficiently small to cross lung barriers, negative ζ potential and high EE (≥86%), suggesting that the PEG molecular weight did not significantly affect particle properties. As confirmed by TEM analysis, both the PEGylated NP formulations showed a regular and spherical shape (Figure 27).

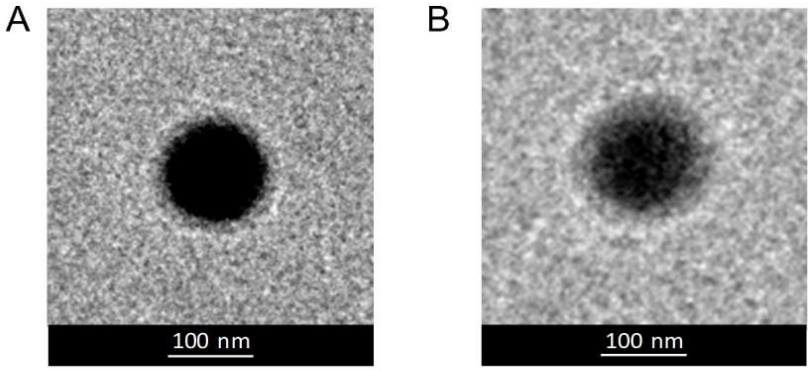

Figure 27. *TEM images of M33-loaded NPs: M33_PEG2000 NPs (A) and M33_PEG5000 NPs (B). Images are representative of the samples.*

The FALT analysis of the PEG shell on the NPs surface, obtained by monitoring the influence of the ionic strength of the dispersing medium on NP surface charge, confirmed the core–shell structure of the NPs, with a PLGA core surrounded by a PEG shell (Figure 28). This hypothesis was also supported by the FALT evaluation of NPs prepared without PEG, which exhibited a very low shell thickness (1.08 nm).

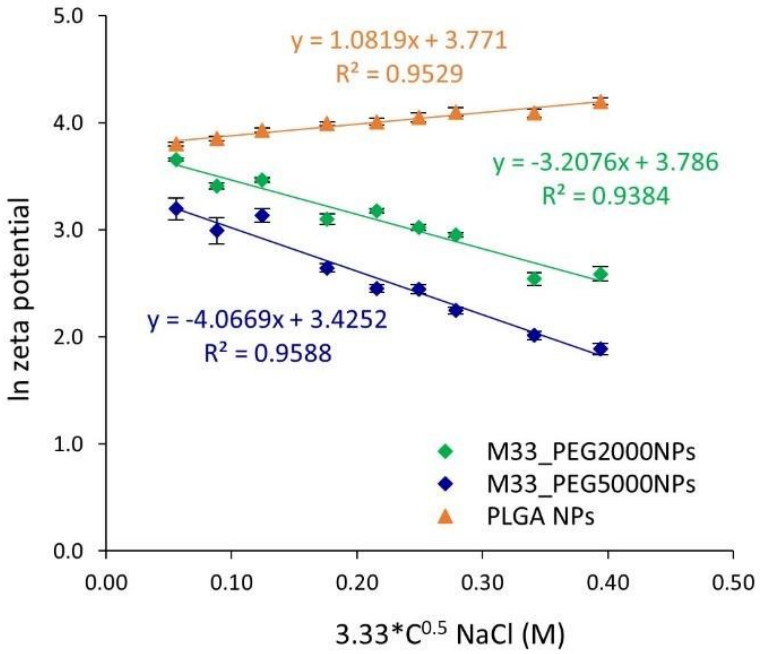

Figure 28. *Fixed aqueous layer thickness (in nm) obtained as the slope of the linear regression of ionic strength of the dispersing medium against NP surface charge: ln (ζ) against k (k = 3.3 c0.5, where k - 1 is the Debye length). There is a significant difference between SET-M33_PEG2000 NPs and SET-M33_PEG5000 NPs (one-way ANOVA; p < 0.05), and between both the two PEGylated formulations and the PLGA NP formulation control (one-way ANOVA; p < 0.0001).*

As expected, particles with PEG 5000 Da showed a higher shell thickness (4.07 nm) than that obtained with PEG 2000 Da (3.21 nm). The *in vitro* kinetics of SET-M33 release were evaluated in PBS employing NPs containing the SET-M33_Rhod. The results are shown in Figure 29 as the percentage of peptide released over time.

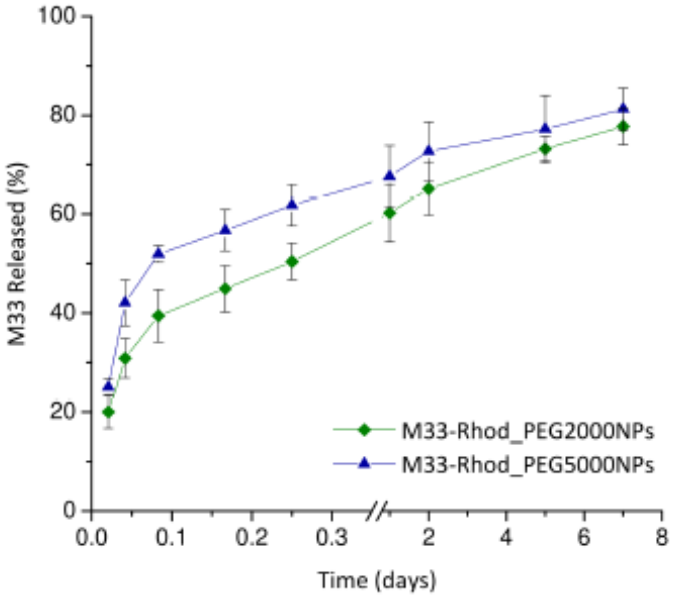

Figure 29. *In vitro release of SET-M33_Rhod from PEG NPs calculated as the percentage of SET-M33 released by NPs (%) ± SD over time. The experiments were run in triplicate for each time point. No significant differences were observed (t-test; $p > 0.05$).*

The two NP formulations showed typical biphasic release profiles characterized by an initial burst (about 60% and 45% of the amount encapsulated released in 6 hours for SET-M33-Rhod_PEG5000 NPs and SET-M33-Rhod_PEG2000 NPs, respectively) followed by controlled release of the peptide lasting about 7 days. In the case of polymeric nanoparticles, the diffusion of the drug is generally faster than polymeric matrix erosion, thus the mechanism of release can be predominantly related to the diffusion process.

IN VITRO AEROSOL PERFORMANCE OF NANOPARTICLES

The *in vitro* aerosol performance of NPs is shown in Figure 30 and Table 11.

Cumulative mass recovered as a function of the cut-off diameter and the fine particle characteristics of the aerosol cloud of SET-M33-Rhod_PE2000 NPs and SET-M33-Rhod_PEG5000 NPs was evaluated upon delivery through Aeroneb® Go and PARI TurboBOY nebulizers. Differences were observed in the deposition patterns of the NP formulations tested. When PARI TurboBOY was used as the nebulizer, both NP formulations generated a NP cloud with a low aerodynamic diameter (<2.7 μm) that reached the deep CUP of the NGI. On the other hand, when Aeroneb Go was used, SET-M33_PEG5000 NPs

showed a higher aerodynamic diameter (3.85±0.70 μm) than SET-M33_PEG2000NPs (2.68±1.59 μm). Nevertheless, all the aerodynamic diameters were less than 5 μm, suggesting that the distribution of the formulation in the lungs by the most widely used nebulizers is uniform.

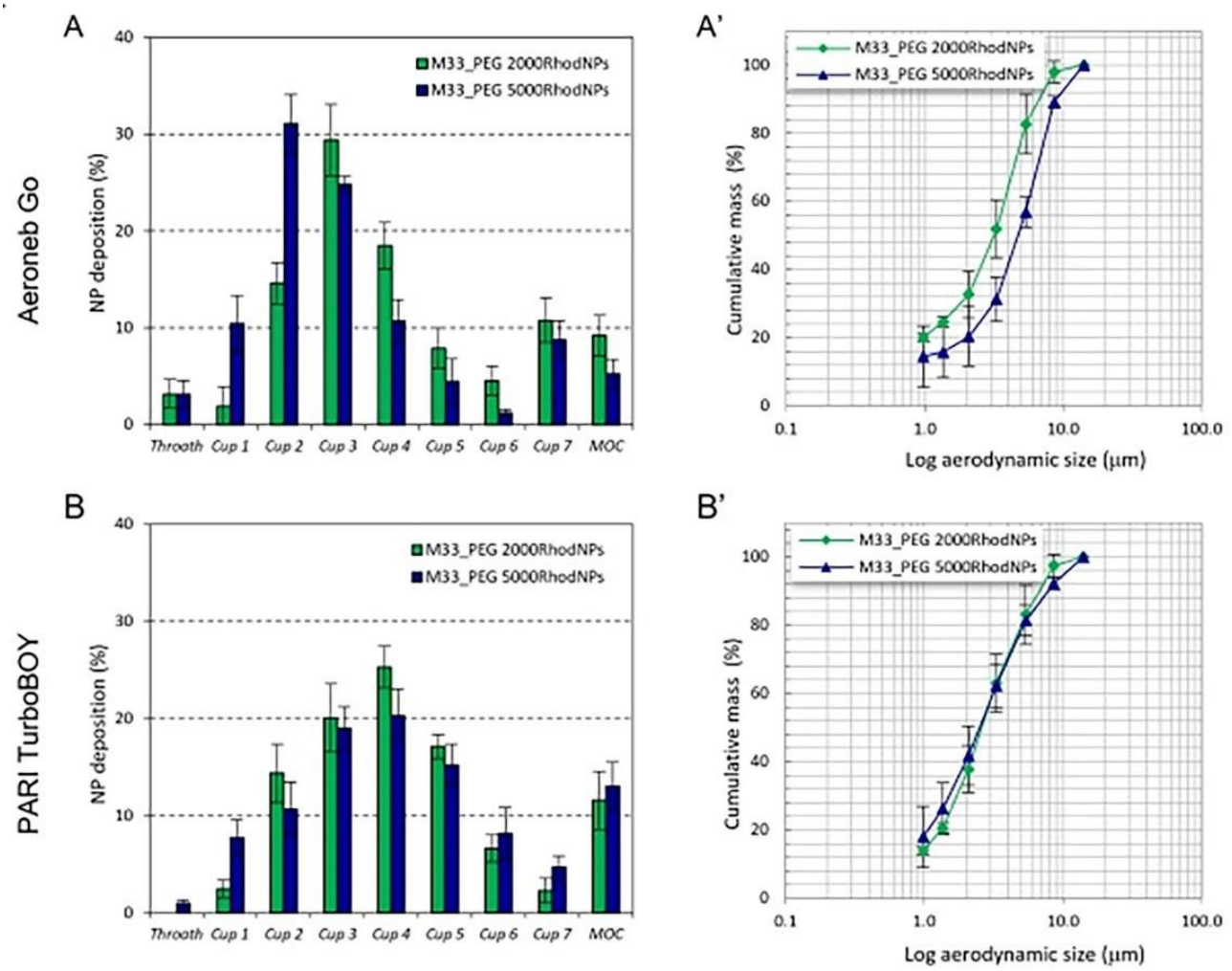

Figure 30. *In vitro aerosol performance of SET-M33_PEG 2000-Rhod and SET-M33_PEG 5000-Rhod delivered through Aeroneb® Go and PARI TurboBOY nebulizers: Cumulative mass recovered was a function of the cut-off diameter of the NGI stages (A, B), NGI deposition pattern (A', B'). The emitted dose was measured as the difference between the total amount of NPs initially placed in the nebulizer chamber and the amount remaining. At the flow rate used (15 L/min), the cut-off diameters of the NGI stages were 0.98 m (Cup 1), 1.36 μm (Cup 2), 2.08 μm (Cup 3), 3.3 μm (Cup 4), 5.39 μm (Cup 5), 8.61 μm (Cup 6), 14.1 μm (Cup 7). No significant differences were observed for all the formulations tested (one-way ANOVA multiple comparison; $p > 0.05$).*

Table 11. *Overall aerosol properties of M33_PEG 2000-Rhod and M33_PEG 5000-Rhod delivered through Aeroneb® Go and PARI TurboBOY nebulizers: Experimental mass median aerodynamic diameter (MMADexp) and geometric standard deviation (GSD) were calculated by plotting cumulative mass of particles retained in each collection cup versus the cut-off diameter of the corresponding stage. The fine particle fraction (FPF) was calculated as the percentage of NPs deposited in stages 3–7 (MMADexp < 5.39 μm) compared to the amount initially loaded in the nebulizer chamber. The respirable fraction (RF) is the total amount recovered from the NGI. Data are reported as mean ± SD (n = 3).*

	M33_PEG 2000RhodNPs		M33_PEG 5000RhodNPs	
	Aeroneb	**PARI TurboBOY**	**Aeroneb**	**PARI TurboBOY**
FPF	37.1 ± 16.3	39.4 ± 9.5	40.5 ± 0.1	43.0 ± 5.7
RF	71.1 ± 1.6	71.2 ± 7.4	50.0 ± 7.8	67.5 ± 2.2
$MMAD_{exp}$	2.68 ± 1.03	2.66 ± 1.02	3.85 ± 0.70	2.53 ± 0.71
GSD	2.91 ±0.98	2.66 ± 0.58	2.62 ± 0.02	2.86 ± 0.47

IN VITRO NPs INTERACTIONS WITH MUCIN AND BACTERIAL ALGINATES

A critical issue in defining the ability of particles to diffuse across lung barriers (i.e., the mucus layer) is the evaluation of the interactions between the particles and major barrier components. An absence of interactions is commonly considered a prerequisite for improving particle diffusion across the mucus layer [193]. We therefore first derived a rough estimation of interactions between NPs and mucin, the major component of airway mucus, and between NPs and BA, a main component of the *P. aeruginosa* biofilm extracellular matrix. This was achieved by measuring NP scattering at 650 nm with and without mucin/BA. As shown in Figure 30 A, both formulations showed the same absorbance in water and in mucin, suggesting that mucin is not absorbed on the surface of NPs, irrespective of the length of the PEG chain on the particle surface. The absence of evident particle interactions was also confirmed by DLS size analysis, where NP dispersion in water and mucin was comparable (Figure 31 B).

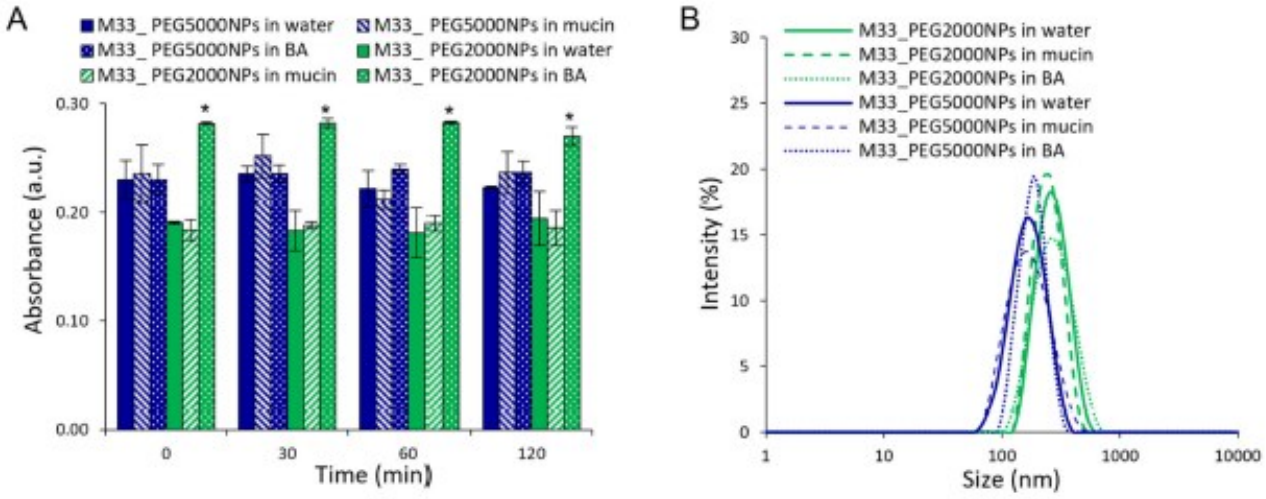

Figure 31. *In vitro assessment of SET-M33-loaded NP interactions with mucin and BA: (A) Time trend of scattering at 650 nm by NPs (1 mg/mL) in the presence of mucin or BA. NP dispersions in water are reported as controls. (B) Size distribution of NPs with mucin or BA evaluated by dynamic light scattering intensity. The size distribution profiles of NP dispersions in water are reported as controls. The statistical analysis was performed by one-way ANOVA (* $p < 0.0001$).*

On the other hand, SET-M33_PEG2000 NP dispersion in BA showed a statistically significant difference ($p < 0.0001$) in the scattering, suggesting an interaction between NPs and BA (Figure 30). This effect was not observed with SET-M33_PEG5000 NPs, where the greater thickness of the PEG shell protected the particle surface from these interactions. Although detectable, the slight increase in scattering by PEG 2000 particles suggests an absence of particle aggregation and strong interactions, as confirmed by size analysis in BA (Figure 31 B).

On the other hand, free SET-M33 strongly interacted with mucin and BA, leading to the formation of nanometric complexes and 60-fold and 200-fold increases in sample turbidity, respectively (Figure 32), while PEGylated NPs efficiently shielded interactions of SET-M33 with mucin and BA, avoiding any formation of complexes or aggregates.

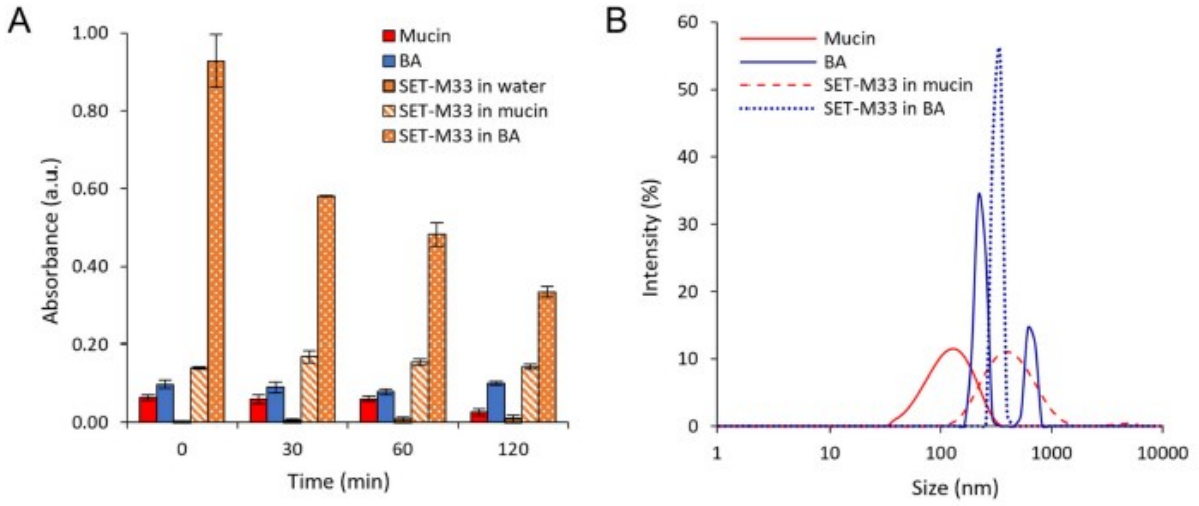

Figure 32. *In vitro assessment of free SET-M33 interactions with mucin and BA: (A) Time trend of scattering at 650 nm by free SET-M33 (40 g/mL) in the presence of mucin or BA. Scattering at 650 nm by SET-M33 solution in water is reported as the control. (B) Size distribution of free SET-M33 NPs with mucin or BA evaluated by dynamic light scattering intensity.*

IN VITRO DIFFUSION STUDIES ACROSS MUCUS AND BIOFILM MODELS

The ability of NPs to aid the diffusion of SET-M33 through artificial mucus (AM) and simulated bacterial biofilm (BA), and the effect of the PEG shell on NP diffusion, were evaluated by a modified Transwell® multiplate assay (Figure 32). After 1 hour, NP percentages as high as 70% for SET-M33_PEG5000 NPs in the acceptor medium were recorded, demonstrating that these PEGylated NPs readily diffused across the artificial mucus layer (Figure 33 A). SET-M33_PEG2000 NPs did not diffuse so readily even after 4 hours (Figure 33 A). Although the two PEGylated NPs diffused rapidly through the mucus layer, the highest diffusion was observed for NPs modified with PEG 5000 Da, which provides an optimal dense PEG shell with a brush conformation, confirming that the PEG molecular weight affects the ability of NPs to diffuse across the mucus layer [194]. On the other hand, in the BA diffusion studies, no differences were found between the two NP formulations in the first 2 hours (see similar diffusion profiles in Figure 33 C). An effect of PEG molecular weight was observed towards the end of the assay at 6 hours, namely, the greater diffusion of SET-M33_PEG5000 NPs (90%) than of SET-M33_PEG 2000 NPs (70%). The ability of PEGylated NPs to aid the diffusion of SET-M33 across simulated lung barriers was confirmed by *in vitro* permeation studies, performed under the same

conditions, with NPs containing fluorescently labeled SET-M33. The results were compared with those of free SET-M33_Rhod (Figure 33 B, D). After deposition of the same amount on the AM layer, the percentage of SET-M33_Rhod encapsulated in SET-M33_PEG 5000 NPs permeating into the acceptor compartment in 1 hour was more than twice that of the free SET-M33_Rhod and SET-M33_Rhod encapsulated in SET-M33_PEG 2000 NPs (80.68% for SET-M33_PEG 5000 NPs versus 37.10% and 26.32% for free SET-M33_Rhod and SET-M33_PEG 2000 NPs, respectively) (Figure 33 B). Interestingly, while a slight decrease in SET-M33_Rhod diffusion was detected in AM, high interaction was detected between free SET-M33_Rhod and BA, as suggested by the permeation profile (Figure 33 D). The encapsulation of SET-M33_Rhod in PEGylated PLGA NPs led to a 7.6-fold increase in SET-M33_Rhod diffusion across the BA layer. After 6 hours, only 12.3% of SET-M33_Rhod had crossed the BA layer, while more than 90% was detected in the acceptor compartment when the peptide was encapsulated in NPs (93.74% and 92.91% for SET-M33_PEG 5000 NPs and SET-M33_PEG 2000 NPs, respectively). These results indicate that PEG5000 NPs were the best formulation. They were therefore selected for further experiments on *in vitro* antimicrobial and anti-biofilm activity and *in vivo* toxicity.

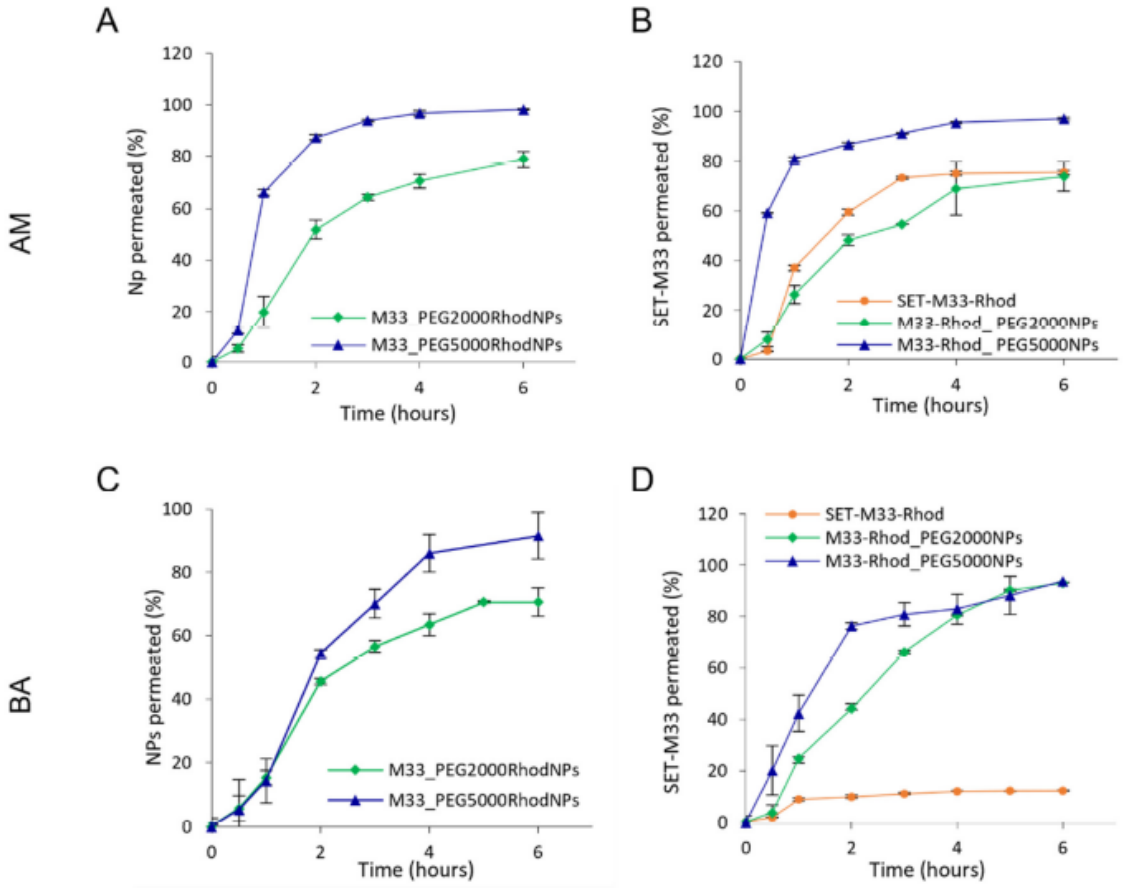

Figure 33. *In vitro transport of SET-M33-loaded fluorescent NPs (A,C) and in vitro transport of SET-M33_Rhod-loaded NPs (B,D) through artificial mucus (AM) and bacterial alginates (BA), as determined by the Transwell® multiplate assay. Results are presented as the percentage of SETM33_Rhod and fluorescent NPs permeating across AM and BA as a function of time. Data are expressed as the mean ± SD calculated for three different batches (n = 6).*

IN VITRO ANTIBACTERIAL ACTIVITY OF SET-M33_PEG 5000 NPS

On the basis of the promising results achieved with PEG5000, only SET-M33_PEG5000 NPs underwent *in vitro* efficacy studies against bacteria. NPs produced with PEG5000 were tested at different final peptide concentrations (24 µM, 12 µM, 6 µM). Unloaded NPs were tested as a control. The activity was evaluated in terms of the growth of *P. aeruginosa* ATCC 27853™24, 48 and 72 hours after treatment, compared with the control sample (untreated bacterial cells). Antibacterial activity persisted up to 72 hours when SET-M33_PEG5000 NPs were loaded at the higher concentrations, and up to 48 hours with SET-M33_PEG5000 NPs loaded with 6 µM SET-M33 (Figure 34). The persistent effect can be related to the sustained release of SET-M33 provided by NPs.

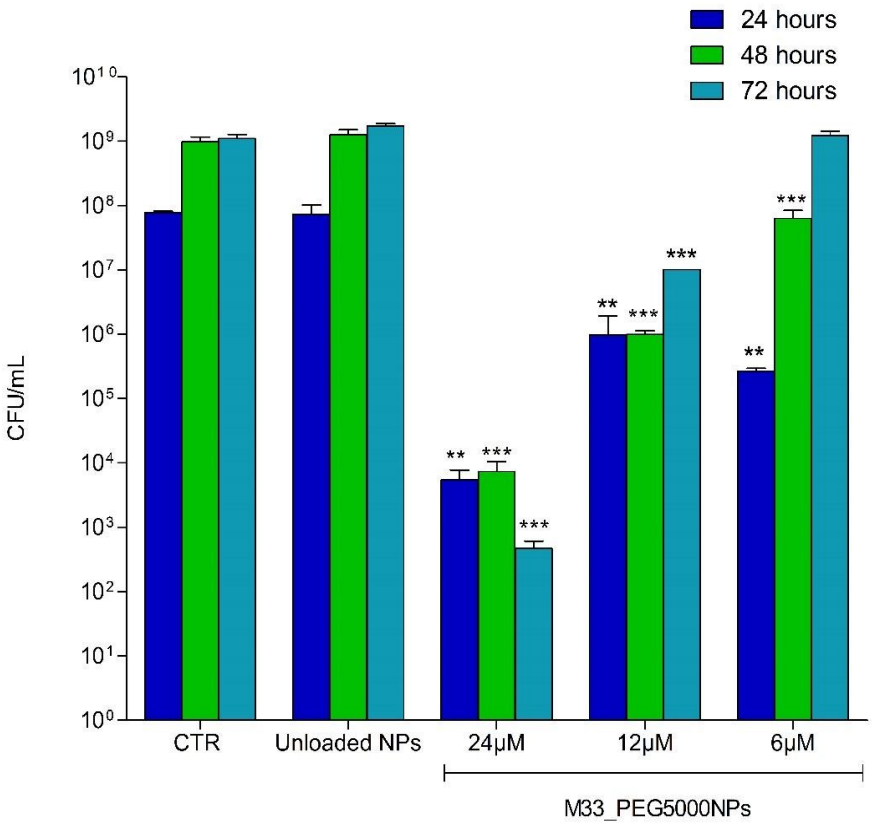

***Figure 34**. Histogram of P. aeruginosa (ATCC 27853™) colonies (CFUs) produced at different times (indicated in the internal legend) and then plated in LB agar medium: CTR indicates the number of colonies produced by untreated bacteria. Unloaded NPs indicates the number of colonies produced by bacteria incubated with NPs without peptide. M33_PEG5000 NPs show the number of colonies produced by bacteria incubated with NPs with the peptide at the concentrations indicated. The experiment was performed in triplicate. Results are expressed as mean ± SD of three wells. Significant differences between groups were evaluated by one-way ANOVA with Dunnett's multiple comparison test using GraphPad Prism 5.03 software, where ***, $p < 0.001$; **, $p < 0.05$. Each column is compared with its control at each time point.*

IN VITRO ANTIBIOFILM ACTIVITY OF FREE SET-M33 AND SET-M33_PEG5000 NPS

Antibiofilm activity of SET-M33_PEG5000 NPs was measured and compared to that of free SET-M33 peptide using *P. aeruginosa* (ATCC 27853™) as a bacterial model. The free peptide showed evident anti-biofilm activity at all concentrations tested, proving to be strongest 72 hours after the initial incubation (Figure 35). This could be due to the high stability of SET-M33 polymeric structure. The profile of anti-biofilm activity of SET-M33_PEG5000 NPs was very similar to that of the free peptide; it had a dose-dependent trend, and the greatest reduction in biomass was at 24 µM. Like the free form, SET-

M33_PEG5000 NP activity was strongest after 72 hours. Of note, when SET-M33_PEG5000 NPs were tested, only a reduced amount of SET-M33 was released and able to exert its anti-biofilm activity. Nonetheless, the effect of SET-M33_PEG5000 NPs appeared comparable to that observed when the total amount of SET-M33 was free. This effect can be related to the ability of NPs to release the peptide in a controlled manner over time.

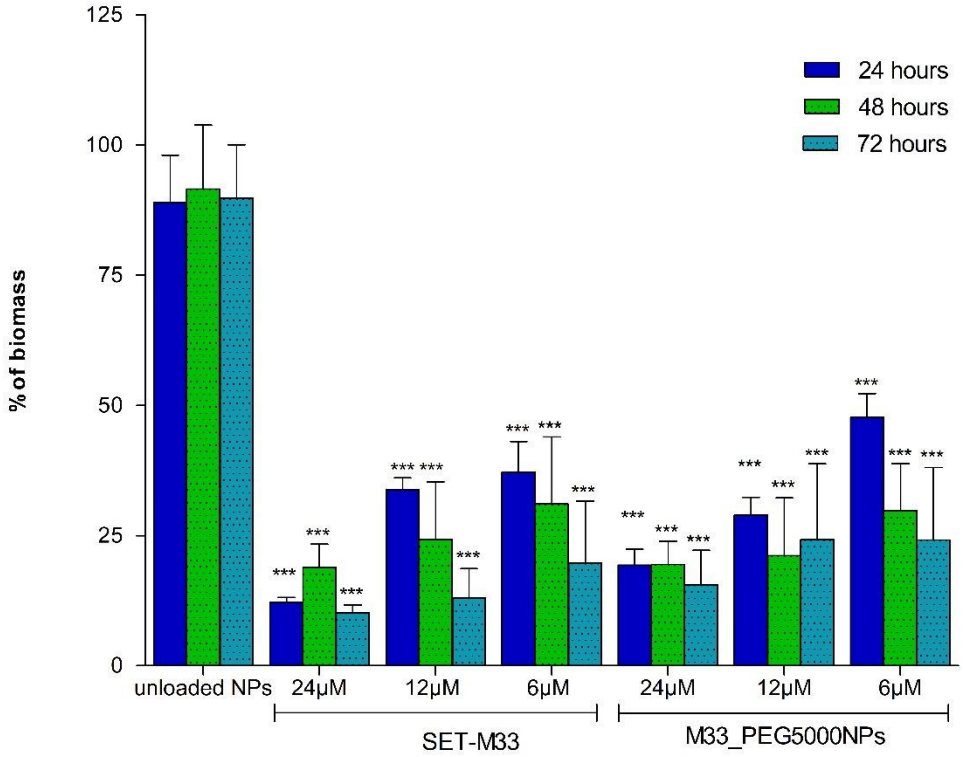

Figure 35. *Histogram of the percentage of P. aeruginosa (ATCC 27853™) biofilm biomass at different times of incubation with free SET-M33 or SET-M33 peptide encapsulated in nanoparticles (M33_PEG5000 NPs): Unloaded NPs indicates the biofilm biomass after incubation with nanoparticles without peptide. Results are expressed as mean ± SD of three wells. Significant differences between groups were evaluated by one-way ANOVA with Dunnett's multiple comparison test using GraphPad Prism 5.03 software, where ***, $p < 0.001$. Each column is compared with its control at each time point.*

CYTOTOXICITY OF FREE SET-M33 AND SET-M33_PEG5000 NPS

Since the NPs described here are intended to treat pneumonia via local delivery to the lungs, cytotoxicity was measured on human bronchial cells from a healthy individual (16HBE140- cells) and a CF patient (CFBE410- cells). SET-M33_PEG5000 NPs and the free peptide were incubated for 48 hours with cells to determine EC_{50}. No toxicity was detected for SET-

M33_PEG5000 NPs, whereas the free peptide at the same concentrations as in the NPs showed an EC_{50} of 23 µM with 16HBE14o- cells (Figure 36 A) and 21 µM with CFBE41ocells (Figure 36 B).

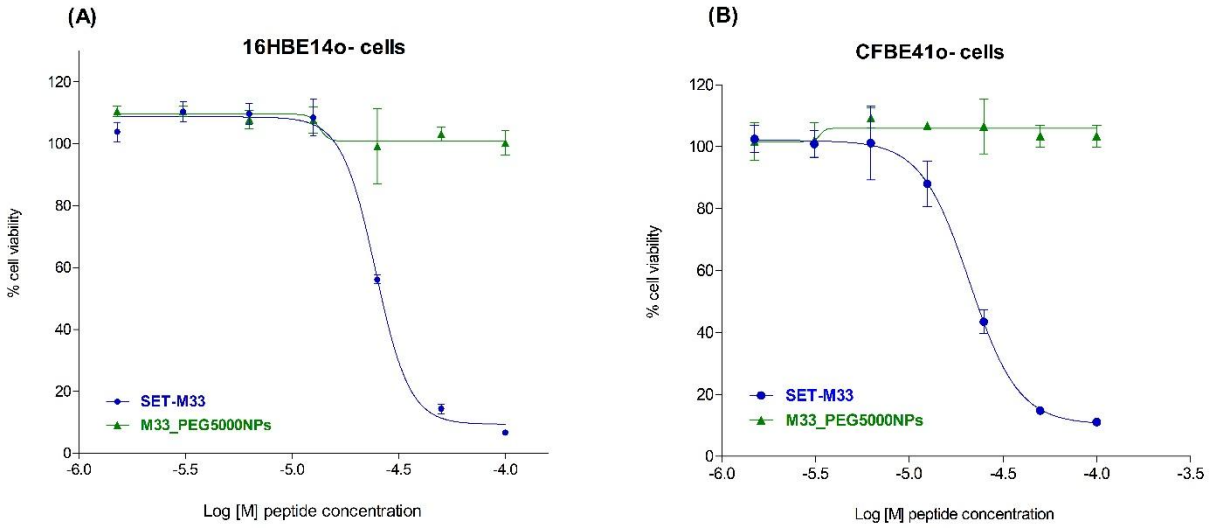

***Figure 36**. Cytotoxicity of free SET-M33 (circle) and M33_PEG5000 NPs (triangle) towards 16HBE14o- (A) and CFBE41o- (B) bronchial cells: The cell lines were incubated with free and encapsulated peptide at the same concentrations (from 100 to 3.125 µM) for 48 h. Cell viability was then evaluated using 0.1% crystal violet staining solution. Cell survival (y-axis), expressed as a percentage with respect to untreated cells, is plotted against peptide concentration (x-axis) on a logarithmic scale. The experiment was performed in triplicate. The data, reported as mean SD (n = 3), were analyzed by non-linear regression using GraphPad Prism 5.03.*

IN VIVO ACUTE TOXICITY OF FREE SET-M33 AND SET-M33_PEG5000 NPS

Mice (n = 5/group) were treated via i.t. administration of free SET-M33 and SET-M33_PEG5000 NPs at the same peptide concentration (10 mg/Kg). A nebulization system reproducing aerosol application was used. Mice were checked for signs of toxicity for up to 96 hours, using the following toxicity score: wiry coat and poor motility = mild signs; very wiry coat, abundant lachrymation and poor motility even under stimulation = manifest signs (Figure 37). No signs of toxicity were observed in mice treated via i.t. administration of SET-M33_PEG5000 NPs and unloaded nanoparticles, confirming the absence of toxicity already seen in cytotoxicity tests, and the high biocompatibility of the material used. On the other hand, i.t. administration of free SET-M33 caused three deaths within 6 hours, mild signs in

one mouse and no signs in another mouse. The situations of the two surviving mice remained unchanged over the 96 hours.

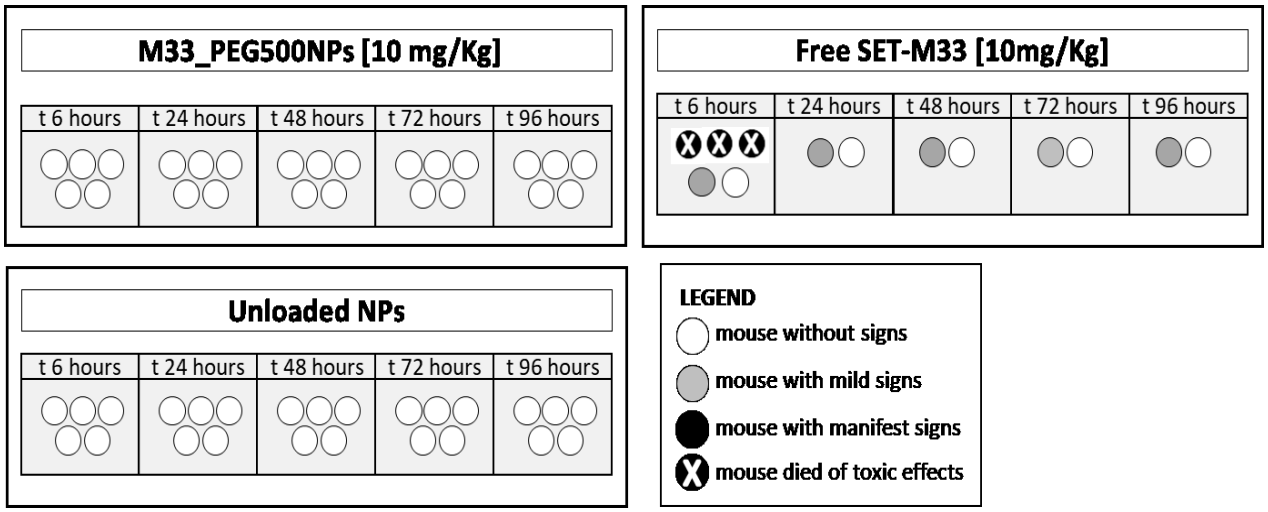

Figure 37. *Acute toxicity of SET-M33_PEG5000 NPs, free SET-M33 and unloaded NPs in vivo: Mice (represented as circles) underwent i.t. inoculation with 10 mg/kg in a single dose and were monitored for 96 hours. Different scales of grey and the X symbols in the circles indicate severity of signs and death, as described in the internal legend.*

DISCUSSION AND CONCLUSIONS

Excessive and inappropriate use of antibiotics in healthcare, agriculture, and veterinary resulted in a significant rise in antimicrobial resistance. This phenomenon poses a significant global threat, underscoring the pressing need for strategic global investments in developing new therapeutic approaches to combat antimicrobial resistance. Among these alternatives, antimicrobial peptides emerged as a noteworthy class of antibacterial molecules. Although they are not a complete alternative to traditional antibiotics due to certain limitations, they could be a valid support to antibiotic therapy [1-12].

The peptide SET-M33 is a synthetic molecule under study for the development of a new antibacterial drug for bacterial infections, including pulmonary ones.

Pneumonia is a common acute respiratory infection that affects the alveoli and distal airways [195]. It is a major health problem and is associated with high morbidity and short- and long-term mortality in all age groups worldwide. A large variety of microorganisms can cause pneumonia, including MDR pathogens such as *S. aureus*, *P. aeruginosa*, *K. pneumoniae* and other bacteria [196-197]. Research focused on new antibacterial drugs to be administered locally into the lungs is of crucial importance for the future. Pneumonia is triggered by bacterial infections that evolve into an inflammatory state, in some cases very severe, in which bacterial toxins such as LPS, LTA, peptidoglycan and others play an important role. However, LPS is the major toxin involved in lung inflammation in pneumonia [198]. The neutralization of LPS and the killing of bacteria are therefore important therapeutic issues for healthcare professionals.

SET-M33 and some of its back-up molecules have already been reported for antibacterial efficacy in different infections and inflammation models *in vivo* and *ex vivo*, including sepsis [115; 169; 174], pneumonia [174- 177] and skin infections [174]. As a novel drug to administer intravenously, SET-M33 entered in a pre-clinical development phase that includes the scale up of the production process, adsorption, excretion [174] and finally toxicity. SET-M33 showed a grade of toxicity, which when combined with the efficacy experiments already reported, suggests that it will have a favourable therapeutic index.

A new therapeutic agent must meet all regulatory agency requirements in order to obtain marketing authorization. Then, the standard procedures specify that before a new therapeutic entity can be given to humans, developers must first test it thoroughly in animals for safety and efficacy [199]. The main aims of pre-clinical studies are roughly to determine:

i) the efficacy and toxicity of the compound; ii) its pharmacokinetics; iii) the formulation for appropriate delivery in humans. Pre-clinical toxicological studies must be conducted in two animal species, including a rodent and a non-rodent, before proceeding to the clinical phases of development [200-201]. In the pre-clinical phase, the ultimate goal is to translate the animal model responses into an understanding of the risk for human subjects [202]. Toxicity testing in animals is therefore valuable for lead compound characterization and further decisions about the direction of development [203].

The Study 1 reported in this Ph.D. thesis describes the activity of SET-M33 in inhibiting the pro-inflammatory action of LPS in the lung through local administration by nebulization in mice. The therapeutic effect of the peptide was evaluated in terms of inhibition of the cells and cytokines involved in inflammation. The strongest activity of SET-M33 was recorded for neutrophils and mononuclear cells, and for cytokines IP-10, MCP-1, MIP1 and TNF-α. Moreover, the inhibition dose dependency result was evident for KC, MIP-1 and TNF-α. The very promising outcomes emerged from a comparison of SET-M33 activity and Budesonide, namely the corticosteroid drug used in clinical practice to reduce lung inflammation and in the present study as a positive control. In particular, as regards IP-10, MIP-1α and TNF-α levels, SET-M33 proved even more active in a dose-dependent manner than Budesonide in inhibiting the inflammatory effect provoked by LPS.

At the same time, the *in vivo* toxicity study showed that doses compatible with anti-inflammatory efficacy could be considered suitable for clinical use. As stated by Palazzi *et al.* [204], changes likely to impair the functional capacity of an organism or degenerative changes associated with inflammation and fibrosis can be considered adverse. For these evaluations, the concentration of peptide in the aerosol, the particle-size distribution in the aerosol, and the estimated achieved dose of the peptide inhaled by the mice were initially estimated. This allowed to calculate that doses of 5 and 20 mg/kg/day corresponded to actual concentrations in aerosol particles of 4.34 and 23.1 mg/kg/day, respectively. These data are important for evaluation of the actual number of molecules inhaled by the animals. The high incidence, nature and range of findings seen in mice treated with SET-M33 at 23.1 mg/kg/day indicated irritation and foreign-body reaction and included a clear local inflammatory response, leading to the conclusion that effects were adverse at this exposure level. On the other hand, pathological effects on the respiratory system were practically absent in mice dosed with 4.34 mg/kg/day, which did not provoke any in-life effects. As

such, the effects were considered non-adverse. Consequently, the present results suggest a reference NOAEL for aerosol administration of 5 mg/kg as a starting point for future clinical studies.

As an outcome of the Study 2, when tested in rats, even at highest dose used, SET-M33 did not have any neurological effects as assessed by Irwin tests of behavioural and physiological states, nor did it affect body temperature, locomotor activity or body weight. Likewise, SET-M33 did not affect lung function in terms of respiratory rate, tidal volume and minute volume when compared with the vehicle-treated control and a baclofen-treated positive control. In prolonged treatment (4-week daily administration and 2-week recovery period) of rats, clinical signs during the recovery period and loss of body weight recorded in some animals showed that animals treated with the high dose (15 mg/kg/day) were unable to recover. Mean plasma concentrations quantified on day 28 were higher than on day 1 in both sexes, but especially in females. In any case, because no quantifiable concentrations were detected in the day 28 pre-dose and 24-hour post-dose samples, the increased drug exposure in females at day 28 is more likely related to a defect in drug elimination than to accumulation of SET-M33.

Systemic exposure of dogs to SET-M33 generally appeared to have nonlinear (dose-dependent) kinetics in the dose range 0.5 to 4.0 mg/kg/day on days 1 and 28 of the 4-week intravenous (infusion) study. Increasing the dose of SET-M33 above 0.5 mg/kg/day is likely to result in higher systemic exposure than would be predicted in the case of a linear relationship. However, the C_{max} of SET-M33 in male dogs appeared to have linear (dose-independent) kinetics. In addition, the data also provided evidence that there were no differences in systemic exposure of male and female dogs to SET-M33 at the 0.5 and 1.5 mg/kg/day dose levels, but that at the highest dose (4.0 mg/kg/day), the systemic exposure of female dogs to SET-M33 was higher than that of males. Systemic exposure was higher after repeated intravenous administration (infusion) of SET-M33 than after a single dose and suggests that SET-M33 has time-dependent kinetics.

Daily intravenous infusion of the peptide at ≥0.5 mg/kg/day in beagle dogs did not produce any observable effect on heart function, as demonstrated by ECG parameters (heart rate, PR, QRS, QT and QTc intervals) in males and females (data not reported here).

In both animal species, daily administration of SET-M33 at the highest doses used in our tests caused renal effects, such as tubule degeneration/regeneration, elevated blood concentrations of urea and creatinine, high glucose (only in rats), all suggesting a functional deficit and identifying the kidneys as a possible target for toxic effects. This confirms the bio-distribution and excretion data obtained previously with radio-iodinate SET-M33 [174], which showed an evident uptake of the peptide by kidneys and bladder after intravenous administration of the peptide to mice. The bioanalytical evaluation of blood parameters and the histological analysis of the present study did not suggest any possible toxic effects on other organs in rats and dogs.

Dogs remain the main non-rodent species used in preclinical drug development [205]. Determination of the NOAEL in these animals is an important part of non-clinical risk assessment [205-206]. The results obtained with SET-M33 in the 4-week toxicity study with 4-week recovery period in dogs, especially regarding the adverse findings of renal tubule degeneration/regeneration and moderate to marked vascular thrombi at infusion sites at doses ≥1.5 mg/kg/day, indicate that the NOAEL is below this latter dosage, presumably around 0.5 mg/kg/day. This dose will be a useful starting point for an eventual Phase I clinical trial.

Study 1 and Study 2 reported in this thesis were designed to comply with accepted pharmacological principles and the requirements of Europe, Japan and the USA [207-215].

The data reported in this thesis, added to that previously published for different animal models [174-177] complete the experimentation of the SET-M33 peptide. SET-M33 has now concluded all pre-clinical stages of development, including safety evaluations and toxicokinetic parameters, for administration by intravenous bolus or infusion and inhalation.

Considering the certain degree of toxicity, reported for other similar peptides as well, a strategies aimed to reduce the toxic effects at the local level maintaining its efficacy need to be implemented. With this purpose, the idea of encapsulation of the peptide in biocompatible nanoparticles (NPs) came up. Indeed, a promising formulation approach is the encapsulation in a poly(lactide-co-glycolide) nanoparticles that can mask the charges of SET-M33, preserve its bioactive structure, reduce side effects, facilitate transport to bacteria and achieve a prolonged therapeutic effect.

As a local delivery route, pulmonary administration through nebulization systems is an ideal way to treat respiratory infections, inflammation and other pathological manifestations affecting the lungs. However, important determinants of the clinical outcomes of inhaled medicines are the concentration/persistency of the drug in the lungs, as well as its ability to overcome airway barriers. Optimized inhalable formulations should be able to deliver the drug intact to the lungs and to shield its interactions with the lung environment [139; 216].

Traditional antibiotic therapies often fail, not only due to recurrent bacterial resistance, but also because of the presence of sticky mucus associated with infections and inflammation [217]. This aspect is especially critical in CF, where the submucosal glands and distal airways are obstructed by thick tenacious secretions. Indeed, CF mucus may strongly limit the drug concentration reaching the target (i.e., bacterial cells in the case of antimicrobial therapy). The route to the target is even more complicated for inhaled antimicrobial agents due to the biofilm-like mode of growth of certain bacterial species, such as *P. aeruginosa*, involved in lung infections.

The toxicity results and efficacy data already reported in this thesis and in previous articles [115; 169; 174; 176] showed a satisfactory therapeutic index, even with the narrow range of doses used. Likewise, preliminary experiments with free SET-M33 administered intratracheally by nebulization systems gave promising results in terms of efficacy and toxicity. However, its clinical application would be greatly improved by a decrease in toxicity.

A possible way to decrease local toxicity, and consequently enlarge the dose range, is encapsulation of the peptide in biocompatible nanoparticles. The encapsulation systems with single-chain dextran nanoparticles has been previously tested [177]. Here, we developed PLGA nanoparticles with a PEG shell. By virtue of their biocompatibility and biodegradability, PLGAs are a promising class of materials for delivery of antimicrobial peptides to the lungs [166-167]. These biocompatible NPs can be administered to the lungs through nebulizers as aqueous dispersions or dry powder [166; 218]. In our study, two different formulations of PEGylated PLGA-based NPs containing SET-M33 were prepared, using PEG of two different molecular weights (2000 or 5000 Da). Since PEG 5000 showed better performance in a translational perspective, SET-M33-containing NPs conjugated with PEG 5000 were chosen for further characterization in terms of antibacterial efficacy and toxicity.

Testing of this well-characterized nanosystem showed three important effects for lung delivery: 1) NPs containing SET-M33 passed biological barriers (lung mucus and bacterial alginate) while maintaining the local activity of the peptide; 2) the active molecule was released from NPs over an extended period of time, producing a prolonged antibacterial effect after a single administration; 3) SET-M33 toxicity was much reduced, while the molecule remained active in terms of antibacterial effect. Practically, the peptide contained within NPs did not provoke any detectable side effects in cells or *in vivo* at peptide doses in NPs that caused manifest toxicity when used as a free molecule [219].

In conclusion of the Study 3, the combination of polymeric NPs with a strong new antibacterial agent, such as the peptide SET-M33, produced an ideal antibacterial nanosystem for the development of a novel antibacterial agent. This nanosystem is attractive for the treatment of lung pathologies, where traditional antibiotics are losing their activity due to multidrug-resistant bacteria.

REFERENCES

1. Aslam B, Wang W, Arshad MI, Khurshid M, Muzammil S, Rasool MH, Nisar MA, Alvi RF, Aslam MA, Qamar MU, Salamat MKF, Baloch Z. Antibiotic resistance: a rundown of a global crisis. *Infect Drug Resist*. **2018**; *11:*1645-1658. doi: 10.2147/IDR.S173867.
2. Gajdács M, Albericio F. Antibiotic Resistance: From the Bench to Patients. *Antibiotics (Basel)*. **2019**; *8(3)*:129. doi: 10.3390/antibiotics8030129.
3. Baran A, Kwiatkowska A, Potocki L. Antibiotics and Bacterial Resistance-A Short Story of an Endless Arms Race. *Int J Mol Sci.* **2023**; *24*(6):5777. doi: 10.3390/ijms24065777.
4. Christaki E, Marcou M, Tofarides A. Antimicrobial Resistance in Bacteria: Mechanisms, Evolution, and Persistence. *J Mol Evol.* **2020**; 88(1):26-40. doi: 10.1007/s00239-019-09914-3.
5. Davies J, Davies D. Origins and evolution of antibiotic resistance. *Microbiol Mol Biol Rev.* **2010**; *74(3)*:417-33. doi: 10.1128/MMBR.00016-10.
6. Rice LB. Federal funding for the study of antimicrobial resistance in nosocomial pathogens: no ESKAPE. *J Infect Dis.* **2008**; *197*:1079–1081. doi: 10.1086/533452.
7. World Health Organization. 2017. Global priority list of antibiotic-resistant bacteria to guide research, discovery, and development of new antibiotics. https://www.who.int/news/item/27-02-2017-who-publishes-list-of-bacteria-for-which-new-antibiotics-are-urgently-needed
8. Larsson DG, Flach CF. Antibiotic resistance in the environment. *Nat Rev Microbiol*. **2022**; *20*:257–269. doi: 10.1038/s41579-021-00649-x.
9. The Review on Antimicrobial Resistance. Antimicrobial Resistance: Tackling A Crisis For The Health And Wealth Of Nations (Wellcome Trust and UK Government, 2014).
10. O'Neill, J. Tackling drug-resistant infections globally: Final report and recommendations. London: HM Government and Wellcome Trust; 2016. Review on Antimicrobial Resistance, chaired by Jim O'Neill. https://amr-review.org/sites/default/files/160518_Final%20paper_with% 20cover.pdf (Accessed 2023)
11. CenterWatch. 2020. FDA approved drugs. https://www.centerwatch.com/directories/1067-fda-approved-drugs/topic/546-bacterial-infections
12. Klug DM, Idiris FIM, Blaskovich MAT, von Delft F, Dowson CG, Kirchhelle C, Roberts AP, Singer AC, Todd MH. There is no market for new antibiotics: this allows an open approach to research and development. *Wellcome Open Res*. **2021**; *6*:146. doi: 10.12688/wellcomeopenres.16847.1.
13. European Medicines Agency. 2020. Vaborem. https://www.ema.europa.eu/en/medicines/human/EPAR/vaborem
14. European Medicines Agency. 2020. Xerava. https://www.ema.europa.eu/en/medicines/human/EPAR/xerava
15. European Medicines Agency. 2020. Quofenix. https://www.ema.europa.eu/en/medicines/human/EPAR/quofenix
16. European Medicines Agency. 2020. Recarbrio. https://www.ema.europa.eu/en/medicines/human/EPAR/recarbrio
17. Lin DM, Koskella B, Lin HC. Phage therapy: An alternative to antibiotics in the age of multi-drug resistance. *World J Gastrointest Pharmacol Ther*. **2017**; *8(3)*:162-173. doi: 10.4292/wjgpt.v8.i3.162.
18. Rappuoli R, Bloom DE, Black S. Deploy vaccines to fight superbugs. *Nature.* **2017**; *552(7684)*:165-167. doi: 10.1038/d41586-017-08323-0.
19. De Oliveira DMP, Forde BM, Kidd TJ, Harris PNA, Schembri MA, Beatson SA, Paterson DL, Walker MJ. Antimicrobial Resistance in ESKAPE Pathogens. *Clin Microbiol Rev.* **2020**; *33(3)*:e00181-19. doi: 10.1128/CMR.00181-19.
20. Bloom DE, Black S, Salisbury D, Rappuoli R. Antimicrobial resistance and the role of vaccines. *Proc Natl Acad Sci U S A.* **2018**; *115(51)*:12868-12871. doi: 10.1073/pnas.1717157115. PMID: 30559204; PMCID: PMC6305009
21. Mahlapuu M, Björn C, Ekblom J. Antimicrobial peptides as therapeutic agents: opportunities and challenges. *Crit Rev Biotechnol.* **2020**; *40(7)*:978-992. doi: 10.1080/07388551.2020.1796576.
22. Lourenço ALP, Rios TB, da Silva ÁP, Franco OL, Ramada MHS. Peptide Stapling Applied to Antimicrobial Peptides. *Antibiotics (Basel)*. **2023**; *12(9)*:1400. doi: 10.3390/antibiotics12091400.
23. Fjell CD, Hiss JA, Hancock RE, Schneider G. Designing antimicrobial peptides: form follows function. *Nat Rev Drug Discov.* **2011**; *11(1)*:37-51. doi: 10.1038/nrd3591. Erratum in: Nat Rev Drug Discov. 2012 Feb;11(2):168.
24. Chen N, Jiang C. Antimicrobial peptides: Structure, mechanism, and modification. *Eur J Med Chem*. **2023**; 255:115377. doi: 10.1016/j.ejmech.2023.115377.
25. Nijnik A, Hancock RE. The roles of cathelicidin LL-37 in immune defences and novel clinical applications. *Curr Opin Hematol.* **2009**; *16(1)*:41-7. doi: 10.1097/moh.0b013e32831ac517.
26. Takahashi D, Shukla SK, Prakash O, Zhang G. Structural determinants of host defense peptides for antimicrobial activity and target cell selectivity. *Biochimie.* **2010**; *92(9)*:1236-41. doi: 10.1016/j.biochi.2010.02.023.
27. Haney EF, Straus SK, Hancock REW. Reassessing the Host Defense Peptide Landscape. *Front Chem.* **2019**; *7*:43. doi: 10.3389/fchem.2019.00043.
28. Guan Q, Huang S, Jin Y, Campagne R, Alezra V, Wan Y. Recent Advances in the Exploration of Therapeutic Analogues of Gramicidin S, an Old but Still Potent Antimicrobial Peptide. *J Med Chem.* **2019**; *62(17)*:7603-7617. doi: 10.1021/acs.jmedchem.9b00156.
29. Magana M, Pushpanathan M, Santos AL, Leanse L, Fernandez M, Ioannidis A, Giulianotti MA, Apidianakis Y, Bradfute S, Ferguson AL, Cherkasov A, Seleem MN, Pinilla C, de la Fuente-Nunez C, Lazaridis T, Dai T, Houghten RA, Hancock REW, Tegos GP. The value of antimicrobial peptides in the age of resistance. *Lancet Infect Dis*. **2020**; *20(9)*:e216-e230. doi: 10.1016/S1473-3099(20)30327-3.

30. Mookherjee N, Hancock RE. Cationic host defence peptides: innate immune regulatory peptides as a novel approach for treating infections. *Cell Mol Life Sci.* **2007**; *64(7-8)*:922-33. doi: 10.1007/s00018-007-6475-6.
31. Lazzaro BP, Zasloff M, Rolff J. Antimicrobial peptides: Application informed by evolution. *Science*. **2020**; *368*(6490):eaau5480. doi: 10.1126/science.aau5480.
32. Bin Hafeez A, Jiang X, Bergen PJ, Zhu Y. Antimicrobial Peptides: An Update on Classifications and Databases. *Int J Mol Sci.* **2021**; *22(21)*:11691. doi: 10.3390/ijms222111691.
33. Yi HY, Chowdhury M, Huang YD, Yu XQ. Insect antimicrobial peptides and their applications. *Appl Microbiol Biotechnol.* **2014**; *98(13)*:5807-22. doi: 10.1007/s00253-014-5792-6.
34. Rončević T, Puizina J, Tossi A. Antimicrobial Peptides as Anti-Infective Agents in Pre-Post-Antibiotic Era? *Int J Mol Sci.* **2019**; *20(22)*:5713. doi: 10.3390/ijms20225713.
35. Wang G, Li X, Wang Z. APD3: the antimicrobial peptide database as a tool for research and education. *Nucleic Acids Res.* **2016**; *44(D1)*:D1087-93. doi: 10.1093/nar/gkv1278.
36. Gao X, Ding J, Liao C, Xu J, Liu X, Lu W. Defensins: The natural peptide antibiotic. *Adv Drug Deliv Rev*. **2021**; *179*:114008. doi: 10.1016/j.addr.2021.114008.
37. Luo Y, Song Y. Mechanism of Antimicrobial Peptides: Antimicrobial, Anti-Inflammatory and Antibiofilm Activities. *Int J Mol Sci*. **2021**; *22(21)*:11401. doi: 10.3390/ijms222111401.
38. Talapko J, Meštrović T, Juzbašić M, Tomas M, Erić S, Horvat Aleksijević L, Bekić S, Schwarz D, Matić S, Neuberg M, Škrlec I. Antimicrobial Peptides-Mechanisms of Action, Antimicrobial Effects and Clinical Applications. *Antibiotics (Basel)*. **2022**; *11(10)*:1417. doi: 10.3390/antibiotics11101417.
39. Dijksteel GS, Ulrich MMW, Middelkoop E and Boekema BKHL. Review: Lessons Learned from Clinical Trials Using Antimicrobial Peptides (AMPs). *Front. Microbiol*. **2021**; *12*:616979. doi: 10.3389/fmicb.2021.616979.
40. Ebenhan T, Gheysens O, Kruger HG, Zeevaart JR, Sathekge MM. Antimicrobial peptides: their role as infection-selective tracers for molecular imaging. *Biomed Res Int*. **2014**; *2014*:867381. doi: 10.1155/2014/867381
41. Huang Y, Huang J, Chen Y. Alpha-helical cationic antimicrobial peptides: relationships of structure and function. *Protein Cell.* **2010**; *1(2)*:143-52. doi: 10.1007/s13238-010-0004-3.
42. Godballe T, Nilsson LL, Petersen PD, Jenssen H. Antimicrobial β-peptides and α-peptoids. *Chem Biol Drug Des.* **2011**; *77(2)*:107-16. doi: 10.1111/j.1747-0285.2010.01067.x.
43. Wang G. Improved methods for classification, prediction, and design of antimicrobial peptides. *Methods Mol Biol.* **2015**; *1268*:43-66. doi: 10.1007/978-1-4939-2285-7_3.
44. Lee TH, Hall KN, Aguilar MI. Antimicrobial Peptide Structure and Mechanism of Action: A Focus on the Role of Membrane Structure. *Curr Top Med Chem*. **2016**; *16(1)*:25-39. doi: 10.2174/1568026615666150703121700.
45. Lyu Z, Yang P, Lei J, Zhao J. Biological Function of Antimicrobial Peptides on Suppressing Pathogens and Improving Host Immunity. *Antibiotics*. **2023**; *12*:1037. Doi: 10.3390/antibiotics12061037.
46. Lin TT, Yang LY, Lin CY, Wang CT, Lai CW, Ko CF, Shih YH, Chen SH. Intelligent De Novo Design of Novel Antimicrobial Peptides against Antibiotic-Resistant Bacteria Strains. *Int J Mol Sci.* **2023**; *24(7)*:6788. doi: 10.3390/ijms24076788.
47. Levin JM, Oprea TI, Davidovich S, Clozel T, Overington JP, Vanhaelen Q, Cantor CR, Bischof E, Zhavoronkov A. Artificial intelligence, drug repurposing and peer review. *Nat Biotechnol*. **2020**; *38(10)*:1127-1131. doi: 10.1038/s41587-020-0686-x.
48. Réda C, Kaufmann E, Delahaye-Duriez A. Machine learning applications in drug development. *Comput Struct Biotechnol J.* **2019**; *18*:241-252. doi: 10.1016/j.csbj.2019.12.006
49. Torres MDT, Cao J, Franco OL, Lu TK, de la Fuente-Nunez C. Synthetic Biology and Computer-Based Frameworks for Antimicrobial Peptide Discovery. *ACS Nano*. **2021**; *15(2)*:2143-2164. doi: 10.1021/acsnano.0c09509.
50. Smith GP. Filamentous fusion phage: novel expression vectors that display cloned antigens on the virion surface. *Science*. **1985**; *228(4705)*:1315-7. doi: 10.1126/science.4001944.
51. Pitt A, Nims Z. Peptide Display Technologies. *Methods Mol Biol.* **2019**; *2001*:285-298. doi: 10.1007/978-1-4939-9504-2_13.
52. Lyu Z, Yang P, Lei J, Zhao J. Biological Function of Antimicrobial Peptides on Suppressing Pathogens and Improving Host Immunity. *Antibiotics (Basel)*. **2023**; *12(6)*:1037. doi: 10.3390/antibiotics12061037.
53. Musa M, Radman M, Krisko A. Decreasing translation error rate in Escherichia coli increases protein function. *BMC Biotechnol.* **2016**; 16:28. doi: 10.1186/s12896-016-0259-8.
54. Mattanovich D, Branduardi P, Dato L, Gasser B, Sauer M, Porro D. Recombinant protein production in yeasts. *Methods Mol Biol.* **2012**; *824*:329-58. doi: 10.1007/978-1-61779-433-9_17.
55. Shanmugaraj B, Bulaon CJI, Malla A, Phoolcharoen W. Biotechnological Insights on the Expression and Production of Antimicrobial Peptides in Plants. *Molecules*. **2021**; 26(13):4032. doi: 10.3390/molecules26134032.
56. Holaskova E, Galuszka P, Frebort I, Oz MT. Antimicrobial peptide production and plant-based expression systems for medical and agricultural biotechnology. *Biotechnol Adv.* **2015**; *33(6 Pt 2)*:1005-23. doi: 10.1016/j.biotechadv.2015.03.007.
57. Merrifield RB. Solid phase peptide synthesis. i. the synthesis of a tetrapeptide. *J. Am. Chem. Soc.* **1963**; **85**:2149–2154.
58. Behrendt R, White P, Offer J. Advances in Fmoc solid-phase peptide synthesis. *J Pept Sci.* **2016**; *22(1)*:4-27. doi: 10.1002/psc.2836.
59. Roque-Borda CA, da Silva PB, Rodrigues MC, Azevedo RB, Di Filippo L, Duarte JL, Chorilli M, Festozo Vicente E, Pavan FR. Challenge in the Discovery of New Drugs: Antimicrobial Peptides against WHO-List of Critical and High-Priority Bacteria. *Pharmaceutics.* **2021**; *13(6)*:773. doi: 10.3390/pharmaceutics13060773.

60. Dorato MA, Buckley LA. Toxicology in the drug discovery and development process. *Curr Protoc Pharmacol.* **2006**; Chapter 10:Unit10.3. doi: 10.1002/0471141755.ph1003s32.
61. Hannappel M. Biopharmaceuticals: From peptide to drug. *AIP Conf. Proc.* **2017**; *1871(1)*:060004. doi: 10.1063/1.4996533
62. Agyei D, Ahmed I, Akram Z, Iqbal HM, Danquah MK. Protein and Peptide Biopharmaceuticals: An Overview. *Protein Pept Lett.* **2017**; *24(2)*:94-101. doi: 10.2174/0929866523666161222150444.
63. Payne DJ, Gwynn MN, Holmes DJ, Pompliano DL. Drugs for bad bugs: confronting the challenges of antibacterial discovery. *Nat Rev Drug Discov*. **2007**; *6(1)*:29-40. doi: 10.1038/nrd2201.
64. Miethke M, Pieroni M, Weber T, Brönstrup M, Hammann P, Halby L, Arimondo PB, Glaser P, Aigle B, Bode HB, Moreira R, Li Y, Luzhetskyy A, Medema MH, Pernodet JL, Stadler M, Tormo JR, Genilloud O, Truman AW, Weissman KJ, Takano E, Sabatini S, Stegmann E, Brötz-Oesterhelt H, Wohlleben W, Seemann M, Empting M, Hirsch AKH, Loretz B, Lehr CM, Titz A, Herrmann J, Jaeger T, Alt S, Hesterkamp T, Winterhalter M, Schiefer A, Pfarr K, Hoerauf A, Graz H, Graz M, Lindvall M, Ramurthy S, Karlén A, van Dongen M, Petkovic H, Keller A, Peyrane F, Donadio S, Fraisse L, Piddock LJV, Gilbert IH, Moser HE, Müller R. Towards the sustainable discovery and development of new antibiotics. *Nat Rev Chem*. **2021**; *5(10)*:726-749. doi: 10.1038/s41570-021-00313-1.
65. Sharma K, Sharma KK, Sharma A, Jain R. Peptide-based drug discovery: Current status and recent advances. *Drug Discov Today*. **2023**; *28(2)*:103464. doi: 10.1016/j.drudis.2022.103464.
66. Muttenthaler M, King GF, Adams DJ, Alewood PF. Trends in peptide drug discovery. *Nat Rev Drug Discov*. **2021**; *20(4)*:309–325. doi: 10.1038/s41573-020-00135-8.
67. Anand U, Bandyopadhyay A, Jha NK, Pérez de la Lastra JM, Dey A. Translational aspect in peptide drug discovery and development: An emerging therapeutic candidate. *Biofactors*. **2023**; *49(2)*:251-269. doi: 10.1002/biof.1913.
68. U.S Food and Drug Administration. FDA approved drug products. http://www.accessdata.fda.gov/scripts/cder/drugsatfda/index.cfm?fuseaction=Search.DrugDetails (Accessed on December, 2023)
69. Tran TB, Velkov T, Nation RL, Forrest A, Tsuji BT, Bergen PJ, Li J. Pharmacokinetics/pharmacodynamics of colistin and polymyxin B: are we there yet?. *Int J Antimicrob Agents*. **2016**; *48(6)*:592-597. doi: 10.1016/j.ijantimicag.2016.09.010.
70. Roscia G, Falciani C, Bracci L, Pini A. The development of antimicrobial peptides as new antibacterial drugs. *Curr Protein Pept Sci.* **2013**; *14(8)*:641-9. doi: 10.2174/1389203714081312271553O8.
71. Gregoire N, Chauzy A, Buyck J, Rammaert B, Couet W, Marchand S. Clinical Pharmacokinetics of Daptomycin. *Clin Pharmacokinet.* **2021**; *60(3)*:271-281. doi: 10.1007/s40262-020-00968-x.
72. Tally FP, DeBruin MF. Development of daptomycin for gram-positive infections. *J Antimicrob Chemother.* **2000**; *46(4)*:523-6. doi: 10.1093/jac/46.4.523.
73. LiverTox: Clinical and Research Information on Drug-Induced Liver Injury [Internet]. Bethesda (MD): National Institute of Diabetes and Digestive and Kidney Diseases; 2012–. Vancomycin. 2020 Aug 20. PMID: 31644188
74. Zhanel GG, Calic D, Schweizer F, Zelenitsky S, Adam H, Lagacé-Wiens PR, Rubinstein E, Gin AS, Hoban DJ, Karlowsky JA. New lipoglycopeptides: a comparative review of dalbavancin, oritavancin and telavancin. *Drugs*. **2010**; *70(7)*:859-86. doi: 10.2165/11534440-000000000-00000.
75. Vimberg V. Teicoplanin-A New Use for an Old Drug in the COVID-19 Era? *Pharmaceuticals (Basel)*. **2021**; 14(12):1227. doi: 10.3390/ph14121227.
76. Pavithrra G, Rajasekaran R. Gramicidin Peptide to Combat Antibiotic Resistance: A Review. *Int. J. Pept. Res. Ther.* **2020**; *26:* 191–199.
77. van der Does AM, Hensbergen PJ, Bogaards SJ, Cansoy M, Deelder AM, van Leeuwen HC, Drijfhout JW, van Dissel JT, Nibbering PH. The human lactoferrin-derived peptide hLF1-11 exerts immunomodulatory effects by specific inhibition of myeloperoxidase activity. *J Immunol*. **2012**; *188(10)*:5012-9. doi: 10.4049/jimmunol.1102777.
78. van Groenendael R, Beunders R, Kox M, van Eijk LT, Pickkers P. The Human Chorionic Gonadotropin Derivate EA-230 Modulates the Immune Response and Exerts Renal Protective Properties: Therapeutic Potential in Humans. *Semin Nephrol.* **2019**; *39(5)*:496-504. doi: 10.1016/j.semnephrol.2019.06.009.
79. van Groenendael R, Beunders R, Hemelaar P, Hofland J, Morshuis WJ, van der Hoeven JG, Gerretsen J, Wensvoort G, Kooistra EJ, Claassen WJ, Waanders D, Lamberts MGA, Buijsse LSE, Kox M, van Eijk LT, Pickkers P. Safety and Efficacy of Human Chorionic Gonadotropin Hormone-Derivative EA-230 in Cardiac Surgery Patients: A Randomized Double-Blind Placebo-Controlled Study. *Crit Care Med.* **2021**; *49(5)*:790-803. doi: 10.1097/CCM.0000000000004847.
80. Kaplan CW, Sim JH, Shah KR, Kolesnikova-Kaplan A, Shi W, Eckert R. Selective membrane disruption: mode of action of C16G2, a specifically targeted antimicrobial peptide. *Antimicrob Agents Chemother*. **2011**; *55(7)*:3446-52. doi: 10.1128/AAC.00342-11.
81. https://www.dentistryiq.com/dentistry/article/16350459/c3-jian-completes-second-phase-2-clinical-trial-of-anticavity-drug (Accessed on December, 2023).
82. Mercer DK, Robertson JC, Miller L, Stewart CS, O'Neil DA. NP213 (Novexatin®): A unique therapy candidate for onychomycosis with a differentiated safety and efficacy profile. *Med Mycol*. **2020**; *58(8)*:1064-1072. doi: 10.1093/mmy/myaa015.
83. Kudrimoti M, Curtis A, Azawi S, Worden F, Katz S, Adkins D, Bonomi M, Elder J, Sonis ST, Straube R, Donini O. Dusquetide: A novel innate defense regulator demonstrating a significant and consistent reduction in the duration of oral mucositis in

preclinical data and a randomized, placebo-controlled phase 2a clinical study. *J Biotechnol*. **2016**; *239*:115-125. doi: 10.1016/j.jbiotec.2016.10.010.
84. https://www.soligenix.com/pipeline-programs/sgx942-treatment-for-oral-mucositis/ (accessed on December, 2023).
85. Fritsche TR, Rhomberg PR, Sader HS, Jones RN. Antimicrobial activity of omiganan pentahydrochloride tested against contemporary bacterial pathogens commonly responsible for catheter-associated infections. *J Antimicrob Chemother*. **2008**; *61(5)*:1092-8. doi: 10.1093/jac/dkn074.
86. Niemeyer-van der Kolk T, Buters TP, Krouwels L, Boltjes J, de Kam ML, van der Wall H, van Alewijk DCJG, van den Munckhof EHA, Becker MJ, Feiss G, Florencia EF, Prens EP, Moerland M, Burggraaf J, Rissmann R, van Doorn MBA. Topical antimicrobial peptide omiganan recovers cutaneous dysbiosis but does not improve clinical symptoms in patients with mild to moderate atopic dermatitis in a phase 2 randomized controlled trial. *J Am Acad Dermatol*. **2022**; *86(4)*:854-862. doi: 10.1016/j.jaad.2020.08.132.
87. Rijsbergen M, Rijneveld R, Todd M, Feiss GL, Kouwenhoven STP, Quint KD, van Alewijk DCJG, de Koning MNC, Klaassen ES, Burggraaf J, Rissmann R, van Poelgeest MIE. Results of phase 2 trials exploring the safety and efficacy of omiganan in patients with human papillomavirus-induced genital lesions. *Br J Clin Pharmacol*. **2020**; *86(11)*:2133-2143. doi: 10.1111/bcp.14181.
88. Alshrari AS, Hudu SA, Elmigdadi F, Imran M. The Urgent Threat of Clostridioides difficile Infection: A Glimpse of the Drugs of the Future, with Related Patents and Prospects. *Biomedicines.* **2023**; *11(2)*:426. doi: 10.3390/biomedicines11020426.
89. Laverty G. Cationic antimicrobial peptide cytotoxicity. *SOJ Microbiol. Infect. Dis.* **2014**; *2*:112. doi: 10.15226/sojmid.2013.00112.
90. Dijksteel GS, Ulrich MMW, Middelkoop E, Boekema BKHL. Review: Lessons Learned From Clinical Trials Using Antimicrobial Peptides (AMPs). *Front Microbiol*. **2021**; *12*:616979. doi: 10.3389/fmicb.2021.616979.
91. Li J, Koh JJ, Liu S, Lakshminarayanan R, Verma CS, Beuerman RW. Membrane Active Antimicrobial Peptides: Translating Mechanistic Insights to Design. *Front Neurosci*. **2017**; 11:73. doi: 10.3389/fnins.2017.00073.
92. McCrudden MTC, McLean DTF, Zhou M, Shaw J, Linden GJ, Irwin CR, Lundy FT. The host defence peptide LL-37 is susceptible to proteolytic degradation by wound fluid isolated from foot ulcers of diabetic patients. *Int. J. Pept. Res. Ther.* **2014**; *20*:457–464. 10.1007/s10989-014-9410-3.
93. Kohanski MA, Dwyer DJ, Collins JJ. How antibiotics kill bacteria: from targets to networks. *Nat Rev Microbiol.* **2010**; *8(6)*:423-35. doi: 10.1038/nrmicro2333.
94. Mookherjee N, Anderson MA, Haagsman HP, Davidson DJ. Antimicrobial host defence peptides: functions and clinical potential. *Nat Rev Drug Discov*. **2020**; *19(5)*:311-332. doi: 10.1038/s41573-019-0058-8.
95. Spohn R, Daruka L, Lázár V, Martins A, Vidovics F, Grézal G, Méhi O, Kintses B, Számel M, Jangir PK, Csörgő B, Györkei Á, Bódi Z, Faragó A, Bodai L, Földesi I, Kata D, Maróti G, Pap B, Wirth R, Papp B, Pál C. Integrated evolutionary analysis reveals antimicrobial peptides with limited resistance. *Nat Commun*. **2019**; *10(1)*:4538. doi: 10.1038/s41467-019-12364-6.
96. Bauer ME, Shafer WM. On the in vivo significance of bacterial resistance to antimicrobial peptides. *Biochim Biophys Acta.* **2015**; *1848(11 Pt B)*:3101-11. doi: 10.1016/j.bbamem.2015.02.012.
97. Andersson DI, Hughes D, Kubicek-Sutherland JZ. Mechanisms and consequences of bacterial resistance to antimicrobial peptides. *Drug Resist Updat*. **2016**; *26*:43-57. doi: 10.1016/j.drup.2016.04.002.
98. Anaya-López JL, López-Meza JE, Ochoa-Zarzosa A. Bacterial resistance to cationic antimicrobial peptides. *Crit Rev Microbiol.* **2013**; *39(2)*:180-95. doi: 10.3109/1040841X.2012.699025.
99. Peschel A, Sahl HG. The co-evolution of host cationic antimicrobial peptides and microbial resistance. *Nat Rev Microbiol.* **2006**; *4(7)*:529-36. doi: 10.1038/nrmicro1441.
100. Lazzaro BP, Zasloff M, Rolff J. Antimicrobial peptides: Application informed by evolution. *Science*. **2020**; *368(6490)*:eaau5480. doi: 10.1126/science.aau5480.
101. Liu Y, Shi J, Tong Z, Jia Y, Yang B, Wang Z. The revitalization of antimicrobial peptides in the resistance era. *Pharmacol Res.* 2021; *163*:105276. doi: 10.1016/j.phrs.2020.105276.
102. Liu YY, Wang Y, Walsh TR, Yi LX, Zhang R, Spencer J, Doi Y, Tian G, Dong B, Huang X, Yu LF, Gu D, Ren H, Chen X, Lv L, He D, Zhou H, Liang Z, Liu JH, Shen J. Emergence of plasmid-mediated colistin resistance mechanism MCR-1 in animals and human beings in China: a microbiological and molecular biological study. *Lancet Infect Dis.* **2016**; *16(2)*:161-8. doi: 10.1016/S1473-3099(15)00424-7.
103. Sun J, Zhang H, Liu YH, Feng Y. Towards Understanding MCR-like Colistin Resistance. *Trends Microbiol.* **2018**; *26(9)*:794-808. doi: 10.1016/j.tim.2018.02.006.
104. Hu Y, Liu F, Lin IY, Gao GF, Zhu B. Dissemination of the mcr-1 colistin resistance gene. *Lancet Infect Dis.* **2016**; *16(2)*:146-7. doi: 10.1016/S1473-3099(15)00533-2.
105. Veronese FM, Mero A. The impact of PEGylation on biological therapies. *BioDrugs.* **2008**; *22(5)*:315-29. doi: 10.2165/00063030-200822050-00004.
106. Falciani C, Lozzi L, Scali S, Brunetti J, Bracci L, Pini A. Site-specific pegylation of an antimicrobial peptide increases resistance to Pseudomonas aeruginosa elastase. *Amino Acids.* **2014**; *46(5)*:1403-7. doi: 10.1007/s00726-014-1686-2.
107. Park H, Otte A, Park K. Evolution of drug delivery systems: From 1950 to 2020 and beyond. *J Control Release*. **2022**; *342*:53-65. doi: 10.1016/j.jconrel.2021.12.030.

108. Kamysz E, Sikorska E, Jaśkiewicz M, Bauer M, Neubauer D, Bartoszewska S, Barańska-Rybak W, Kamysz W. Lipidated Analogs of the LL-37-Derived Peptide Fragment KR12-Structural Analysis, Surface-Active Properties and Antimicrobial Activity. *Int J Mol Sci.* **2020**; *21(3)*:887. doi: 10.3390/ijms21030887.
109. Rounds T, Straus SK. Lipidation of Antimicrobial Peptides as a Design Strategy for Future Alternatives to Antibiotics. *Int J Mol Sci.* **2020**; *21(24)*:9692. doi: 10.3390/ijms21249692.
110. Bellavita R, Braccia S, Galdiero S, Falanga A. Glycosylation and Lipidation Strategies: Approaches for Improving Antimicrobial Peptide Efficacy. *Pharmaceuticals (Basel).* **2023**; *16(3)*:439. doi: 10.3390/ph16030439.
111. Jiang H, Zhang X, Chen X, Aramsangtienchai P, Tong Z, Lin H. Protein Lipidation: Occurrence, Mechanisms, Biological Functions, and Enabling Technologies. *Chem Rev.* **2018**; *118(3)*:919-988. doi: 10.1021/acs.chemrev.6b00750.
112. Deo S, Turton KL, Kainth T, Kumar A, Wieden HJ. Strategies for improving antimicrobial peptide production. *Biotechnol Adv.* **2022;** *59*:107968. doi: 10.1016/j.biotechadv.2022.107968.
113. Chen N, Jiang C. Antimicrobial peptides: Structure, mechanism, and modification. *Eur J Med Chem.* **2023**; 255:115377. doi: 10.1016/j.ejmech.2023.115377.
114. Falciani C, Lozzi L, Pollini S, Luca V, Carnicelli V, Brunetti J, Lelli B, Bindi S, Scali S, Di Giulio A, Rossolini GM, Mangoni ML, Bracci L, Pini A. Isomerization of an antimicrobial peptide broadens antimicrobial spectrum to gram-positive bacterial pathogens. *PLoS One.* **2012**; *7(10)*:e46259. doi: 10.1371/journal.pone.0046259.
115. Brunetti J, Carnicelli V, Ponzi A, Di Giulio A, Lizzi AR, Cristiano L, Cresti L, Cappello G, Pollini S, Mosconi L, Rossolini GM, Bracci L, Falciani C, Pini A. Antibacterial and Anti-Inflammatory Activity of an Antimicrobial Peptide Synthesized with D Amino Acids. *Antibiotics (Basel)*. **2020**; *9(12)*:840. doi: 10.3390/antibiotics9120840.
116. Tam JP. Synthetic peptide vaccine design: synthesis and properties of a high-density multiple antigenic peptide system. *Proc. Natl. Acad. Sci. USA.* **1988**; *85(15)*:5409-5413. doi: 10.1073/pnas.85.15.5409.
117. Pini A, Falciani C, Bracci L. Branched peptides as therapeutics. *Curr Protein Pept Sci.* **2008**; *9(5)*:468-77. doi: 10.2174/138920308785915227.
118. Bracci L, Falciani C, Lelli B, Lozzi L, Runci Y, Pini A, De Montis MG, Tagliamonte A, Neri P. Synthetic peptides in the form of dendrimers become resistant to protease activity. *J Biol Chem.* **2003**; *278(47)*:46590-5. doi: 10.1074/jbc.M308615200.
119. Wei D, Zhang X. Biosynthesis, bioactivity, biotoxicity and applications of antimicrobial peptides for human health. *Biosafety and Health*. **2022**; *4(2)*:118-134. doi: 10.1016/j.bsheal.2022.02.003.
120. Greco I, Molchanova N, Holmedal E, Jenssen H, Hummel BD, Watts JL, Håkansson J, Hansen PR, Svenson J. Correlation between hemolytic activity, cytotoxicity and systemic in vivo toxicity of synthetic antimicrobial peptides. *Sci Rep.* **2020**; *10(1)*:13206. doi: 10.1038/s41598-020-69995-9.
121. Spaller BL, Trieu JM, Almeida PF. Hemolytic activity of membrane-active peptides correlates with the thermodynamics of binding to 1-palmitoyl-2-oleoyl-sn-glycero-3-phosphocholine bilayers. *J Membr Biol.* **2013**; 246(3):257-62. doi: 10.1007/s00232-013-9525-z.
122. Edwards IA, Elliott AG, Kavanagh AM, Blaskovich MAT, Cooper MA. Structure-Activity and -Toxicity Relationships of the Antimicrobial Peptide Tachyplesin-1. *ACS Infect Dis.* **2017**; *3(12)*:917-926. doi: 10.1021/acsinfecdis.7b00123.
123. Bamgbola O. Review of vancomycin-induced renal toxicity: an update. *Ther Adv Endocrinol Metab.* **2016**; *7(3)*:136-47. doi: 10.1177/2042018816638223.
124. Ordooei Javan A, Salamzadeh J, Shokouhi S, Sahraei Z. Evaluation of Renal Toxicity of Colistin Therapy With Neutrophil Gelatinase-associated Lipocalin: a Biomarker of Renal Tubular Damage. *Iran J Kidney Dis*. **2017**; *11(6)*:447-455.
125. Kelesidis T, Falagas ME. The safety of polymyxin antibiotics. *Expert Opin Drug Saf.* **2015**; *14(11)*:1687-701. doi: 10.1517/14740338.2015.1088520.
126. Zavascki AP, Nation RL. Nephrotoxicity of Polymyxins: Is There Any Difference between Colistimethate and Polymyxin B? *Antimicrob Agents Chemother.* **2017**; *61(3)*:e02319-16. doi: 10.1128/AAC.02319-16.
127. Dai C, Li J, Tang S, Li J, Xiao X. Colistin-induced nephrotoxicity in mice involves the mitochondrial, death receptor, and endoplasmic reticulum pathways. *Antimicrob Agents Chemother*. **2014**; *58(7)*:4075-4085. doi: 10.1128/AAC.00070-14.
128. Azad MA, Finnin BA, Poudyal A, Davis K, Li J, Hill PA, Nation RL, and Velkov T. Polymyxin B induces apoptosis in kidney proximal tubular cells. *Antimicrob Agents Chemother.* **2013**; *57*:4329–4335. doi: 10.1128/AAC.02587-12.
129. Li J, Milne RW, Nation RL, Turnidge JD, Smeaton TC, Coulthard K. Pharmacokinetics of colistin methanesulphonate and colistin in rats following an intravenous dose of colistin methanesulphonate. *J Antimicrob Chemother*. **2004**; *53(5)*:837-840. doi: 10.1093/jac/dkh167.
130. Cresti L, Falciani C, Cappello G, Brunetti J, Vailati S, Melloni E, Bracci L, Pini A. Safety evaluations of a synthetic antimicrobial peptide administered intravenously in rats and dogs. *Sci Rep.* **2022**; *12(1)*:19294. doi: 10.1038/s41598-022-23841-2.
131. Cresti L, Cappello G, Vailati S, Melloni E, Brunetti J, Falciani C, Bracci L, Pini A. In Vivo Efficacy and Toxicity of an Antimicrobial Peptide in a Model of Endotoxin-Induced Pulmonary Inflammation. *Int J Mol Sci.* **2023**; *24(9)*:7967. doi: 10.3390/ijms24097967.
132. Ho DK, Nichols BLB, Edgar KJ, Murgia X, Loretz B, Lehr CM. Challenges and strategies in drug delivery systems for treatment of pulmonary infections. *Eur J Pharm Biopharm*. **2019**; *144*:110-124. doi: 10.1016/j.ejpb.2019.09.002.
133. d'Angelo I, Conte C, La Rotonda MI, Miro A, Quaglia F, Ungaro F. Improving the efficacy of inhaled drugs in cystic fibrosis: challenges and emerging drug delivery strategies. *Adv Drug Deliv Rev.* **2014**; *75*:92-111. doi: 10.1016/j.addr.2014.05.008.
134. Gao W, Chen Y, Zhang Y, Zhang Q, Zhang L. Nanoparticle-based local antimicrobial drug delivery. *Adv Drug Deliv Rev*. **2018**; *127*:46-57. doi: 10.1016/j.addr.2017.09.015.

135. O'Sullivan BP, Freedman SD. Cystic fibrosis. *Lancet.* **2009**; *373(9678)*:1891-904. doi: 10.1016/S0140-6736(09)60327-5.
136. Gaspar MC, Couet W, Olivier JC, Pais AA, Sousa JJ. Pseudomonas aeruginosa infection in cystic fibrosis lung disease and new perspectives of treatment: a review. *Eur J Clin Microbiol Infect Dis.* **2013**; *32(10)*:1231-1252. doi: 10.1007/s10096-013-1876-y.
137. Ibrahim BM, Tsifansky MD, Yang Y, Yeo Y. Challenges and advances in the development of inhalable drug formulations for cystic fibrosis lung disease. *Expert Opin Drug Deliv*. **2011**; *8(4)*:451-66. doi: 10.1517/17425247.2011.561310.
138. Patra JK, Das G, Fraceto LF, Campos EVR, Rodriguez-Torres MDP, Acosta-Torres LS, Diaz-Torres LA, Grillo R, Swamy MK, Sharma S, Habtemariam S, Shin HS. Nano based drug delivery systems: recent developments and future prospects. J *Nanobiotechnology.* **2018**; *16(1)*:71. doi: 10.1186/s12951-018-0392-8.
139. Cano A, Ettcheto M, Espina M, López-Machado A, Cajal Y, Rabanal F, Sánchez-López E, Camins A, García ML, Souto EB. State-of-the-art polymeric nanoparticles as promising therapeutic tools against human bacterial infections. *J Nanobiotechnology*. **2020**; *18(1)*:156. doi: 10.1186/s12951-020-00714-2.
140. Cavalieri F, Tortora M, Stringaro A, Colone M, Baldassarri L. Nanomedicines for antimicrobial interventions. *J Hosp Infect*. **2014**; *88(4)*:183-90. doi: 10.1016/j.jhin.2014.09.009.
141. Eleraky NE, Allam A, Hassan SB, Omar MM. Nanomedicine Fight against Antibacterial Resistance: An Overview of the Recent Pharmaceutical Innovations. *Pharmaceutics.* **2020**; *12(2)*:142. doi: 10.3390/pharmaceutics12020142.
142. Bhatia S. Nanoparticles types, classification, characterization, fabrication methods and drug delivery applications, Natural polymer drug delivery systems. *Natural Polymer Drug Delivery Systems*. **2016**; pp. 33-93. doi: 10.1007/978-3-319-41129-3_2
143. Shnoudeh AJ, Hamad I, Abdo RW, Qadumii L, Jaber AY, Surchi HS, Alkelany SZ. Synthesis, Characterization, and Applications of Metal Nanoparticles. *Advances in Pharmaceutical Product Development and Research, Biomaterials and Bionanotechnology: Elsevier*. **2019**. *Chapter 15*, pp. 527-612
144. Mitchell MJ, Billingsley MM, Haley RM, Wechsler ME, Peppas NA, Langer R. Engineering precision nanoparticles for drug delivery. *Nat Rev Drug Discov*. **2021**; *20(2)*:101-124. doi: 10.1038/s41573-020-0090-8.
145. Anselmo AC, Mitragotri S. Nanoparticles in the clinic: An update. *Bioeng Transl Med.* **2019**; 4(3):e10143. doi: 10.1002/btm2.10143.
146. FDA News Release. FDA approves first treatment for certain types of poor-prognosis acute myeloid leukemia. 2017. http://www.fda.gov/news-events/press-announcements/fda-approves-first-treatment-certain-types-poor-prognosis-acute-myeloid-leukemia. Accessed December, 2023
147. Zhang L, Pornpattananangku D, Hu CM, Huang CM. Development of nanoparticles for antimicrobial drug delivery. *Curr Med Chem.* **2010**; *17(6)*:585-94. doi: 10.2174/092986710790416290.
148. Sharma S, Parmar A, Kori S, Sandhir R. PLGA-based nanoparticles: a new paradigm in biomedical applications, *TrAC Trends in Analytical Chemistry*, **2016**; *80*:30-40. doi: 10.1016/j.trac.2015.06.014
149. Lu Y, Cheng D, Niu B, Wang X, Wu X, Wang A. Properties of Poly (Lactic-co-Glycolic Acid) and Progress of Poly (Lactic-co-Glycolic Acid)-Based Biodegradable Materials in Biomedical Research. *Pharmaceuticals (Basel).* **2023**; *16(3)*:454. doi: 10.3390/ph16030454.
150. Galindo R, Sánchez-López E, Gómara MJ, Espina M, Ettcheto M, Cano A, Haro I, Camins A, García ML. Development of Peptide Targeted PLGA-PEGylated Nanoparticles Loading Licochalcone-A for Ocular Inflammation. *Pharmaceutics.* **2022**; 14(2):285. doi: 10.3390/pharmaceutics14020285.
151. Zhang D, Liu L, Wang J, Zhang H, Zhang Z, Xing G, Wang X, Liu M. Drug-loaded PEG-PLGA nanoparticles for cancer treatment. *Front Pharmacol.* **2022**; *13*:990505. doi: 10.3389/fphar.2022.990505.
152. Saxena J, Bisen M, Misra A, Srivastava VK, Kaushik S, Siddiqui AJ, Mishra N, Singh A, Jyoti A. Targeting COPD with PLGA-Based Nanoparticles: Current Status and Prospects. *Biomed Res Int.* **2022**; *2022*:5058121. doi: 10.1155/2022/5058121.
153. Lester MK, Flume PA, Gray SL, Anderson D, Bowman CM. Nebulizer use and maintenance by cystic fibrosis patients: a survey study. *Respir Care*. **2004**; *49(12)*:1504-8.
154. Ho DK, Nichols BLB, Edgar KJ, Murgia X, Loretz B, Lehr CM. Challenges and strategies in drug delivery systems for treatment of pulmonary infections. *Eur J Pharm Biopharm.* **2019**; *144*:110-124. doi: 10.1016/j.ejpb.2019.09.002.
155. Merchant Z, Buckton G, Taylor KM, Stapleton P, Saleem IY, Zariwala MG, Somavarapu S. A New Era of Pulmonary Delivery of Nano-antimicrobial Therapeutics to Treat Chronic Pulmonary Infections. *Curr Pharm Des*. **2016;** 22(17):2577-2598. doi: 10.2174/1381612822666160317142139.
156. Teixeira MC, Carbone C, Sousa MC, Espina M, Garcia ML, Sanchez-Lopez E, Souto EB. Nanomedicines for the Delivery of Antimicrobial Peptides (AMPs). *Nanomaterials (Basel).* **2020**; *10(3)*:560. doi: 10.3390/nano10030560.
157. Lam SJ, Wong EHH, Boyer C, Qiao GG. Antimicrobial polymeric nanoparticles. *Prog Polym Sci.* **2018**; *76*:40–64.
158. Sánchez-López E, Gomes D, Esteruelas G, Bonilla L, Lopez-Machado AL, Galindo R, Cano A, Espina M, Ettcheto M, Camins A, Silva AM, Durazzo A, Santini A, Garcia ML, Souto EB. Metal-Based Nanoparticles as Antimicrobial Agents: An Overview. *Nanomaterials (Basel)*. **2020**; *10(2)*:292. doi: 10.3390/nano10020292.
159. Diniz FR, Maia RCAP, Rannier L, Andrade LN, V Chaud M, da Silva CF, Corrêa CB, de Albuquerque Junior RLC, P da Costa L, Shin SR, Hassan S, Sanchez-Lopez E, Souto EB, Severino P. Silver Nanoparticles-Composing Alginate/Gelatine Hydrogel Improves Wound Healing In Vivo. *Nanomaterials (Basel)*. **2020**; *10(2)*:390. doi: 10.3390/nano10020390.

160. Chen WY, Chang HY, Lu JK, Huang YC, Harroun SG, Tseng YT, Li YJ, Huang CC, Chang HT Self-Assembly of Antimicrobial Peptides on Gold Nanodots: Against Multidrug-Resistant Bacteria and Wound-Healing Application. *Adv. Funct. Mater.* **2015**; *25*:7189–7199. Doi: 10.1002/adfm.201503248.
161. Salouti M, Mirzaei F, Shapouri R, Ahangari A. Synergistic Antibacterial Activity of Plant Peptide MBP-1 and Silver Nanoparticles Combination on Healing of Infected Wound Due to Staphylococcus aureus. *Jundishapur J Microbiol*. **2016**; *9(1)*:e27997. doi: 10.5812/jjm.27997.
162. Sonia TA, Sharma CP. Chitosan and Its Derivatives for Drug Delivery Perspective. *Adv. Polym. Sci*. **2011**; *243*:23–53. doi: 10.1007/12_2011_117.
163. Piras AM, Maisetta G, Sandreschi S, Esin S, Gazzarri M, Batoni G, Chiellini F. Preparation, physical-chemical and biological characterization of chitosan nanoparticles loaded with lysozyme. *Int. J. Biol. Macromol*. **2014**; *67*:124–131. doi: 10.1016/j.ijbiomac.2014.03.016.
164. Piras AM, Maisetta G, Sandreschi S, Gazzarri M, Bartoli C, Grassi L, Esin S, Chiellini F, Batoni G. Chitosan nanoparticles loaded with the antimicrobial peptide temporin B exert a long-term antibacterial activity in vitro against clinical isolates of Staphylococcus epidermidis. *Front Microbiol.* **2015**; *6*:372. doi: 10.3389/fmicb.2015.00372.
165. Cerchiara T, Abruzzo A, di Cagno M, Bigucci F, Bauer-Brandl A, Parolin C, Vitali B, Gallucci MC, Luppi B. Chitosan based micro- and nanoparticles for colon-targeted delivery of vancomycin prepared by alternative processing methods. *Eur. J. Pharm. Biopharm.* **2015**; *92*:112–119. doi: 10.1016/j.ejpb.2015.03.004.
166. d'Angelo I, Casciaro B, Miro A, Quaglia F, Mangoni ML, Ungaro F. Overcoming barriers in Pseudomonas aeruginosa lung infections: Engineered nanoparticles for local delivery of a cationic antimicrobial peptide. *Colloids Surf. B Biointerfaces*. **2015**; *135*:717–725. doi: 10.1016/j.colsurfb.2015.08.027.
167. Casciaro B, d'Angelo I, Zhang X, Loffredo MR, Conte G, Cappiello F, Quaglia F, Di YP, Ungaro F, Mangoni ML. Poly(lactide-co-glycolide) Nanoparticles for Prolonged Therapeutic Efficacy of Esculentin-1a-Derived Antimicrobial Peptides against Pseudomonas aeruginosa Lung Infection: in Vitro and in Vivo Studies. *Biomacromolecules.* **2019**; *20(5)*:1876-1888. doi: 10.1021/acs.biomac.8b01829.
168. Cappiello F, Casciaro B, Loffredo MR, Puglisi E, Lin Q, Yang D, Conte G, d'Angelo I, Ungaro F, Ferrera L, Barbieri R, Cresti L, Pini A, Di YP, Mangoni ML. Pulmonary Safety Profile of Esc Peptides and Esc-Peptide-Loaded Poly(lactide-co-glycolide) Nanoparticles: A Promising Therapeutic Approach for Local Treatment of Lung Infectious Diseases. *Pharmaceutics*. **2022**; *14(11)*:2297. doi: 10.3390/pharmaceutics14112297.
169. Pini A, Falciani C, Mantengoli E, Bindi S, Brunetti J, Iozzi S, Rossolini GM, Bracci L. "A novel tetrabranched antimicrobial peptide that neutralizes bacterial lipopolysaccharide and prevents septic shock in vivo", *FASEB Journal*; **2010**; *24*:1015-1022. doi: 10.1096/fj.09-145474.
170. Pini A, Giuliani A, Falciani C, Runci Y, Ricci C, Lelli B, Malossi M, Neri P, Rossolini GM, Bracci L. Antimicrobial activity of novel dendrimeric peptides obtained by phage display selection and rational modification. *Antimicrob Agents Chemother*. **2005**; *49(7)*:2665-72. doi: 10.1128/AAC.49.7.2665-2672.2005.
171. Pini A, Lozzi L, Bernini A, Brunetti J, Falciani C, Scali S, Bindi S, Di Maggio T, Rossolini GM, Niccolai N, Bracci L. Efficacy and toxicity of the antimicrobial peptide M33 produced with different counter-ions. *Amino Acids*. **2012**; *43(1)*:467-73. doi: 10.1007/s00726-011-1103-z.
172. Pini A, Giuliani A, Falciani C, Fabbrini M, Pileri S, Lelli B, Bracci L. Characterization of the branched antimicrobial peptide M6 by analyzing its mechanism of action and in vivo toxicity. *J Pept Sci.* **2007**; *13(6):*393-9. doi: 10.1002/psc.858.
173. van der Weide H, Brunetti J, Pini A, Bracci L, Ambrosini C, Lupetti P, Paccagnini E, Gentile M, Bernini A, Niccolai N, Jongh DV, Bakker-Woudenberg IAJM, Goessens WHF, Hays JP, Falciani C. Investigations into the killing activity of an antimicrobial peptide active against extensively antibiotic-resistant K. pneumon iae and P. aeruginosa. *Biochim Biophys Acta Biomembr.* **2017**; *1859(10)*:1796-1804. doi: 10.1016/j.bbamem.2017.06.001.
174. Brunetti J, Falciani C, Roscia G, Pollini S, Bindi S, Scali S, Arrieta UC, Gómez-Vallejo V, Quercini L, Ibba E, Prato M, Rossolini GM, Llop J, Bracci L, Pini A. In vitro and in vivo efficacy, toxicity, bio-distribution and resistance selection of a novel antibacterial drug candidate. *Sci Rep.* **2016;** *6*:26077. doi: 10.1038/srep26077.
175. Brunetti J, Roscia G, Lampronti I, Gambari R, Quercini L, Falciani C, Bracci L, Pini A. Immunomodulatory and Anti-inflammatory Activity in Vitro and in Vivo of a Novel Antimicrobial Candidate. *J Biol Chem*. **2016**; *291(49)*:25742-25748. doi: 10.1074/jbc.M116.750257.
176. Quercini L, Brunetti J, Riolo G, Bindi S, Scali S, Lampronti I, D'Aversa E, Wronski S, Pollini S, Gentile M, Lupetti P, Rossolini GM, Falciani C, Bracci L, Pini A. An antimicrobial molecule mitigates signs of sepsis in vivo and eradicates infections from lung tissue. *FASEB J.* **2020**; *34(1)*:192-207. doi: 10.1096/fj.201901896RR.
177. Falciani C, Zevolini F, Brunetti J, Riolo G, Gracia R, Marradi M, Loinaz I, Ziemann C, Cossío U, Llop J, Bracci L, Pini A. Antimicrobial Peptide-Loaded Nanoparticles as Inhalation Therapy for *Pseudomonas aeruginosa* Infections. *Int J Nanomedicine*. **2020**; *15*:1117-1128. doi: 10.2147/IJN.S218966.
178. Percie du Sert N, Hurst V, Ahluwalia A, Alam S, Avey MT, Baker M, Browne WJ, Clark A, Cuthill IC, Dirnagl U, Emerson M, Garner P, Holgate ST, Howells DW, Karp NA, Lazic SE, Lidster K, MacCallum CJ, Macleod M, Pearl EJ, Petersen OH, Rawle F, Reynolds P, Rooney K, Sena ES, Silberberg SD, Steckler T, Würbel H. The ARRIVE guidelines 2.0: Updated guidelines for reporting animal research. *PLoS Biol.* **2020**; *18(7)*:e3000410. doi: 10.1371/journal.pbio.3000410.
179. Alexander DJ, Collins CJ, Coombs DW, Gilkison IS, Hardy CJ, Healey G, Karantabias G, Johnson N, Karlsson A, Kilgour JD, McDonald P. Association of Inhalation Toxicologists (AIT) working party recommendation for standard delivered dose

calculation and expression in non-clinical aerosol inhalation toxicology studies with pharmaceuticals. *Inhal Toxicol*. **2008**; *20(13)*:1179-89. doi: 10.1080/08958370802207318.
180. Timmerman P, White S, McDougall S, Kall MA, Smeraglia J, Fjording MS, Knutsson M. Tiered approach into practice: scientific validation for chromatography-based assays in early development - a recommendation from the European Bioanalysis Forum. *Bioanalysis.* **2015**; *7(18)*:2387-2398. doi: 10.4155/bio.15.168.
181. Angervall L, Carlström E. Theoretical criteria for the use of relative organ weights and similar ratios in biology. *J Theor Biol.* **1963**; *4(3)*:254-9. doi: 10.1016/0022-5193(63)90004-3.
182. Irwin S. Comprehensive observational assessment: Ia. A systematic, quantitative procedure for assessing the behavioral and physiologic state of the mouse. *Psychopharmacologia*. **1968**; *13(3)*:222-57. doi: 10.1007/BF00401402.
183. Mathiasen JR, Moser VC. The Irwin Test and Functional Observational Battery (FOB) for Assessing the Effects of Compounds on Behavior, Physiology, and Safety Pharmacology in Rodents. *Curr Protoc Pharmacol*. **2018**; *83(1)*:e43. doi: 10.1002/cpph.43.
184. Flénet T, Fontecave-Jallon J, Guméry PY, Eynard C, Boucher F, Baconnier P, Tanguy S. High-resolution respiratory inductive plethysmography in rats: validation in anesthetized conditions. *Physiol Meas.* **2017**; *38(7)*:1362-1372. doi: 10.1088/1361-6579/aa6737.
185. d'Angelo I, Parajó Y, Horváth A, Kéri G, La Rotonda MI, Alonso MJ. Improved delivery of angiogenesis inhibitors from PLGA:poloxamer blend micro- and nanoparticles. *J Microencapsul*. **2010**; *27(1)*:57-66. doi: 10.3109/02652040902954729.
186. Ungaro F, d'Angelo I, Coletta C, d'Emmanuele di Villa Bianca R, Sorrentino R, Perfetto B, Tufano MA, Miro A, La Rotonda MI, Quaglia F. Dry powders based on PLGA nanoparticles for pulmonary delivery of antibiotics: modulation of encapsulation efficiency, release rate and lung deposition pattern by hydrophilic polymers. *J Control Release*. **2012**; 157(1):149-59. doi: 10.1016/j.jconrel.2011.08.010.
187. Sadzuka Y, Nakade A, Hirama R, Miyagishima A, Nozawa Y, Hirota S, Sonobe T. Effects of mixed polyethyleneglycol modification on fixed aqueous layer thickness and antitumor activity of doxorubicin containing liposome. *Int J Pharm.* **2002**; *238(1-2)*:171-80. doi: 10.1016/s0378-5173(02)00075-3.
188. Moss OR. Simulants of lung interstitial fluid. *Health Phys*. **1979**; *36(3)*:447-8.
189. Vogel HJ, Bonner DM. Acetylornithinase of Escherichia coli: Partial purification and some properties. *J. Biol. Chem*. **1956**; *218(1)*:97–106.
190. Luca V, Stringaro A, Colone M, Pini A, Mangoni ML. Esculentin(1-21), an amphibian skin membrane-active peptide with potent activity on both planktonic and biofilm cells of the bacterial pathogen Pseudomonas aeruginosa. *Cell Mol Life Sci.* **2013**; *70(15)*:2773-86. doi: 10.1007/s00018-013-1291-7.
191. Duret C, Wauthoz N, Merlos R, Goole J, Maris C, Roland I, Sebti T, Vanderbist F, Amighi K. In vitro and in vivo evaluation of a dry powder endotracheal insufflator device for use in dose-dependent preclinical studies in mice. *Eur J Pharm Biopharm*. **2012**; 81(3):627-34. doi: 10.1016/j.ejpb.2012.04.004.
192. Hoppentocht M, Hoste C, Hagedoorn P, Frijlink HW, de Boer AH. In vitro evaluation of the DP-4M PennCentury insufflator. *Eur J Pharm Biopharm*. **2014**; *88(1)*:153-9. doi: 10.1016/j.ejpb.2014.06.014.
193. Ensign LM, Tang BC, Wang YY, Tse TA, Hoen T, Cone R, Hanes J. Mucus-penetrating nanoparticles for vaginal drug delivery protect against herpes simplex virus. *Sci Transl Med*. **2012**; *4(138):*138ra79. doi: 10.1126/scitranslmed.3003453.
194. Xu Q, Boylan NJ, Cai S, Miao B, Patel H, Hanes J. Scalable method to produce biodegradable nanoparticles that rapidly penetrate human mucus. *J Control Release*. **2013**; *170(2)*:279-86. doi: 10.1016/j.jconrel.2013.05.035.
195. Niederman MS, Torres A. Severe community-acquired pneumonia. *Eur Respir Rev*. **2022**; *31(166)*:220123. doi: 10.1183/16000617.0123-2022.
196. Torres A, Cilloniz C, Niederman MS, Menéndez R, Chalmers JD, Wunderink RG, van der Poll T. Pneumonia. *Nat Rev Dis Primers*. **2021**; 7(1):25. doi: 10.1038/s41572-021-00259-0.
197. Mandell LA, Niederman MS. Aspiration Pneumonia. *N Engl J Med.* **2019**; *380(7)*:651-663. doi: 10.1056/NEJMra1714562.
198. Sender V, Stamme C. Lung cell-specific modulation of LPS-induced TLR4 receptor and adaptor localization. *Commun Integr Biol.* **2014**; *7:*e29053. doi: 10.4161/cib.29053.
199. Prior H, Haworth R, Labram B, Roberts R, Wolfreys A, Sewell F. Justification for species selection for pharmaceutical toxicity studies. *Toxicol Res (Camb)*. **2020**; *9(6)*:758-770. doi: 10.1093/toxres/tfaa081.
200. Prior H, Baldrick P, de Haan L, Downes N, Jones K, Mortimer-Cassen E., Kimber I. Reviewing the utility of two species in general toxicology related to drug development. *Int J Toxicol.* **2018**; *37*:121–124.
201. Blaich G, Baumann A, Kronenberg S, de Haan L, Ulrich P, Richter WF, Tibbitts J, Chivers S, Tarcsa E, Caldwell R, Crameri F. Non-clinical Safety Evaluation of Biotherapeutics - Challenges, Opportunities and new Insights. *Regul Toxicol Pharmacol*. **2016**; *80S*:S1-S14. doi: 10.1016/j.yrtph.2016.08.012.
202. Robinson NB, Krieger K, Khan FM, Huffman W, Chang M, Naik A, Yongle R, Hameed I, Krieger K, Girardi LN, Gaudino M. The current state of animal models in research: A review. *Int J Surg*. **2019**; *72*:9-13. doi: 10.1016/j.ijsu.2019.10.015.
203. Chi LH, Burrows AD, Anderson RL. Can preclinical drug development help to predict adverse events in clinical trials?. *Drug Discov Today*. **2022**; *27(1*):257-268. doi: 10.1016/j.drudis.2021.08.010.
204. Palazzi X, Burkhardt JE, Caplain H, Dellarco V, Fant P, Foster JR, Francke S, Germann P, Gröters S, Harada T, Harleman J, Inui K, Kaufmann W, Lenz B, Nagai H, Pohlmeyer-Esch G, Schulte A, Skydsgaard M, Tomlinson L, Wood CE, Yoshida M. Characterizing "Adversity" of Pathology Findings in Nonclinical Toxicity Studies: Results from the 4th ESTP International Expert Workshop. *Toxicol Pathol.* **2016**; *44(6)*:810-24. doi: 10.1177/0192623316642527.

205. Bailey J, Thew M, Balls M. An analysis of the use of dogs in predicting human toxicology and drug safety. *Altern Lab Anim.* **2013**; *41(5)*:335-50. doi: 10.1177/026119291304100504.
206. Zhang Y, Deng C, Gong D, Kang Y, Liu J, Zhang W. Preclinical safety evaluation of ET-26 hydrochloride, a novel intravenous anesthetic agent, in beagle dogs. *J Appl Toxicol.* **2020**; *40(5)*:679-690. doi: 10.1002/jat.3936.
207. European Medicines Agency. ICH guideline S6 (R1)—Preclinical safety evaluation of biotechnology-derived pharmaceuticals. EMA/CHMP/ICH/731268/1998. **1998**.
208. European Medicines Agency. ICH M3 (R2)—Non-clinical safety studies for the conduct of human clinical trials and marketing authorization for pharmaceuticals. EMA/CPMP/ICH/286/95. **1995**.
209. European Medicines Agency. Coommittee for Medicinal Products for Human Use (CHMP). Guideline on repeated dose toxicity EMA/CPMP/SWP/1042/99. **2010**.
210. European Medicines Agency. Committee for Medicinal Products for Human Use (CHMP). Questions and answers on the withdrawal of the 'Note for guidance on single dose toxicity'. EMA/CHMP/SWP/81714/2010. **2010**.
211. European Medicines Agency. Committee for Medicinal Products for Human Use (CHMP). Guideline on similar biological medicinal products containing biotechnology-derived proteins as active substance: Non-clinical and clinical issues. EMEA/CHMP/BMWP/42832/2005 Rev1. **2014**.
212. European Medicines Agency. Committee for Medicinal Products for Human Use (CHMP). Guideline on similar biological medicinal products. CHMP/437/04 Rev 1. **2014**.
213. European Medicines Agency. Committe for proprietary medicinal products (CPMP). Position paper on non-clinical safety studies to support clinical trials with single microdose. CPMP/SWP/2599/02. **2003**.
214. European Medicines Agency. Concept Paper. Need for revision of the guideline single dose toxicity 3BS1a. EMEA/CHMP/SWP/302413/08. **2008**.
215. European Medicines Agency. ICH S3A Toxicokinetics: The assessment of systemic exposure in toxicity studies. EMA/CPMP/ICH/384/95. 1995.
216. Casciaro B, Ghirga F, Quaglio D, Mangoni ML. Inorganic Gold and Polymeric Poly(Lactide-co-glycolide) Nanoparticles as Novel Strategies to Ameliorate the Biological Properties of Antimicrobial Peptides. *Curr Protein Pept Sci*. **2020**; *21(4)*:429-438. doi: 10.2174/1389203720666191203101947.
217. Jackson L, Waters V. Factors influencing the acquisition and eradication of early Pseudomonas aeruginosa infection in cystic fibrosis. *J Cyst Fibros*. **2021**; *20(1)*:8-16. doi: 10.1016/j.jcf.2020.10.008.
218. d'Angelo I, Conte C, Miro A, Quaglia F, Ungaro F. Pulmonary drug delivery: a role for polymeric nanoparticles? *Curr Top Med Chem.* **2015**; *15(4)*:386-400. doi: 10.2174/1568026615666150108123256.
219. Cresti L, Conte G, Cappello G, Brunetti J, Falciani C, Bracci L, Quaglia F, Ungaro F, d'Angelo I, Pini A. Inhalable Polymeric Nanoparticles for Pulmonary Delivery of Antimicrobial Peptide SET-M33: Antibacterial Activity and Toxicity In Vitro and In Vivo. *Pharmaceutics*. **2022**; *15(1)*:3. doi: 10.3390/pharmaceutics15010003.